Degradation rates and mechanisms of acid-resistant coatings in copper-leaching tanks

Møller, Victor Buhl

Publication date:
2017

Document Version
Publisher's PDF, also known as Version of record

Degradation rates and mechanisms of acid-resistant coatings in copper-leaching tanks

Victor Buhl Møller

PhD Thesis

December 2017

DTU Chemical Engineering
Department of Chemical and Biochemical Engineering

Degradation rates and mechanisms of acid-resistant coatings in copper-leaching tanks

By Victor Buhl Møller

PhD thesis
December 2nd, 2017

Supervisor	Søren Kiil (DTU Chemical Engineering)
Co-supervisors	Kim Dam-Johansen (DTU Chemical Engineering)
	Sarah Maria Frankaer (Hempel A/S)

DTU Chemical Engineering
Department of Chemical and Biochemical Engineering

Preface

This dissertation is the result of three years of collaborative research between the Technical University of Denmark (DTU), the coating producer Hempel A/S, and the cement and minerals process company FLSmidth A/S. It is part of the project 'Minerals and Cement Process Technology - MiCeTech' funded by Innovation Fund Denmark, FLSmidth A/S, Hempel A/S, the Hempel Foundation, and the Technical University of Denmark (DTU). An approximate two years were spent for designing, constructing and refining experimental set-ups at the center for Combustion and Harmful Emission Control (CHEC) at DTU Chemical Engineering, and the remaining time on performing experiments and disseminating the results.

This work was made possible by the support of my supervisors, colleagues, supporting staff, family and friends. I would like to thank Søren Kiil for his advice, guidance and inspiration, not only in the PhD, but also through my master thesis. His care for details has been a great counterweight to my sometimes more rushed approach to problems. I would like to thank Kim Dam-Johansen for giving insight in industry needs, and for providing me with the opportunity to do this PhD. I am also grateful for Sarah Frankærs continued motivation and optimism, whenever prospects were sour.
I would like to acknowledge the contribution of Ilsur Khusainov and Ting Wang to the work on diffusion cells. Without them there would not have been time to dive into detailed predictions of coating barrier properties. I would also like to acknowledge the supporting staff at DTU who minimized the time I had to spend on paper work. Special thanks to the KT workshop and technicians who taught me numerous practical lessons, and without whom the experimental set-ups would have remained purely theoretical.
Furthermore, I would like to thank my fellow PhD students at CHEC and CoaST who made the workplace a great place to be, in particular Gerard Capellades Mendez for his scientific input and who's refined humor entertained the whole office. Finally I would like to thank my family for their support, especially my wife for keeping me well-nourished, my daughter for not keeping me up at night, and my mother, who believes people always forget always to acknowledge their mothers, there you go.

Summary

Modern society is reliant on high purity metals, making mineral processing and refining of metals vital to everyday life. However, unit operations, associated with the extraction and purification of metals, can come into contact with highly acidic substances, which may lead to corrosion of tanks, reactors and process equipment. To reduce the required maintenance, operational downtime, and thereby the overall production costs, steel and concrete surfaces need to be protected from these chemicals. Organic coating technology has been proved to provide protection against acidic environments, but its potential in the mineral industry has not yet been thoroughly investigated. This particular industry poses unique challenges, with high operational temperatures (around 75 °C) and combined acidic-erosive environments.

The use of organic coatings to protect tanks, pipes, and secondary exposure areas, may provide significant savings compared to utilizing ceramic or metal alloys with similar acid resistance. Nevertheless, organic coatings are often disregarded in favor of their inorganic counterparts. This is in part due to a lack of knowledge regarding the limitations of organic coatings, and the inability to accurately predict coating lifetime. More know-how is required before organic coatings can compete against materials with a proven track-record.

In this PhD project, state-of-the-art literature on acid resistant organic coatings was collected and reviewed. The subsequent investigations concerned predicting coating lifetimes and investigating degradation mechanisms in the harsh acidic environments found in agitated leaching reactors, where failure can occur due to chemical reactions, erosive wear, acid diffusion, or a mixture of the three. The research conducted can be summarized by the five main parts below.

Part I An in-depth literature study was performed to uncover and review uses and limitations of acid-resistant coatings in the chemical industry, with a comparison to alternative resistant materials based on metals and ceramics. In addition, coating degradation phenomena caused by acid exposure, were mapped to the extent possible, and analysis methods for detecting coating degradation type and severity were listed and discussed. It was found that more knowledge on chemical and physical degradation mechanisms was required. Improvements in resistance to elevated temperatures and abrasion would decrease the risk of use and increase the potential application areas of organic coatings exposed to acidic environments in the chemical industry.

Part II A series of thermoset coatings with some degree of acid resistance were selected for sulfuric acid and water immersion experiments: one vinyl ester, one polyurethane and three different novolac epoxies. The measured outputs were weight change, visual observations, FTIR, and SEM/EDS analysis of coating cross-sections.

One of the selected novolac epoxies failed so rapidly in sulfuric acid, that it was excluded from further experimentation. The two other novolac epoxy coatings showed a fast and high weight gain, along with delamination or blistering in the warm acid, but no hard evidence of chemical changes. The polyurethane coating showed a gradual drop in weight due to acid exposure, caused by the dissolution of limestone fillers. The vinyl ester coating showed little weight gain, no deformation, and no EDS-detectable sulfur element in the film after 53 days of immersion.

Part III To explore the performance of the coatings in a realistic environment, a pilot-scale agitated leaching reactor containing sulfuric acid and micron-size ore particles, was designed and constructed. The most important scaling factor was the stirring intensity.

Failure, attributed to erosion, was observed via dry film thickness change during exposure. This output parameter was found to be a function of film swelling and contraction, due to chemical exposure, as well as the polishing caused by the erosive particles. For coating samples placed on the reactor bottom, film reduction rates varied with radial position. Maximum rates were found about halfway between reactor center and wall. Polishing rates also varied significantly with acid concentration, most likely due to chemical degradation of the coatings which damaged the surface mechanical properties. The vinyl ester-based coating was most resistant to the simultaneous erosive/acidic exposure; a 1000 μm thick film would have an estimated lifetime of 5.9 ± 1.1 years, compared to a similar novolac epoxy or polyurethane coating where the lifetime was estimated to 1.6 ± 0.2 and 1.4 ± 0.1 years, respectively.

Part IV A series of newly designed and constructed diffusion cells were used to measure sulfuric acid diffusion rates through the coatings. A mathematical model was developed to simulate the experimental data, and diffusion mechanisms were studied through the modeling results.

It was found that sulfuric acid deteriorated the coating barrier properties as it diffused through the films. This was expressed in the modeling results, where the diffusion coefficient required continuous concentration dependency, combined with a simplified three-step time dependence, to accurately simulate the acid breakthrough time and the subsequent steady state flux. Using the model developed, it was possible to estimate a coating lifetime, based on the acid breakthrough time. Coating degradation reactions with the sulfuric acid proved the most significant factor in determining barrier properties. A vinyl ester-based coating proved the most effective barrier to sulfuric acid diffusion, where a 735 μm thick film showed no acid permeation after 118 days of exposure. Comparatively, a 1000 μm thick polyurethane coating was simulated to last 278$\pm$13 days, a 100% solids amine-cured novolac epoxy would last 56$\pm$3 days, and a regular amine-cured novolac epoxy would last 3.2$\pm$0.5 days before acid permeated the film.

Part V A summary of coating performance was provided, and the lifetime of the coatings in the agitated leaching environment was evaluated based on the diffusion, reaction, and erosion failure mechanisms.

The vinyl ester was the peak performer in terms of chemical inertness, barrier properties and erosive resistance. The polyurethane came second, while novolac epoxies had the poorest performance of the coatings investigated. The combined polishing and acid diffusion would yield lifetimes below the previous estimate from diffusion cells experiments, due a reduction of the effective coating thickness, but diffusion barrier properties were found to be the most significant factor. For coatings in agitated leaching reactors, the importance of considering all degradation mechanisms was emphasized, since they showed synergistic behavior: ionic diffusion enabled chemical reactions in the film, the following chemical reactions speeded up acid diffusion rates, the combined reaction/diffusion increased the erosion rates, and finally erosive wear would speed up diffusion rates.

Dansk resumé

Det moderne samfund er afhængig af metaller med en høj renhed, hvilket gør mineralforarbejdning og raffinering af metaller, afgørende for hverdagen. I forbindelse med udvinding og rensning af mineraler til metal produktion, kan enhedsoperationer komme i kontakt med stærk syrlige stoffer, som kan korroderer reaktorer og proces udstyr. Beskyttelse af stål- og betonflader fra disse ætsende kemikalier, er vigtig for at reducere den nødvendige vedligeholdelse samt driftstop, og derved reducere de samlede produktionsomkostninger. Organisk coating teknologi har vist sig at kunne bruges som beskyttelse mod stærkt syrlige miljøer, men dets potentiale i mineralindustrien er endnu ikke grundigt undersøgt, da der er unikke udfordringer med høje driftstemperaturer og syre samt erosive miljøer.

Anvendelsen af organiske coatings til beskyttelse af tanke, rør og sekundære eksponeringsområder, kan medføre betydelige besparelser sammenlignet med anvendelsen af keramiske eller metallegeringer, med tilsvarende syrebestandighed. Ikke desto mindre, ignoreres organiske coatings ofte til fordel for deres uorganiske modparter. Dette skyldes til dels manglende viden om begrænsningerne af organiske coatings, og en manglende evne til at forudsige levetiden nøjagtigt. Der kræves mere know-how, inden organiske coatings kan konkurrere mod materialer med en veldokumenteret historik.

Denne PhD. afhandling samler og reviewer litteratur vedrørende syre-resistente coatings, for at samle et billede af hvor vi står i dag. Derefter forsøges det at forudsige coating levetider og undersøge nedbrydningsmekanismerne, i det barske syrelige miljø fundet i omrørte leaching reaktorer, hvor coatings kan nedbrydes af kemiske reaktioner, erosivt slid, syre diffusion, eller en blanding af alle tre. Forskningen kan deles i fem hovedstykker, som er opsummeret nedenfor.

Del I Et dybtgående litteratur studie blev udført for at undersøge brugen og begrænsningerne af syre-resistente coatings i den kemiske industri, i sammenligning med alternative metalliske og keramiske materialer. Derudover, blev coating nedbrydnings fænomener i syreligt miljø, og analyse metoder til at observere graden og typen af nedbrydning kortlagt. Det blev konkluderet at mere viden om de kemiske og fysiske nedbrydningsmekanismer kræves, og at forbedringer i temperatur og slid resistens ville reducere risikoen af brug, og øge potentielle anvendelses områder af organiske coatings i sure miljøer i den kemiske industri.

Del II En række termosætte coatings med en vis grad af syrebestandighed blev valgt til svovlsyre og vandneddypningsforsøg: en vinyl ester, en polyurethan og tre novolak-epoxier. De målte outputs var vægt ændring, visuel observationer samt FTIR og SEM/EDS analyse af coating tværsnit.

En af de udvalgte novolak-epoxier svigtede så hurtigt i svovlsyre, at den blev udelukket fra resten af projektet. De to andre novolak-epoxy coatinger viste en hurtig og høj vægtforøgelse sammen med delaminering eller blæredannelse i den varme syre, dog ingen tegn på kemiske ændringer ved FTIR-analyse. Polyurethan coatingen oplevede et gradvist fald i vægt grundet syreeksponering, forårsaget af opløsningen af kalksten fyldstoffer. Vinyl ester coatingen viste kun lille vægtforøgelse, ingen deformation og ingen EDS-detekterbart svovlelement i filmen efter 53 dages neddypning.

Del III For at udforske ydeevenen af de udvalgte coatings i et realistisk miljø, blev en pilot-skala omrørt leaching reaktor designet og konstrueret. Den blev bygget til at udsætte coatings for et simultan surt og erosivt miljø.

Nedbrydning grundet erosion blev observeret gennem ændring af filmtykkelse. Denne output parameter viste sig at være en funktion af film hævelse og sammentrækning grundet den kemiske eksponering, samt overflade polering forårsaget af de erosive partikler. For coating prøver placeret i reaktor

bunden varierede filmreduktionshastigheder med radial position. De maksimale polerings hastigheder blev fundet omkring halvvejs mellem reaktor center og væg. Poleringshastighederne varierede også med syrekoncentration, sandsynligvis på grund af kemisk nedbrydning af coatings overflademekaniske egenskaber. Vinyl esteren var mest modstandsdygtig overfor samtidig erosiv/syrlig eksponering, hvor en 1000 μm tyk film ville have en estimeret levetid på $5,9 \pm 1,1$ år, lignende novolak-epoxy og polyurethan belægninger ville henholdsvis holde $1,6 \pm 0,2$ og $1,4 \pm 0,1$ år.

Del IV En række nyligt designet og konstrueret diffusionsceller blev brugt til at observere svovlsyre diffusion gennem de valgte coatinger. En matematisk model blev udviklet til at simulere det resulterende data, og diffusionsmekanismer blev studeret gennem modelleringsresultaterne.

Det blev fundet at svovlsyre forringede barrieregenskaberne for coatingerne samtidig med at syren diffunderede gennem coating filmene. Dette blev udtrykt i modelleringsresultaterne, hvor diffusionskoefficienten blev en funktion af koncentration, kombineret med en simplificeret tre-trins tids afhængighed, for at nøjagtigt simulere både syre gennembrudstid og den følgende steady state flux. Ved hjælp af den udviklede model, var det muligt at estimere coating levetid, baseret på syre gennembrudstiden. Reaktioner mellem coatings og svovlsyren var den væsentligste faktor for bestemmelse af barrieregenskaber. Vinyl esteren viste sig at være det mest effektive barriere for svovlsyre-diffusion, hvor en 735 μm tyk film ikke blev gennembrudt selv efter 118 dages eksponering. Til sammenligning ville en 1000 μm tyk polyurethan belægning varer 278±13 dage, en 100 % faststof-aminhærdet novolak-epoxy ville holde 56±3 dage, og en reguler aminhærdet novolak-epoxy ville holde 3,2±0,5 dage før syre gennemtrængte filmen.

Del V Et resumé af coating ydelse angives, og levetiden af coating produkterne i det omrørt leaching tank miljø blev evalueret baseret på diffusions-, reaktions- og erosionsnedbrydningsmekanismerne.

Vinyl esteren var top-performeren i forhold til kemisk inertitet, barrieregenskaber og slidresistens. Polyurethanen kommer som nummer to, mens novolak-epoxierne var de dårligste af de undersøgte coatings. En simultane erosion og syrediffusion ville resulterer i levetider under det foregående estimat fra diffusionscelle eksperimenterne, som følge af en reduktion af den effektive coatingtykkelse. Dog viste diffusionsbarriereregenskaberne at være de vigtigste faktorer. For coatings i omrørete leaching reaktorer, blev betydningen af at overveje alle nedbrydningsmekanismer understreget, da de viste synergistisk adfærd: ionisk diffusion tillod kemiske reaktioner i coating filmen, de følgende kemiske reaktioner øgede syrediffusionshastighederne, den kombinerede reaktion/diffusion øgede erosionshastigheder, og endelig vil erosiv slid fremskynde syrediffusionshastighederne.

Overview of the Ph.D. thesis

This project started with a question: Where can organic coatings find use in the mineral and cement industry? Among the possibilities, organic coatings were found useful in processes where chemical resistance is of importance, excluding high temperature processes. Focus fell on acid resistance, and the agitated leaching processes used for copper refinery.

Objectives

The overall concept was to investigate new uses of Hempel's products in FLSmidth's industry. The project was therefore a mixture of academic and industrial relevant aims, using agitated leaching tanks as a case study. The main objects were:

- Map acid-resistant coating technology and its uses the chemical industry
- Evaluate performance and estimate lifetimes of organic coatings in the agitated leaching process
- Investigate coating degradation mechanisms in an erosive and acidic environment

Thesis structure

The research was based on three types of experiments: (1) Chemical immersion, of free films and coatings on substrates, (2) erosion experiments, using a pilot-scale agitated leaching reactor, designed and constructed specifically for this project, (3) diffusion experiments, using ionic diffusion cells, also designed and constructed for this project.
The thesis has been divided into five parts.

Part I Is a literature study into acid-resistant organic coatings, their uses and limitations compared to inorganic acid resistant materials. The relevant coating degradation mechanisms are also covered.

Part II Provides details of the coatings used for the study, and immersion experiments performed of coatings on substrates and free films. It also provides an analysis of the observed chemical degradation of the coatings samples.

Part III Introduces the process of agitated leaching of copper. It showcases a pilot-scale agitated leaching set-up, constructed for experimenting with simultaneous chemical and erosive exposure. The resulting coating degradation mechanisms due to erosion/polishing rates are described and lifetimes are estimated.

Part IV Describes the diffusion cells constructed for monitoring coating barrier properties. A mathematical model that simulates the results is presented, and coating lifetimes due to diffusion are estimated.

Part V Provides a perspective of coating performance, lifetime optimization, the relative effect of diffusion and polishing on coating performance, and the synergy of degradation mechanisms.

Part VI Final conclusions and future work.

Scientific hypotheses

1. Protective organic coatings can fail by three main mechanisms:
    - Diffusion of molecules into and through a coating film
    - Reaction of the coating components with, or due to the surrounding media and environment
    - Wear of the coating surface
2. The cause of failure can be a single or a mixture of the three mechanisms. Delamination due to thermal expansion or contraction is neglected.
3. The chemical environment will have a significant impact on organic coating polishing rates.
4. Coating erosion will increase the effective acid diffusion speed through a coating film.

Practical hypotheses

1. Precise measurement of degradation rates can be used to predict coating lifetime:
    - FTIR analysis can be used to predict the type and extent of coating reaction in acid
    - Modeling results from diffusion cells can be used to predict lifetimes of thicker coatings
    - Dry film thickness change can be used to predict coating polishing rates and estimate lifetimes of thicker coatings

Contents

Part I

Acid resistant organic coatings, limitations and failure mechanisms

When starting the project, it quickly became evident that there was no consensus of what defined acid resistance, nor any work that collected and reviewed the literature that existed on the topic. So it was then decided to do exactly that, resulting in a manuscript titled "Acid resistant organic coatings for the chemical industry - a review" [1]. This part is a modified version of said article with the addition of theory on coating erosion, which is of specific relevance to the experiments performed in the project. The current part outlines the main categories of acid resistant materials and the limitations of thermoset coatings in terms of industrial process parameters. It also covers the theory behind three types of organic coating degradation mechanisms.

Nomenclature

C	Concentration [mol/l]
D	Diffusion coefficient [m^2/s]
$\overline{D}$	Average diffusion coefficient [m^2/s]
F	Flux [mol/m^2s]
l	Position in the coating film [m]
l_0	Coating film thickness [m]
R	Gradient of a weight change slope [g/s]
t	Time [s]
T	Temperature [K]
Subscripts	
lag	Time lag
ss	Steady state

List of Abbreviations

ASTM	American Section of the International Association for Testing Materials
CPVC	Critical pigment-volume concentration
DFT	Dry film thickness
EDS	Energy-dispersive X-ray spectroscopy
ETFE	polyethylene tetraflouroethylene
FGD	Flue-gas desulfurization
FRP	Fiber-reinforced plastic
HDEP	High-density polyethylene
HIIR	Halogenrated butyl rubber
LCP	Liquid crystals plastics
LCT	Liquid crystals thermosets
PVC	Pigment-volume concentration
PE	Polyethylene
PP	Polypropylene
PTFE	Polytetraflouroethylene
T_g	Glass transition temperature
SEM	Scanning electron microscope
SS	Steady state
VOC	Volatile organic compounds

1 Organic coatings in acidic environments

Acidic solutions can be a challenge to process because of their ability to corrode common construction steels and concretes [2, 3]. Incorrect handling can result in incidents such as shown in Fig. 1.1, where the acid-resistance of materials surrounding an acid bath was not taken into consideration, or as seen in Fig. 1.2, where sulfuric acid produced by bacteria corroded a sludge tank, producing cavities in the tank [4, 5]. Many processes in the chemical industry consume or produce acidic substances, and often acid resistant alloys or ceramics are used as containment materials without considering the application of organic coatings as an option. This could be due to difficulties with the complex mechanisms of acid-resistance and a general lack of knowledge concerning the limitations and possibilities of organic coatings. This is unfortunate because cost savings can be achieved by coating inexpensive, but corrosion susceptible, construction material with a 0.8 to 3.8 mm thick acid resistant coating, or using fiberglass reinforced plastic (FRP) as the construction material, rather than making all the parts of costly alloy or ceramic material [6, 7]. The value of considering organic protection is evident by looking at some estimated expenses from 2010, where average cost of FRP material and installation is 1000 US\$/m^2, compared to 3000 US\$/m^2 for alloy material with similar acid-resistance [8].

Figure 1.1: Damage on concrete flooring in a chemical etching plant. The floor was exposed to acid drips and spills. Reproduced from [4] with permission from NACE International, Houston, TX. All rights reserved. ©NACE International 2016.

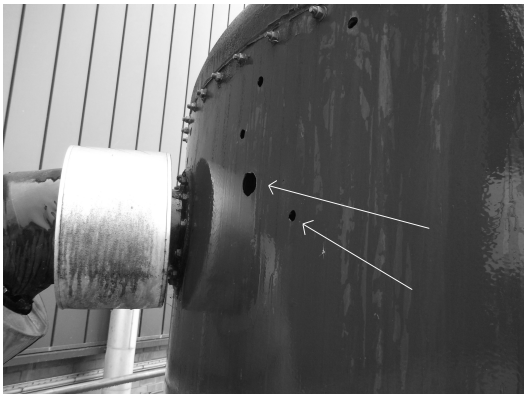

Figure 1.2: Damage on a sludge buffer tank for sewage treatment. The inside of the tank was exposed to sulfuric acid produced by bacteria. Reproduced from [5] with permission from Belzona International and NACE International, Houston, TX. All rights reserved. ©NACE International 2016.

Among the subcategories of organic materials, the chemically cured organic thermosets are of particular interest for harsh chemical exposure. Partly because the coating can be applied in liquid form without heating or excessive use of volatile organic solvents (VOC), but also because the hardened coating consists of a highly cross-linked network yielding good temperature resistance and excellent barrier properties. This makes thermosets the resin of choice when it comes to handling aggressive chemicals in industry [9, 10], and thus is the main focus of this paper.

Acid-resistant organic coatings and linings are surface treatments capable of enhancing the acid-

resistance of an underlying ceramic, metallic, or organic substrate. These coating technologies can be used in chemical industries, or any other industrial process that involves the consumption, production or transport of acidic chemicals, to increase the lifetime and performance of vulnerable materials. Organic coating materials can be self-supporting fiber-reinforced structures, or non-reinforced coatings. Fiber reinforced coatings have found use in wet flue gas desulfurization plants (FGD) [11], while non-reinforced coatings have, among others, been used to line rail-car tanks for acid transport, protect sewage pipes against microbial acids, and preserve stirred acid leach reactors in hydro-metallurgical processes [10, 12, 13]. Table 1.1 provides a list of industries where acid resistant organic coatings are used or have potential use, as protective coatings. The use of organic coatings is not limited to acid protection, also caustic environments and organic chemicals can be handled [14].
Like any other material, organic coatings have limitations. Industrial process variables such as temperature, pressure, wear, acid type, and presence of additional chemicals, can limit the usability of an organic coating. This section will give a brief history of organic coatings in acidic environments and an overview of the general process limitation of organic coatings, usable for acid protection.

Table 1.1: Selected industries where acid resistant organic coatings are used or have potential use, as protective coatings.

Industry	Operation (temperature)	Acid types	Erosive particles present
Wet flue gas desulfurization [11, 15]	Absorber (45-55 °C) and stack (70-85 °C)	Sulfuric and hydrochloric acid	Limestone slurry
Pulp and paper production [16]	Acidic magnesium bisulfite pulping (125-135 °C) and Kraft pulping (20-170 °C)	Sulfuric, formic and acetic acid	None
Chemical transport [17]	Rail car tanks and piping (ambient to <90 °C)	Can vary greatly, both organic and inorganic acids	None
Metal refining [8, 18]	Acid leaching (25-80 °C) and electrowinning (65 °C)	Sulfuric and nitric acid	Slurry concentrates
Sewage treatment [12, 19]	Concrete piping (Ambient)	Sulfuric acid (Bacterial)	None
Metal surface treatment [20]	Pickling of low and high alloy stainless steels, aluminum, copper and zinc alloys (25-80 °C)	Sulfuric, hydrochloric, nitric, hydrofluoric, citric, tartaric and chromic acid	None
Inorganic acid production [14]	Depends on the acid in question	All inorganic acids	Not available
Fertilizer production [21, 22]	Production of ammonium nitrate, ammonium phosphate and ammonium sulfate (20-105 °C)	Sulfuric, nitric and phosphoric acid	None

1.1 History

Thermoplastics such as polyethylene (PE), discovered in 1933, and polytetrafluoroethylene (PTFE or Teflon^{TM}), discovered in 1938, are well known for their acid-resistance, particularly towards hydrochloric acid (HCl), which corrodes many steel alloys. This resistance is shared by many thermoset and

thermoplastic materials. Since their invention, such plastics have been used as acid-resistant materials in equipment components, containers and tanks, and barrier coatings. Specially, the chemically hardened thermoset plastics, with their high cross-linking density have found uses in acidic environments. The most important ones are epoxy vinyl esters, phenolic epoxies, and polyurethane.
Polyurethane was invented in 1937 [23] and today is used in mattresses, tires, shoe soles, and many other applications. As protective coating in acidic environments, polyurethane is recommended by some manufactures in power plants, as well as the pulp and paper industry, though always in combination with epoxy based coatings [24].
Phenolic epoxies, such as bisphenol A epoxy, have been used commercially as protective coatings since 1947 [25, 26], and novolac epoxies are known as the resin within this category with the highest chemical resistance. Experience with use of epoxies in acidic environments is greater than for polyurethanes and it is more widely recommended for power plants and pulp and paper production [24].
Epoxy vinyl esters were discovered in the late 1960s, and succeeded the more brittle bisphenol A fumerate polyester as the resin of choice in aggressive chemical environments [27]. The vinyl ester found use as acid-resistant construction material as well as protective coatings in the chemical industry, and has reported lifetimes between 15 to 25 years in such environments [11]. Today all of the resins mentioned are used in industrial acidic environments, as long as the process parameters fall within the coating limitations.

1.2 Process limitations of acid-resistant coatings

1.2.1 Temperature

A disadvantage of organic coatings is that they are only usable within a narrow temperature range. The glass transition temperature (T_g) of a hardened coating is a good indicator of how high temperatures it can handle. The higher the T_g, the higher process temperatures it can resist, but operating above T_g can cause rapid deterioration [28]. It should be noted that temperature resistance is reduced if a coating is immersed in a liquid [11]. This is due to plasticization effects, which is increased segmental mobility of the resin network also seen as increased material flexibility [29], that lowers the coating's effective T_g [30]. A vinyl ester resin can be usable up to 100-120 °C in fluids and 175-200 °C for gas service [8, 11], while application temperatures can reach around 260 °C at immersed conditions for PTFE [31]. The majority of organic coatings should not be used in environments where temperatures exceed approximately 150 °C [10].

1.2.2 Pressure

Effects of pressure on organic coatings in acidic environments has not been investigated in greater detail. However, decompression has been reported to damage coatings, by causing rapid expansion of gases or liquids dissolved in the coating, resulting in e.g. blister formation [28, 32]. An example of organic coatings in high pressure operations includes flouropolymer coatings, such as PTFE, that have found uses in autoclaves operating between 15 and 35 MPa [33].

1.2.3 Erosion and abrasion

Erosive wear occurs when particles flow against a coating surface, chipping or scratching away coating material. Issues with erosion can occur whenever industrial operations process solid substances, it is a complex and diverse topic with entire journals based solely on the subject [34, 35].
Organic coatings can be used in processes with a low level of erosion or mild abrasion. This could be floor coatings for secondary containment where the coating is exposed to the abrasive sliding wear of pedestrians, or internal pipe coatings for transport of slurry material.
A particular property of some organic coatings, is the ability to deform if a force is applied, and reclaim the original shape when relaxed. This elastic property provides a high resistance towards impacts and related erosion, but organic coatings can also be hard and tough, making them useful in many types of abrasive conditions [36, 37].
Limitations in erosive environments depend on the severity of the erosive forces, which can be difficult to classify. As an example, a gas containing 0.2 wt% particles, moving at 76 m/s, is able to reduce the film thickness of a fiber reinforced coating by 3.18 mm a year in high angle impact zones, while slurries moving parallel to similar coatings at 1.8 to 3.7 m/s cause no issues in 10 years of service [38]. Coating limitations are not straightforward when it comes to erosion, see Section 3.3 for more detail on this aspect.

1.2.4 Acids and pH

Acids can occur in industrial processes as reactants, solvents, pH regulators, and as desired or undesired products. The more common acids include sulfuric (H_2SO_4), hydrochloric and nitric acid (HNO_3) [6]. Industrial processes using acidic chemicals can vary from the use of weak to strong acids and low to high concentrations, in the pH range -1.25 to 7. It is possible to formulate coatings capable of resisting these low pH values, but pH is not the only factor relevant for acid-resistance [13].
In general, organic coatings can have excellent resistance towards acids, but the type of acid(s) being processed is important to consider. An acid's oxidative or reducing properties as well as organic or inorganic nature are relevant. A list of common organic, inorganic and oxidizing acids is given in Table 1.2. Very oxidative acids can be troublesome with their ability to cleave important chemical bonds in coating resins and causing irreversible damage. While organic acids can diffuse rapidly through an organic coating, due to chemical similarity with the resin [39]. Therefore, a coating resistant to a reducing hydrochloric acid, might have poor performance in the oxidizing nitric or organic formic (HCOOH) acid.

Table 1.2: A selection of common inorganic acids, as well as the more troublesome organic and oxidizing inorganic acids. pKa values at 25 °C in aqueous solution are provided in parenthesis.

Organic	Inorganic	Oxidizing Inorganic
Citric (3.1)	Hydrochloric (-7.0)	Perchloric (-10)
Malic (3.4)	Phosphoric (2.1)	Hydrobromic (-9.0)
Formic (3.8)	Hydrofluoric (3.5)	Nitric (-2.0)
Benzoic (4.2)	Boric (9.1)	Sulfuric (-2.0)
Acetic (4.8)		Chromic (0.5)
Propionic (4.9)		Arsenic (2.19)

Acid concentration can also alter the properties of an acid. For example, sulfuric acid can chemically dehydrate vinyl ester, and char the surface, at concentrations above 76 wt%, while chromic acid is only non-oxidizing in very dilute concentrations [13]. The interaction of an acid with any given coating depends on the chemistry of both components. The limitations of organic coatings, with regard to acids, has more to do with the acids ability to react with, and rapidly diffuse through, the coating than it has to do with pH values [40].
To summarize, the use of organic coatings in industrial processes is limited to low temperatures, < 150 °C for most coatings, though some can range up to 260 °C, and mild abrasive environments. However, they can have exceptional resistance to acidic chemicals. Pressure limitation is not an area of much study. If an industrial process operates within these limits, organic coatings are an option, either to protect a vulnerable substrate, or to use with fiber re-enforcement as construction material.

2 Acid resistant materials

The need for protective measures against acid attack is a requirement for any industrial process using or producing such chemicals. Not only to create a safe environment, but also to allow a continuous production, without significant operational downtime due to damaged equipment. Choosing the correct material or surface treatment for unit operations in an aggressive environment is therefore vital.
The protective materials can be divided into two categories, *the inorganic*, using ceramics or metallic based protective measures, and *the organic*, including FRP and organic coatings. Though organic thermoset coatings are the main focus in this paper, it is important to know of the alternatives. This section will give an overview of the chemical composition and use of metallic, ceramic and organic acid resistant systems.

2.1 Inorganic

Ceramic and metallic materials have also been developed to resist a wide range of acids. The advantages of utilizing these materials to prevent acid damage is a good abrasion and temperature resistance, properties that organic coatings cannot provide with the same reliability. Inorganic materials can also be applied as thin protective coatings or undergo surface treatment to enhance acid-resistance. These techniques include electroplating, physical or chemical vapor deposition, thermal spraying, and thermochemical diffusion processes, but are too extensive to be covered in this project [35, 41].
Metals are often prone to damage when in contact with acidic material, but it is possible to make alloys capable of resisting a large range of acids with varying concentrations. Small equipment components, as well as large constructions, such as pipes and vessels, can be made of steel alloys [42]. These resistant alloys have the advantage of being very wear resistant, both to sliding and impact abrasion, though material and manufacture can be costly as the alloys are typically very expensive compared to low grade steels with high iron content, see Table 2.1 [43]. Metals are not inert in an acidic environment, but corrosion rates are often halted by the formation of passivating films on the metal surface. A list of acid resilient stainless steels and their compositions is also shown in Table 2.1, while Table 2.2 gives corrosion rates of these alloys immersed in sulfuric and hydrochloric acid solutions [44].
Metal alloys can be used at high temperatures and are resistant to erosion. However, with added contact to acidic substances, increasing temperatures will increase corrosion rates. Wear can also

enhance corrosion rates, by inducing corrosive wear, a continuous removal of the passivating film [35]. Care must be taken if metals are to be used in acidic environments.

Table 2.1: An overview of metal costs in August 2015 as well as alloys and their general composition in wt.% [44–46].

Element	Fe	C	Cr	Ni	Mo	N	Minor components
(Metal cost [€/kg])	(0.049)	-	(1.87)	(9.13)	(9.41)	-	-
Austenitic (S31600)	65	0.03	17	12.0	2.5	-	Si, Mn, P, S
Superaustenitic (N08020)	42.0	0.02	19.5	33.0	2.2	-	Cu
Duplex (S32550)	61.1	0.04	26.0	5.0	3.0	0.25	Si, Cu, Ti, Mn, P, S
Superferritic (S44660)	68.0	0.02	26.0	2.5	3.0	0.03	Ti, Cb
Nickel-Based (N06022)	4	0.01	21.0	57.5	13.5	-	Si, Cu, Mn, Al, S, P, W

Table 2.2: An overview of some relevant alloys and their corrosion rates in sulfuric and hydrochloric acids in mm per year. Concentration and temperature are provided in parenthesis [44].

Alloy family	Sulfuric acid	Hydrochloric acid
Austenitic (S31600)	>1.27 mm $year^{-1}$ (10wt%, 15 °C)	>1.27 mm $year^{-1}$ (20wt%, 15 °C)
Superaustenitic (N08020)	>0.51 mm $year^{-1}$ (10wt%, boiling)	>1.27 mm $year^{-1}$ (20wt%, 15 °C)
Duplex (S32550)	1.02 mm $year^{-1}$ (10wt%, boiling)	0.003 mm $year^{-1}$ (1wt%, boiling)
Superferritic (S44660)	>0.51 mm $year^{-1}$ (10wt%, boiling)	-
Nickel-Based (N06022)	0.28 mm $year^{-1}$ (10wt%, boiling)	0.06 mm $year^{-1}$ (1wt%, boiling)

Ceramic bricks and coatings have found their uses as protective linings, also called refractories, in storage tanks, reaction vessels, fume ducts, and many unit operations in the chemical industry. They are often used for high acid concentrations and high temperature applications [47, 48]. Ceramics are prime candidates for anti-corrosive linings, the materials tend to be crystalline in nature and have a high melting point and chemical resistance, combined with a high resistance towards erosive wear [49, 50]. Ceramic protection also utilizes organic material, such as furan or vinyl esters for mortar adhesives, or organic membranes behind the lining to prevent leaks caused by cracks in the brittle material, an example is shown in Fig. 2.1. Table 2.3 gives the composition of some acid resistant ceramic materials used in industry [51].

Table 2.3: An overview of acid resistant ceramics and their compositions in wt% [51, 52].

Ceramic type	SiO_2	Al_2O_3	Fe_2O_3	K_2O	TiO_2	Carbon	SiC	Other
Red Shale	64.0	20.6	6.2	4.2	1.6	NA	NA	MgO, Na_2O, CaO
Fire Clay	64.0	27.3	2.0	2.6	1.5	NA	NA	MgO, Na_2O, CaO
SiC	9.6	0.8	0.4	0.0	0.1	NA	87.9	MgO, Na_2O, CaO
Silica	98.4	0.8	0.4	0.0	0.1	NA	NA	MgO, Na_2O, CaO
Carbon	0.3	0.1	0.0	0.0	0.0	96.3	NA	MgO, Na_2O, CaO, S
High Alumina	8.5	85.6	0.3	0.1	0.1	NA	NA	MgO, Na_2O, CaO

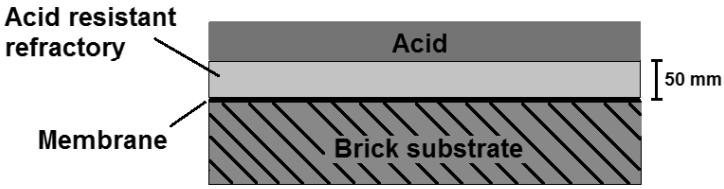

Figure 2.1: Build-up of a protective ceramic coating usable at high temperatures and in concentrated acid exposure from the refractory side. Typically around 50 mm thick coating. Figure modified after [48].

Ceramic linings are capable of resisting very high temperatures, abrasive wear and a wide range of acidic substances, while having lifetimes greater than 12 years [48]. So why would a metal alloy based protective system be preferable? The main reason is the cost. Metallic protective measures are considered higher risk than ceramic systems, they come at a lower total cost of installation. This consideration is important, as we discuss the uses of organic coatings as protective measures. Organic coatings are considered higher risk than the use of metal alloys, but can come at a an even lower cost [8, 42, 53].

2.2 Organic

Organic coatings can be categorized into two major groups, thermoplastic and thermoset. In short, thermoplastics are physically cured, while thermosets are chemically cured via cross-linking reactions. The resin network of hardened thermosets or thermoplastics form the protective organic coating [37]. In between these groups are elastomers, or rubbers, which are cross-linked only to a small degree, see Fig. 2.2 for comparison [54]. This section will give a short overview of the various organic resins that can be utilized in acidic environments to protect a vulnerable substrate.
The terms coating and lining are used for organic protective systems, but their meaning often overlap. The term coating is defined by ASTM as: "A liquid, liquefiable, or mastic composition that is converted by evaporation, cross-linking, or cooling to a solid or semisolid protective, decorative, or functional adherent layer after application" [55]. It often suggests a thin, up to 1 mm thick film on a substrate. Coatings are commonly thermosets as they are easily applied in thin layers, while linings are often a reference to thick, greater than 1 mm films, or coating systems reinforced with glass mats or likewise. Thermoplastic material that is attached to a surface via physical means or with the aid of an adhesive layer often goes by the term lining, and so do multi-layered coating systems and protective coatings on inner surfaces. The ASTM definition of lining is: "Coating or layer of sheet material adhered to or in intimate contact with the interior surface of a container used to protect the container against corrosion by its contents and/or to protect the contents of the container from contamination by the container material." [56]. In this paper, the term coating encompasses linings as well.

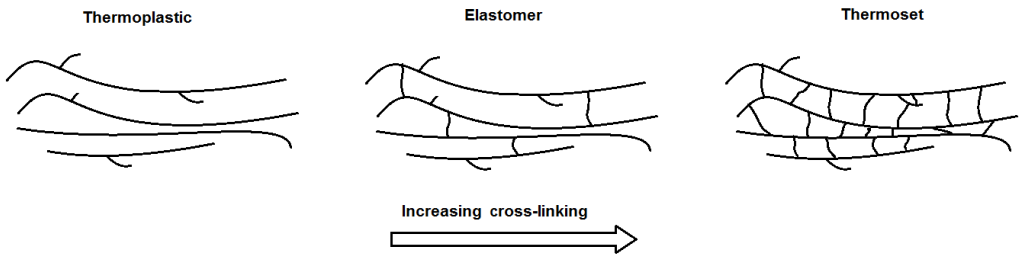

Figure 2.2: Comparison of polymer chain structure of thermoplastics, elastomers, and thermosets. Cross-linking density increases from left to right. For thermoset coatings, a 3D network is formed. Deduced from [37, 54].

2.2.1 Thermoset coatings

Thermoset coatings can be formulated in many varieties based on composition. From a formulation perspective there are many factors affecting the overall performance of a single coating or a coating system. Typically, thermosets are composed of binder, hardener, pigments/fillers, solvents and additives [37].

- Resins (binders) are polymers or network precursors which can cross-link with a curing agent to form the hardened coating film. The chemical structure of hardened polyurethane, amine and anhydride-cured epoxy, and vinyl ester resins are shown in Figs. 2.3 to 2.6.
- Solvents are organic molecules added to dissolve the binder and/or alter the liquid coating viscosity to facilitate application.
- Additives are added in small amounts to control specific properties of the coating.
- Pigments and fillers are small, binder and solvent insoluble, particles.

The acid-resistance of a thermoset coating is a function of all the components as well as curing conditions, substrate pre-treatment, and application method. The most relevant thermoset resins in use for acid-resistance include phenolic epoxy, vinyl ester, and polyurethane [24]. The cross-linked structure and some general notes on these resins are given below. Particular attention should be paid to the various chemical bonds in the cured resins, which make up the backbone of the polymer matrix and play and important role in a coating's acid-resistance.
Polyurethanes are cured by reaction of an isocyanate with a polyol, forming a network with urethane linkages, see Fig. 2.3. The polyol contains alchohol end groups and could be a polyester, polyether, or polycarbonate. Polyurethanes have excellent impact and abrasion resistance but reduced acid-resistance in comparison to epoxy, and vinyl esters [37]. They are often used in combination with epoxies on secondary exposure (spillage) areas [57].

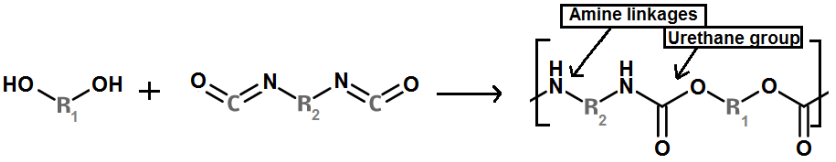

Figure 2.3: Formation of the repeating unit of a polyurethane coating. Chemical groups and linkages that could be involved in chemical degradation are highlighted [58].

Phenolic epoxies are based on resins containing epoxide (oxirane) groups and are known to be tough, non-brittle coatings. The choice of hardener is important for the acid-resistance of the cured resin. If the right hardener is chosen, epoxies can be used in acid service, but they are not recommended for oxidizing acids [14]. Amine and anhydride-cured epoxies, shown in Fig. 2.4 and 2.5 respectively, can be used for acid service. Anhydride-cured epoxies are known to be more acid resistant, but due to slow curing and a need to postcure, the more practical amine-cured epoxies are more common as protective coatings [59].

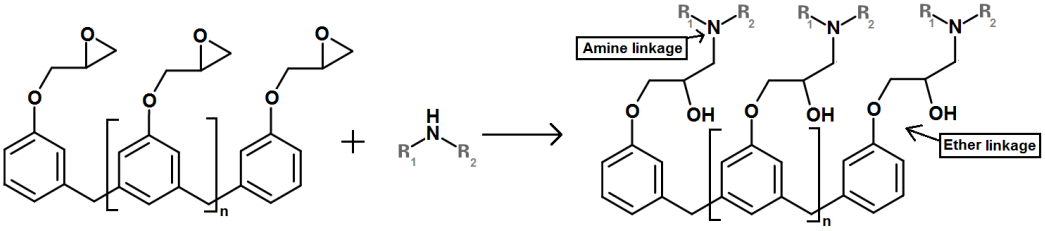

Figure 2.4: The chemical curing and composition of amine-cured novolac epoxy. R groups can contain amines capable of cross-binding with more epoxy and n ≈ 0.2. Chemical groups and linkages that could be involved in chemical degradation are highlighted [59].

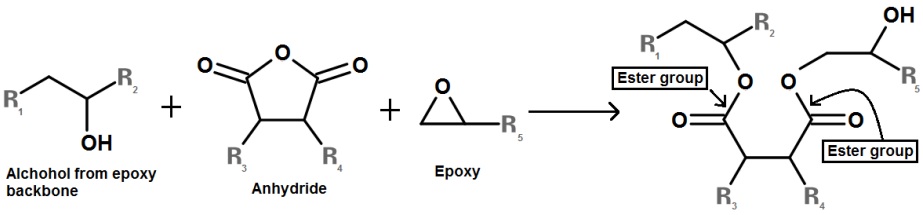

Figure 2.5: The chemical curing and composition of an anhydride-cured epoxy. R_3 and R_4 will vary depending on the anhydride type, they can e.g. combine to make a benzene ring for phthalic anhydride. Not shown in this image is the epoxy backbone, which contains ether linkages [59].

Vinyl esters have high resistance towards both oxidizing and non-oxidizing acids [14, 60]. They can form highly cross-linked networks by radical initiated reactions with monomers such as styrene. Fig. 2.6 shows a typical vinyl ester cross-linked with styrene. Vinyl esters have a good overall resistance to chemical exposure, due to ester-stabilizing methyl groups and the many aromatic groups in the

resin. This, together with a sufficient degree of flexibility makes, the resin useful in many applications. Furthermore, they have been widely used together with fiber reinforcement to improved mechanical properties [13, 27, 61].

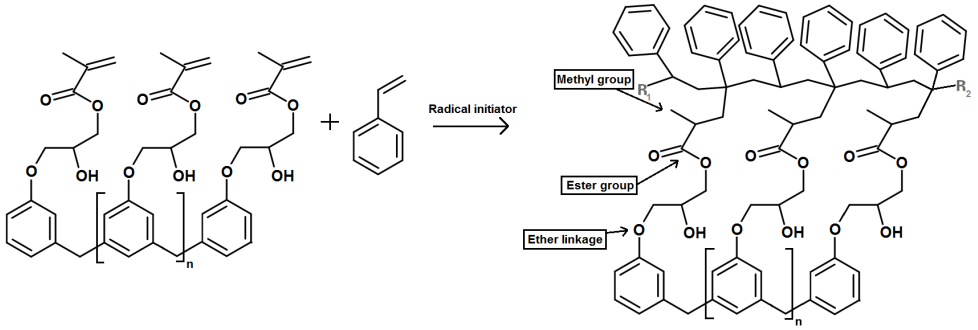

Figure 2.6: Vinyl ester cross-linked with styrene, using a radical initiator such as a peroxide. The vinyl ester shown is based on novolac epoxy reacted with methacrylic acid. R indicates a continuous chain, linking more components to form the resin network, n ≈ 0.2. Chemical groups and linkages that could be involved in chemical degradation are highlighted [59].

Acid resistant coatings based on polyurethane, epoxy or vinyl ester can be found with many small variations, depending on the particular environment they have to resist, leading to numerous brands as shown in Tables 2.4 and 2.5. The list is not exhaustive and does not include resin products, which can be supplied from companies like AOC, Ashland, DSM, Interplastic and Reichhold. It should be noted that sufficient caution and protective measures must be taken during the handling processes of these chemicals. Compounds like styrene, but also epoxy and isocyanates, can be harmful upon skin contact ingestion or inhalation. Details of health issues and correct handling can often be found in the safety data sheet of the selected product.

Table 2.4: Selection of commercial organic coating products with advertised usability in corrosive environments, often categorized under industrial and/or protective coatings. Vinyl esters are typically hardened using styrene and a radical initiator. See the companies' specific product data sheet for further details.

Resin	Company	Product Name	Application areas/environment
Vinyl ester	**Carboline** (carboline.com)	Plasite^{TM}	Highly aggressive environments
		Semstone^{TM}	Aggressive chemicals
	Corrocoat (corrocoat.com)	Corroglass^{TM}	Heavy duty equipment
	Hempel (hempel.com)	Hempaline^{TM}	High temperatures and acidic conditions
	International (international-pc.com)	Ceilcote^{TM}	High-performance corrosion control
	Jotun (jotun.com)	Chemflake^{TM}	Chemical tanks, cooling towers, pipes, water tanks
	Sauereisen (sauereisen.com)	NovolaK Vinyl Ester FibreLine^{TM}	Pulp and paper, superior chemical resistance
	Sherwin-Williams (protective.sherwin-williams.com)	Cor-Cote VEN^{TM}	FGD Systems, Chemical processing, Food and beverage, Metal and mining, Pharmaceutical, Pulp and paper, Water and wastewater, Petrochemical

Table 2.5: Selection of commercial organic coating products with advertised usability in corrosive environments, often categorized under industrial and/or protective coatings. Epoxies are typically amine-cured. See the companies' specific product data sheet for further details.

Resin	Company	Product Name	Application areas/environment
Epoxy	**Belzona** (belzona.com)	Belzona 5811™	Excellent resistance to sulfuric and hydrochloric acid
	Carboline	Phenoline™	Chemically resistant coatings
	Corrocoat	Corrocoat™	Resistant to high concentrations of sulfuric acid
	Hempel	Hempaline™	Tank lining with excellent chemical resistance
	International	Enviroline™	Chemical attack, corrosion and leaks
	PPG (ppgpmc.com)	Phenguard™	Aggressive cargo such as methanol, ethylene dichloride and fatty acids
	Sauereisen	FibreCrete™	For processing and storage. Resists strong sulfuric acids
Polyurethane	**International**	Polibrid™	Corrosion protection for immersion, chemical, abrasion and impact resistant applications
	Sauereisen	ConoFlex Urethane™	Both primary and secondary containment. Highly impermeable, chemically resistant towards a wide range of acids

2.2.2 Thermoplastics

As protective coatings, thermoplastics can be applied as solid plastic sheets with an adhesive layer in between the substrate and plastic, or adhered via mechanical means. In liquid form, thermoplastics can be applied as a melt or dissolved in a solvent, where-after the plastic cools or solvent evaporates, resulting in a hardened coating [37]. When not protecting a substrate, thermoplastics are used as construction material such as containers or components for acid service.
Among many thermoplastics, capable of acid service, the cheap polypropylene (PP) or PE and the more expensive fluoropolymers are common examples [62]. Repeating polymer units of these thermoplastics are shown in Fig. 2.7.

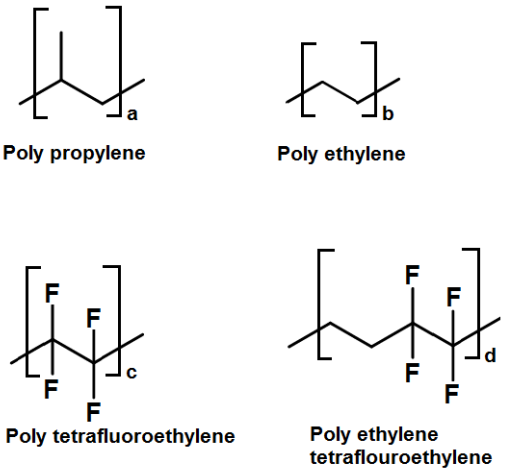

Figure 2.7: Repeating units of some thermoplastic polymers capable of acid immersion service. The common number of the repeating units are: a) 100 to 2400, b) 650 to 1580, c) 10^4 to 10^6, d) 3130 to 6140 [63–65].

PP is made of a pure hydrocarbon backbone and has a high resistance towards inorganic as well as organic acids. It is also one of the cheapest thermoplastics available. It is, however, noted to oxidize slowly in highly oxidizing acids, such as nitric acid [62].
Fluoropolymers such as PTFE and polyethylene tetraflouroethylene (ETFE), have higher resistance towards acids and various solvents than any of the other thermoplastics mentioned. Most of these resins are unaffected by common organic solvents as well as hot concentrated oxidizing and non-oxidizing acids [31]. Flouropolymers are, however, challenging and costly to apply to surfaces, because the polymer resin often has to be applied as multiple thin (40 μm) films and baked above it's melting point, 327 °C for PTFE [65, 66].

2.2.3 Elastomers

Elastomers, also known as rubbers, are special kinds of plastics with unique physical properties. A rubber is able to deform when force is applied and reclaim the original shape when relaxed. This prop-

erty gives rubbers a high resistance towards impacts, such as a hammer strike or particle impingement [35].

To form a rubber, a pre-polymer has to be partially cross-linked through curing or vulcanization reactions. The network formed is closely packed, and can have around 1 to 2 cross-links per 200 repeating polymer units, much less than for typical thermosets. The elastic properties of the rubber is a result of this low cross-linking density, while the close packing yields low permeability [67].

A rubber that has found use as protective lining in acid service is halogenated butyl rubber (HIIR). The rubber material is made by reacting isobutylene and isoprene into a high density polymer, followed by a halogenation of the polymer, shown as the reactant in Fig. 2.8. It is then cured to produce the final product. HIIR such as chlorobutyl and bromobutyl rubber have good resistance towards inorganic acids and so does polychloroprene. For a more comprehensive view on rubbers for corrosion protection, see the book by Chandrasekaran [67] and the chapter by Webb et al. [68].

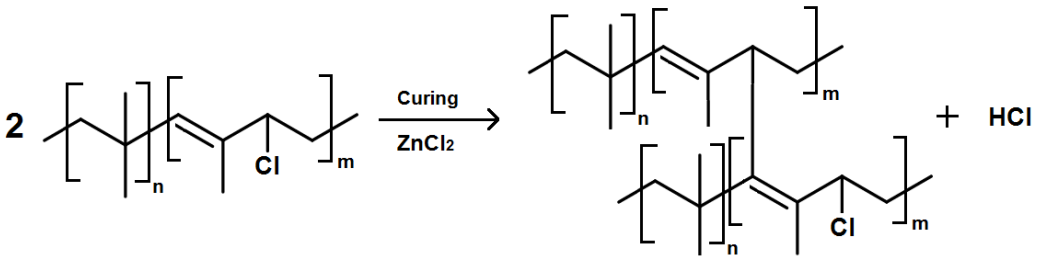

Figure 2.8: Curing of chlorobutyl rubber using zinc chloride catalyst [69]. The ratio n/m is around 200 to produce a low cross-linking density [54]. Typical rubber coating thickness is 6 mm.

2.2.4 FRP thermoset systems

Glass fiber reinforcement for thermoset resins can be either flake filled resin, fiber mat or woven fabric reinforced as shown in Fig. 2.9. Glass fiber reinforcement of thermosets functions similar to steel reinforcement of concrete, by improving a number of mechanical properties of the material such as higher abrasion resistance, enhanced mechanical strength, and better elongation properties. Additionally, flake filled thermosets increase permeation resistance, while fiber mat and woven fabric reinforcement lower the thermal expansion coefficient of the coating close to that of steel, preventing stress cracking and damage from thermal shock [6, 10].

It is possible to use FRP as construction material to prepare pipes and vessels from a desired polymeric material instead of coating existing equipment [53], Fig. 2.10 shows FRP cross-sections, and Fig. 2.11 shows an example of a tank made out of FRP.

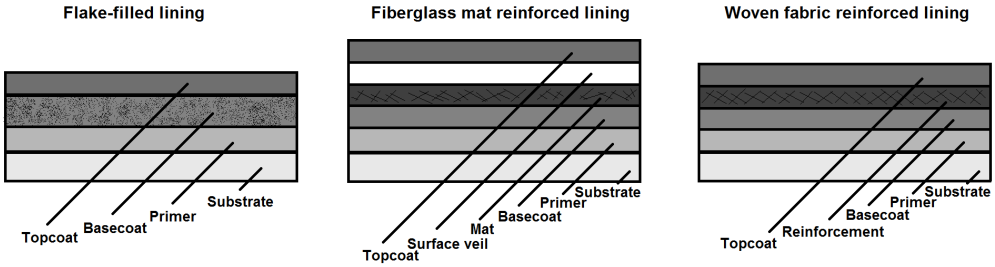

Figure 2.9: Flake filled, fiber mat and woven FRP linings on a substrate, typical lining thickness is 2, 4 and 3 mm from left to right [6].

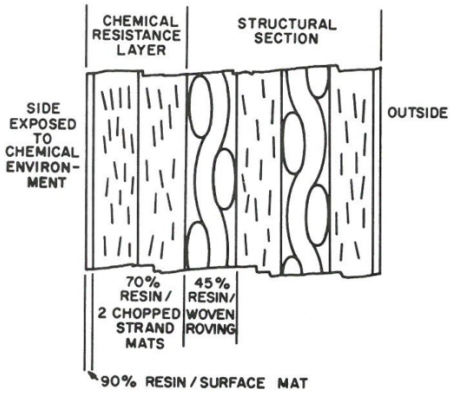

Figure 2.10: Cross-sectional build of a FRP structure without substrate support. The resin is present in the woven glass mat, and in greater quantities, combined with glass flakes, in layers closer to the exposed side to provide a chemical barrier. Reproduced from [53] with permission from NACE International, Houston, TX. All rights reserved. ©NACE International 2016.

Figure 2.11: Example of a FRP tank made of Derakane vinyl ester [70]. Courtesy of Ashland Inc. and Owens Corning

3 Degradation mechanisms

Acid and chemical resistance of organic coatings depend on two categories of degradation, physical and chemical [61, 71, 72]. Physical degradation entails the unavoidable diffusion of chemicals into and through a protective coating. Reactions of coating constituents with the environment are categorized as chemical degradation.
Physical and chemical degradation occur either separately or simultaneously, with a physical diffusion followed by chemical interactions. This section includes the current theories for both degradation mechanisms, with a more detailed look at important thermoset resins. Mechanical degradation by erosive wear is a third failure mechanisms, and can occur whenever coatings come into contact with solid surfaces. These three mechanisms are the causes of barrier coating failure if one disregards failure due to de-bonding caused by poor surface pre-treatment and thermal shock.

3.1 Physical degradation by diffusion

The diffusion of substances into organic coatings cannot be completely prevented, and coatings made to separate an aggressive solution from a given substrate, can fail due to this fact. The diffusion process enables contact between the coating and the diffusing species, and eventually the underlying substrate. This can cause film swelling, cracking and a loss of mechanical properties [6, 7, 11, 37, 61, 71–78], but it also allows chemical degradation to take place inside the coating.
The movement of molecules through a coating film is dependent on the presence of free volume and cohesive forces in the resin matrix, and the frequency and distance with which penetrant molecules can "jump" from one void to another [79]. Penetrating molecules can exist in an unbound state in free volume or in a bound state, where cohesive forces attach the penetrant to the coating network [80]. It is also important to note that for a dissociated acid, the proton and anion likely move simultaneously to maintain charge neutrality [53].
Diffusion rates of molecules through a coating film depend on exposure conditions and choice of coating system [61]. Important parameters for the coating are cross-linking density, crystallinity, pigments, and T_g, while for the penetrating molecule, molecular size, and chemical similarity can have large effects on diffusion [81].
Diffusion coefficients are challenging to generalize, with recorded values for acid resistant resins ranging from 10^{-11} to 10^{-16} m^2/s. Reducing the diffusion rate will prolong the time a coating is able to hinder contact between the aggressive substance and substrate, which, in turn, increases the coating's effective lifetime [82].

3.1.1 Cross-linking density and crystallinity

Increasing the cross-linking density of a thermoset resin typically leads to an increased solvent resistance, chemical resistance, and T_g, with reduced permeation speeds [6, 11, 13, 25, 27, 74, 83, 84]. The cross-linking density is defined as the number of moles of elastically effective network chains per sample volume or weight. Network chains are elastically effective when all ends are attached to the network [85]. Increasing cross-linking density reduces the segmental mobility of a resin network [29, 37] and decreases the free volume. This affects the above mentioned resistances, by limiting the diffusion rate

of molecules through the coating. However, a higher degree of cross-linking will also make a coating more rigid and brittle, a property that can cause major issues in industrial applications.

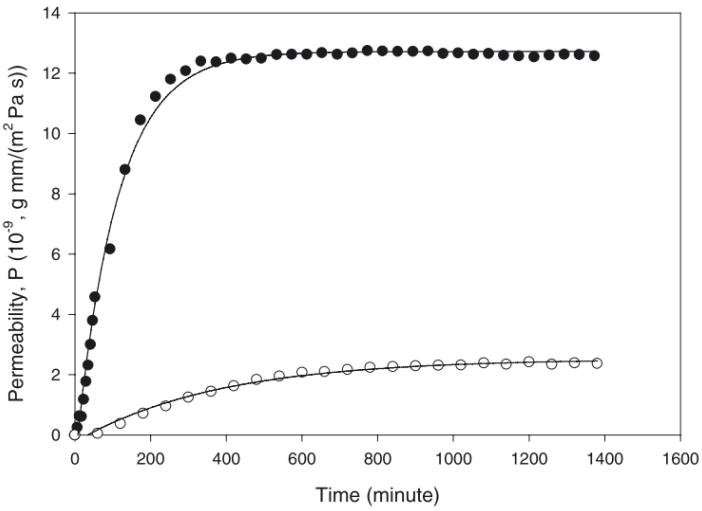

Figure 3.1: Permeation rates of water vapor through a liquid-crystalline (○) and non-crystalline (●) amine-cured epoxy at 37.8 °C. The solid lines are fits to the data points assuming Fickian diffusion. Reprinted from [86] with permission of Springer.

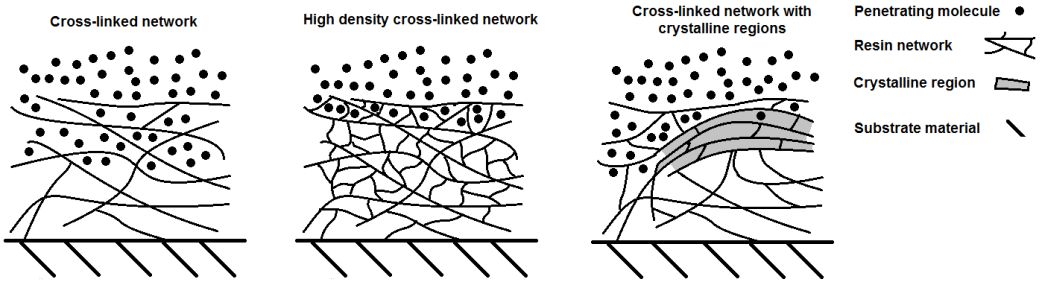

Figure 3.2: Increased rigidity and reduced free volume limits the diffusion rate of molecules through a coating film. Drawings based on [83, 86].

Similar reductions in diffusion rates can be obtained by having crystalline regions in a resin network, because crystalline structures have a closer chain packing than purely amorphous types [58]. Liquid crystal plastics (LCP) and liquid crystal thermosets (LCT) form crystalline domains in a melt or solution [87], and are made by including rod or disk like groups in the polymer backbone [88, 89]. As an example, Fig. 3.1 shows the permeability of water through an LCT amine-cured epoxy, which was found to be much lower than the amorphous counterpart [86]. The effects of cross-link density and crystallinity on diffusion rates are visualized in Fig. 3.2.

3.1.2 Cohesive and chemical factors

The type of chemical(s) a coating is exposed to can effect the coating's diffusion properties without breaking intra-molecular bonds in the resin. Cohesive interactions between the diffusing molecules and coating resin can account for this occurrence.

Molecules can diffuse through a coating using the free volume available, but they can also interact with the resin network via cohesive forces such as hydrogen bonding. A diffusing molecule can attach to a resin chain by cohesive forces and disrupt existing interchain bonds in the resin according to Vanlandingham [80]. This bonding can cause the network to expand in size, observed as swelling of the coating, and reduce the rigidity of the network, causing plasticization.

Plasticization has been connected to increases in internal stress and causes of cracks formation in a coating [86]. Swelling and plasticization effects can be caused by any diffusing molecules be they solvents, or non-solvents like water in amine-cured epoxy. Other side effects of plasticization include decreases in coating's T_g and increased diffusion rates [30, 90]. These enhanced diffusion rates do not only apply for the molecules that cause plasticization, other molecules such as acids can be carried more rapidly into a coating film, thereby facilitating diffusion of secondary chemicals [14].

However, cohesive forces such as hydrogen bonding between coating and the diffusing molecule do not always increase diffusion rates. If the disruption to the resin network is minimal, these interactions can actually decrease diffusion rates by holding on to the diffusing molecule and decreasing the frequency at which the penetrant can jump from one free volume to another. A known case is, once again, water into amine-cured epoxy resins, where the amine and hydroxyl groups in the resin are able to hydrogen bond with the water [86].

Cohesive forces are particularly strong for solvent molecules. A chemical works as a solvent if it has a solubility parameter close to or the same as the coating. The Hilderand solubility parameter is defined as the energy required to vaporize a unit volume of liquid against the intermolecular forces between the molecules [91], and can be divided into the three previously mentioned cohesive forces, also called Hansens solubility parameters, hydrogen bonding, dipole-dipole and dispersion [92]. A solvent can cause greater swelling and plasticization in a thermoset than non-solvents, since the cohesive forces are similar to that of the coating. Solvent-like acids of particular trouble, are the smaller organic acids such as acetic ($C_2H_4O_2$), formic and propionic acid ($C_3H_6O_2$) [14], as shown by Kalenda [39], see Figs. 3.3 and 3.6B.

It is possible to determine which chemicals are particularly troublesome for a given coating using solubility parameters [61, 91]. Based on the parameters of various chemicals, and their effect on either physical attributes, such as flexural strength or degree of swelling, it is possible to map a solubility range for a given coating material. A rule of thumb states, that the closer a chemical's solubility parameter is to the material in question, the higher the degree of swelling and the loss of flexural strength [93]. Figs. 3.4 and 3.5 show the relationship between the solubility parameter and swelling and flexural strength retention, respectively. A high swelling ratio or large drops in flexural strength indicate severe solvation is occurring.

If there is a high degree of rigidity in a coating network, the diffusion can be described as Fickian [39, 94–96]. Deviations from this behavior, also called non-Fickian diffusion, can be associated to relaxation of the network chains caused by the diffusing media [86, 97] and is seen often when the coating experiences extensive swelling [98], that is when cohesive factors are strong. According to

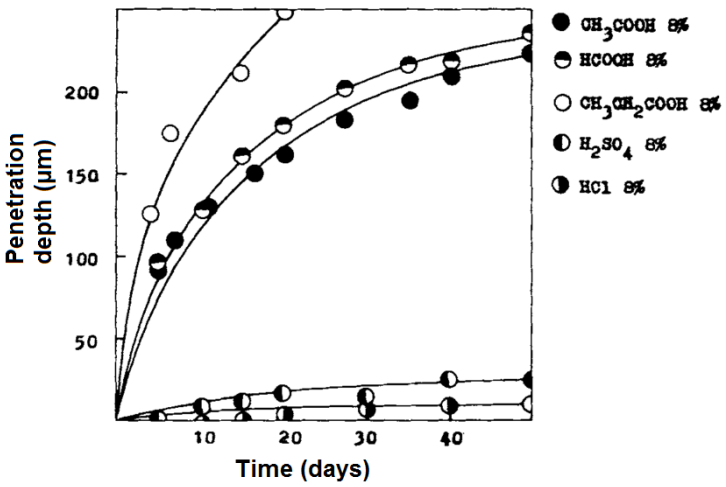

Figure 3.3: The penetration depth vs. time, of 8 wt% acidic solutions into an amine-cured epoxy resin at ambient temperature. The organic acids diffuse rapidly compared to the mineral acids. Reprinted from [39] by permission of John Wiley and Sons ©.

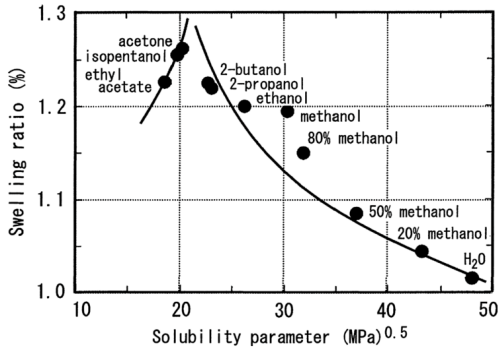

Figure 3.4: Changes in swelling ratio of a hardened polyester resin vs. solubility parameter of various solutions. Reprinted from [71] by permission of the Japan Petroleum Institute.

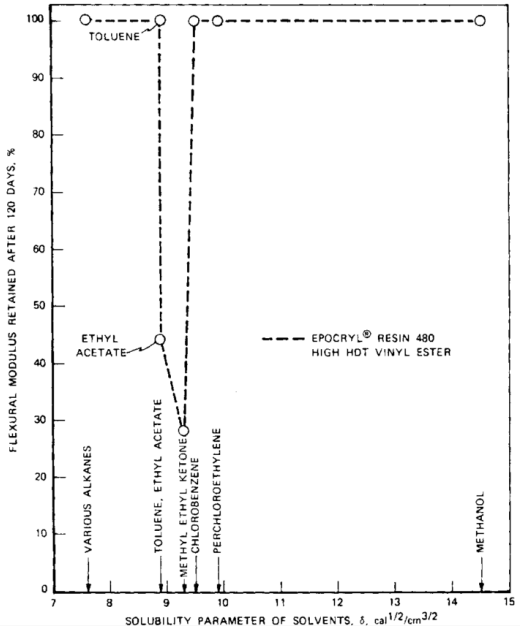

Figure 3.5: Changes in flexural modulus of a vinyl ester in various solutions. Reprinted from [61] by permission of John Wiley and Sons ©.

a FRP material guide from Reichhold A/S [13], solvent penetration following Fickian diffusion, will eventually diffuse all the way through a coating and lead to failure, while for situations when non-Fickian diffusion is valid, an asymptote can be reached after a certain diffusing depth, limiting further penetration. Whether this phenomenon is valid for acidic environments is not stated.
Finally, acid concentration can also play a role in enhancing or even decreasing diffusion coefficients. Kalenda [99] noted that at increasing concentrations, the diffusion coefficient of acetic acid through amine-cured epoxy also increased. While in the same experiment, for sulfuric acid, a peak was reached at around 20-25 wt% acid, any reduction or increase in acid concentration caused a drop in diffusion coefficient value. No explanation was given for these trends, but it indicates that the diffusion coefficients were concentration-dependent.

3.1.3 Fillers and pigments

Fillers and pigments can be used to reduce diffusion rates of unwanted species through a coating, but one has to be careful and ensure the fillers themselves do not have antagonistic interactions with the diffusing medium and accelerate coating failure [100]. Pigments can play many protective roles in a coating system and using barrier pigments is common for reducing molecular and ionic diffusion. Adding pigments, that are inert to the diffusing solution, into a coating will create a physical barrier to diffusion and force the penetrant to take a longer, tortuous, path through the film [101, 102]. This increases the effective lifetime of a coating by delaying contact with the substrate. But pigments can also have the opposite effect, allowing rapid diffusion along the filler-binder interface, and reducing the coating lifetime [103].
Optimizing the shape, orientation, and concentration of pigments will enhance their positive functionality. Pigment volume concentrations (PVC) should be close, to but not above, the critical PVC value (CPVC) [37], and lamellar pigments oriented parallel to the surface, will provide a strong barrier to diffusion [102]. Fig. 3.6A shows the diffusion path of unwanted species through a coating, comparing the effect of spherical and lamellar shaped pigments on the length of this path, while Fig. 3.6B shows this effect with experimental data.
Forming a physical barrier is not the only way to reduce permeation by use of pigments. Reactive pigments have been investigated as an alternative or addition to the typical inert flake fillers. Reactive pigments work by partly reacting with, thus removing, and blocking the permeating substance [96, 104]. A combination of reactive and inert pigments is claimed to reduce the diffusion of aggressive species through a coating to a greater degree, than if used individually [101].
To summarize, physical degradation does not involve bond breaking or formation, but entails the effects caused by the diffusion of molecules into a coating film. Diffusion can be limited by increasing cross-linking density and crystallinity, using barrier pigments and avoiding contact with solvent molecules. The adverse effects on physical properties, caused by molecular diffusion, can be recovered, if the penetrants are removed, as long as no chemical reactions have taken place in the coating [105].

A)

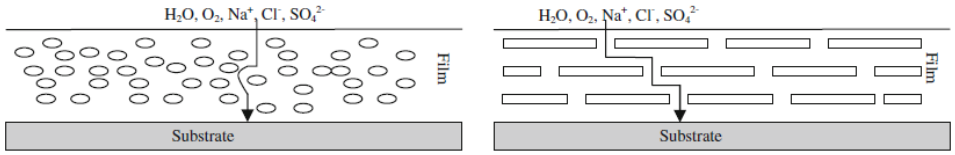

B)

Medium	*Diffusion coefficient, $D \times 10^{10}$ ($mm^2\ s^{-1}$)*								
	0%	*Spherical particles*				*Chip-shaped particles*			
		3%	*6%*	*9%*	*12%*	*3%*	*6%*	*9%*	*12%*
H_2SO_4	183	179	169	144	103	189	115	91	42
HCl	141	135	159	189	175	62	45	34	17
HCOOH	1692	1528	1694	1652	1667	894	651	594	398
CH_3COOH	510	568	552	574	690	495	418	372	302
CH_3CH_2COOH	2816	3352	3271	2890	2931	2274	2007	1850	1528

Figure 3.6: **A:** Idealized migration of species through a coating with spherical and lamellar barrier pigments. The lamellar pigments provide the longest most tortuous diffusion path of the two. Reprinted from [106] by permission of Springer. **B:** Diffusion coefficients of 8 wt% acidic solutions through amine-cured epoxy coating with varying particle concentration [wt%] and shape. No temperature was provided in the reference. Reprinted from [104] by permission of Elsevier.

3.1.4 Mathematics of diffusion coefficients

Diffusion coefficients can be obtained experimentally by methods such as: measuring weight gain of immersed coatings, observing the diffusion front of a penetrant, or monitoring penetrant flux using diffusion cells.

The common for the data treatment of the different methods is the use of Ficks first and second laws of diffusion, presented in Eqns. 1 and 2 respectively, assuming slap geometry and diffusion in only in the l direction.

$$F = -D\frac{\partial C}{\partial l} \text{ Ficks } 1^{st} \text{ law} \tag{1}$$

$$\frac{\partial C}{\partial t} = \frac{\partial}{\partial l}\left(D\frac{\partial C}{\partial l}\right) \text{ Ficks } 2^{nd} \text{ law} \tag{2}$$

The diffusion coefficient is an elusive value, because it is often a function of multiple variables, such as penetrant concentration, environmental temperature, and/or time:

$$D = f(C, T, t) \tag{3}$$

Nevertheless, most analytic solutions to Ficks law assume constant diffusion coefficients, to provide a neater, more approachable solution. The following is a short description of some of these solutions.

One method is the gravimetric method, which is used to determine diffusion coefficients based on weight change, from immersion experiments. Crank [98] derives two simple equations for the determination of an average diffusion coefficient, shown in Eqns. 4 and 5. The two equations are derived from Ficks 2nd law, more detail in Appendix A. $\left(\frac{t}{l^2}\right)_{\frac{1}{2}}$ is the time it takes for the weight gain to reach half the saturation weight, while R is the initial gradient of a weight change slope shown in Fig. 3.7.

$$\overline{D} = \frac{0.049}{\left(\frac{t}{l^2}\right)_{\frac{1}{2}}} \tag{4}$$

$$\overline{D} = \frac{\pi}{16} \cdot R^2 \tag{5}$$

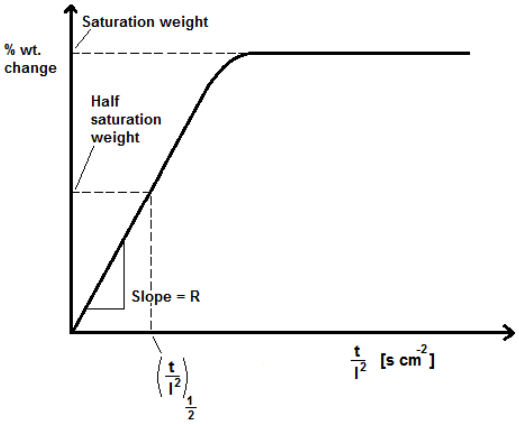

Figure 3.7: Weight change vs time plot for an immersed sample. The values $\left(\frac{t}{l_0^2}\right)_{\frac{1}{2}}$ and R can be inserted in Eqn. 4 or 5.

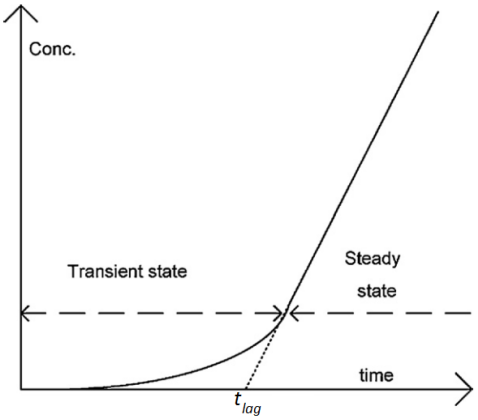

Figure 3.8: Typical concentration vs time data from a diffusion cell, with the time-lag constant, t_{lag} extrapolated from the steady state concentration profile [107].

Another method is to use the time-lag equations. This is useful if the flux of penetrant is monitored in a diffusion cell. A typical plot from such an experiment is shown in Fig. 3.8. The diffusion occurs with an initial transient state, followed by a steady state flux, from which the time-lag can be found by interpolating the steady state curve to intercept with the x-axis. This time-lag can be used in to determine a steady state diffusion coefficient using Eqn. 6. Appendix A provides an overview of the derivation performed by Crank [98].

$$D_{ss} = \frac{l_0^2}{6 \cdot t_{lag}} \tag{6}$$

Finally, the penetration method is useful if one is able to track the moving front of a penetrant through

the coating film as used by Kalenda [39]. Eqn. 7 can be derived by making Eqn. 12 dimensionless and can be used for simple determination of diffusion coefficients.

$$D = \frac{l^2}{t} \tag{7}$$

Eqns. 5, 6, and 7 are all derived on the assumption of uni-directional Fickian diffusion, with constant diffusion coefficients and constant boundary conditions. These idealized equations are useful for rapid comparison of coating barrier properties.

3.2 Chemical degradation

An important property of an acid resistant coating is to remain inert, any reaction with acidic substances or any other additives will damage the coating, causing premature failures, such as cracks in the film, and expose the substrate. Chemical degradation mechanisms are not plentiful in literature but some work can be found for coatings applied in severe acidic environments, and acid rain etching studies in the automotive industry.
The chemical composition and structure of a coating determines it's susceptibility to chemical exposure, and particular chemical bonds, or functional groups, in a resin network can be more or less reactive with the medium in which it is immersed. However, reactivity can be challenging to evaluate, and looking at functional groups and chemical bonds is not sufficient to determine a resins' chemical resistance. The molecular structure of the resin will determine the frequency of reactive sites and the presence of sterical obstructions to reaction. Furthermore, the reaction itself can be either harmless or damaging, and can involve changes in functionality, bond scissoring or bond formation.
This section considers the effects of chemical composition and structure of coating resins on the susceptibility to unwanted chemical reactions with the surrounding medium, and the possible mechanisms of this degradation.

3.2.1 Functional groups

As noted by Hare [14, 40], Allen [61] and Hojo [72], hydrolysis and chemical oxidation are two important reactions that can cause bond breaking in a resin. Acids are commonly found in aqueous solutions, and acid-induced hydrolysis is a reaction with water at low pH [40]. Oxidizing acids, such as nitric acid, are more prone to react with a resin, and can cause greater damage than the stronger but non-oxidizing acids. Bond scission can severely damage a resin, but the same is true for additional bond formation in a cured resin. Additional cross-links can cause increases in internal stress and induce cracks in a coating [71, 108]. Reactions that cause changes in functional groups in a resin, like the conversion of alcohol groups to ketones, have not been noted as an issue, unless it results in bond scissoring.
Functional groups such as esters, amides, ureas, urethanes and acetal are susceptible to acid hydrolysis, even ether, siloxanes and amino groups are said to be vulnerable, but to a lesser extent [40, 72, 109]. Linkages containing non-carbon atoms such as oxygen, nitrogen, and sulfur atoms and their bonds with carbon, are susceptible to hydrolysis reactions; the fewer such weak linkages, the higher the hydrolysis resistance [40].
The reaction rate of coatings undergoing hydrolysis was studied in the automotive industry, with a focus on acrylic-melamine clearcoats in acid rain conditions. By observing changes in absorbance,

using FTIR, for important functional groups, reaction rates can be estimated [110], see Section 4.3 for more details. Such studies of reactivity are, however, rare. Reaction schemes of acid hydrolysis of the above mentioned functional groups and relative reactivities are shown in Fig. 3.9.

Oxidizing acids pose particular problems because the coating has to be resistant to both acidic and oxidizing environments, see Table 1.2 for examples of oxidizing acids. Where research on photo and thermal oxidation of organic coatings is extensive, information on purely chemical oxidation is rather scarce. Hare [40] and Allen [61] note that unsaturated carbon bonds as well as alcohol and aldehyde groups are vulnerable to chemical oxidation. Hojo [72] also mentions chemical oxidation as a typical corrosion reaction of resins, and specifies esters, aliphatics, phenols, and ethers as vulnerable functional groups. Ono [105] observed chain scission of amine linkages in nitric acid.
The ability of an acid to act as an oxidizing agent shows that acid chemistry and not acid strength is of most importance when choosing a protective coating. Fig. 3.10 summarizes the functional groups mentioned to be vulnerable to chemical oxidation along side example reactions.
The chemical structure of a cured film can have significant effects on oxidation resistance and/or hydrolytic susceptibility. An example of this is found in vinyl esters where steric hindrance brought by a methyl group near the ester linkage (see Fig. 2.6) prevents contact between diffusing molecules and the vulnerable ester. The sterical effect also hinders the hydrolysis products from diffusing away from the reaction site, limiting reactions to the surface only [61, 114].
Induced cross-linking can also be detrimental to coating performance [71]. Chemical degradation through the formation of additional cross-links can be monitored by increasing T_g and E-modulus [108, 115], and causes increased brittleness and internal stress in a coating. However, chemical reactions responsible for increased cross-linking have not been mapped.
For an organic coating to be acid resistant, it should have either a slow or no reaction with the dissociated proton in aqueous solution. For a coating to be resistant to a specific acid, the same rule has to apply to the de-protonated anion in conjunction. Thus, the chemistry of a coating as well as the environment are of utmost importance, and if the resin, potential hardener, or their cross-linking sites are susceptible to interaction with the acidic medium, the integrity of the coating could be compromised.

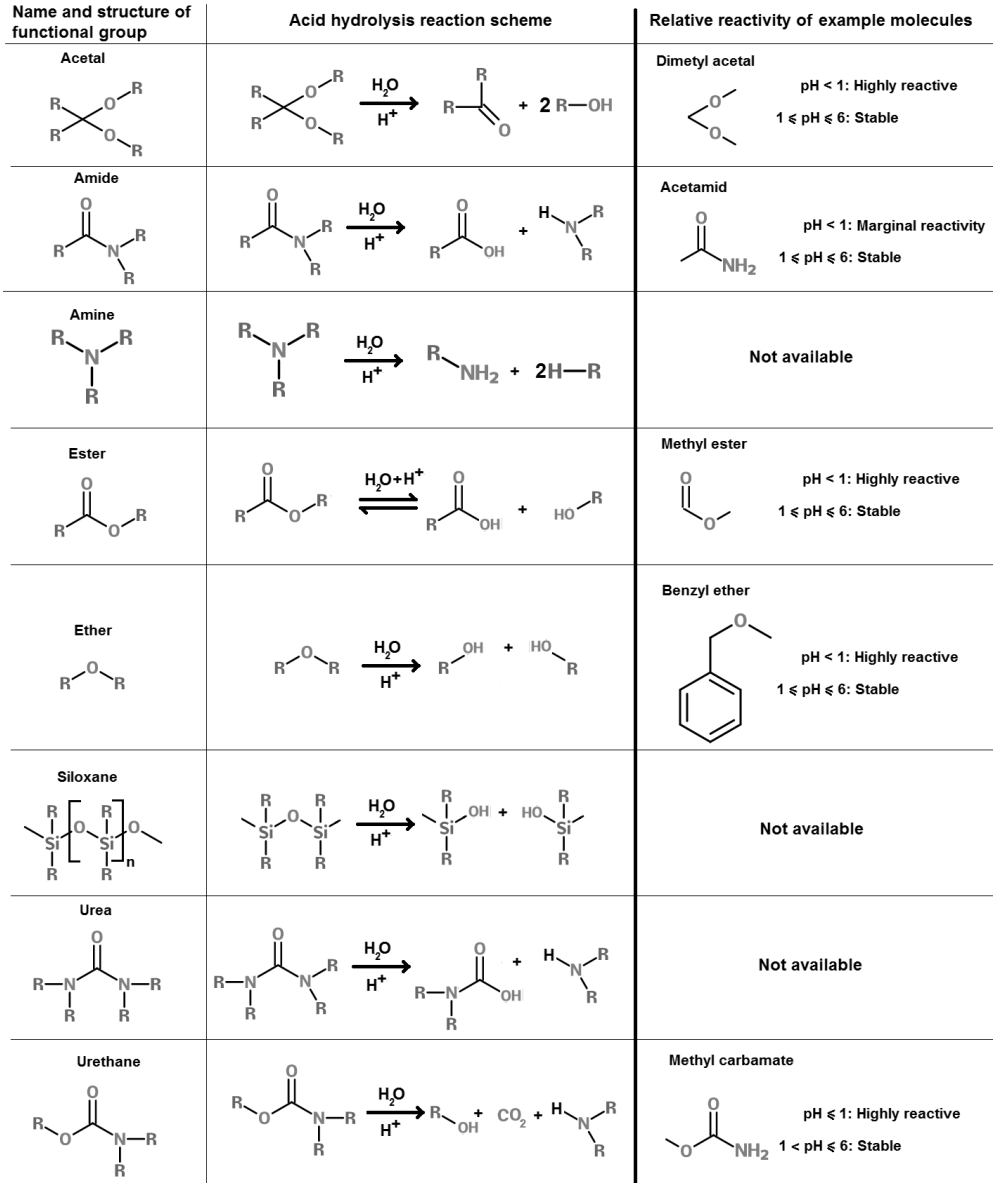

Figure 3.9: Name and structure of functional groups that can be present in coating resins and are vulnerable to acid induced hydrolysis. Proposed chain scissoring reaction schemes [40, 111, 112], and relative reactivity of similar molecules in acidic aqueous conditions are shown [113].

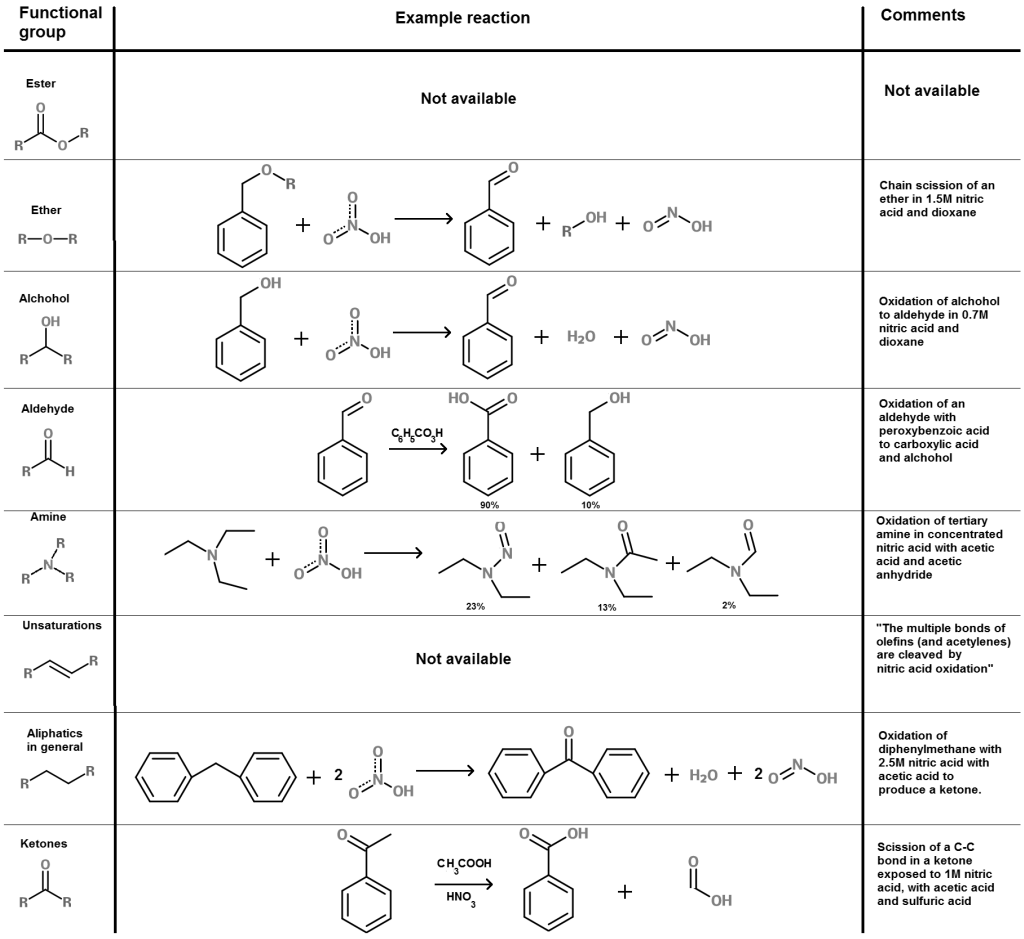

Figure 3.10: Name and structure of functional groups that are vulnerable to chemical oxidation [40, 61, 72, 105], as well as example reactions of organic molecules with oxidizing peroxy acids or nitric acid and comments from Trahanovsky [116].

3.2.2 Mechanisms

Hojo et al. and Tsuda [71, 72] describe various chemical reaction scenarios of polymers, summarized in Fig. 3.11. Whenever a coating is not completely inert towards the environment, one of these degradation mechanisms will occur. Each depends on the reaction and diffusion rate of aggressive media through the coating, as well as the frequency of chemical scissoring in the resin. The three mechanisms are described below:

- **Surface reaction** occurs when the penetrating solution is capable of rapid reaction with the

coating film, i.e. reaction rate $\gg$ diffusion rate, and the susceptible linkages are abundant in the coating. This causes the binder to slowly break apart at the surface and a reduced film thickness can be observed. This is seen e.g. for amine-cured epoxy in nitric acid solutions.

- **Corroded layer** differs slightly from the previous mechanisms. Here the susceptible linkages in the coating are less frequent, leaving behind a degraded leached layer. Still the reaction rate $\gg$ diffusion rate. There are two types: In type 1 the leached layer provides no diffusion barrier, for type 2 the leached layer is partly intact and can act as a diffusion barrier, reducing the diffusion rate.

- A **penetration type** mechanism occurs when the reaction with the coating is very slow, i.e. reaction rate $\ll$ diffusion rate. The coating degradation is therefore dominated by the diffusion process rather than the rate of reaction. The solution diffuses into the coating film and then some time after a reaction is observed between the coating and penetrating molecules.

Hojo's corrosion mechanisms stress the important effects of both physical diffusion and potential chemical reactions in a coating with regards to a coating's overall chemical resistance. Diffusion can be accelerated by chemical interactions between the solution and coating, so chemical resistance is a function of a coating's ability to prevent diffusion of species through the film, as well as chemical inertness in the environment.

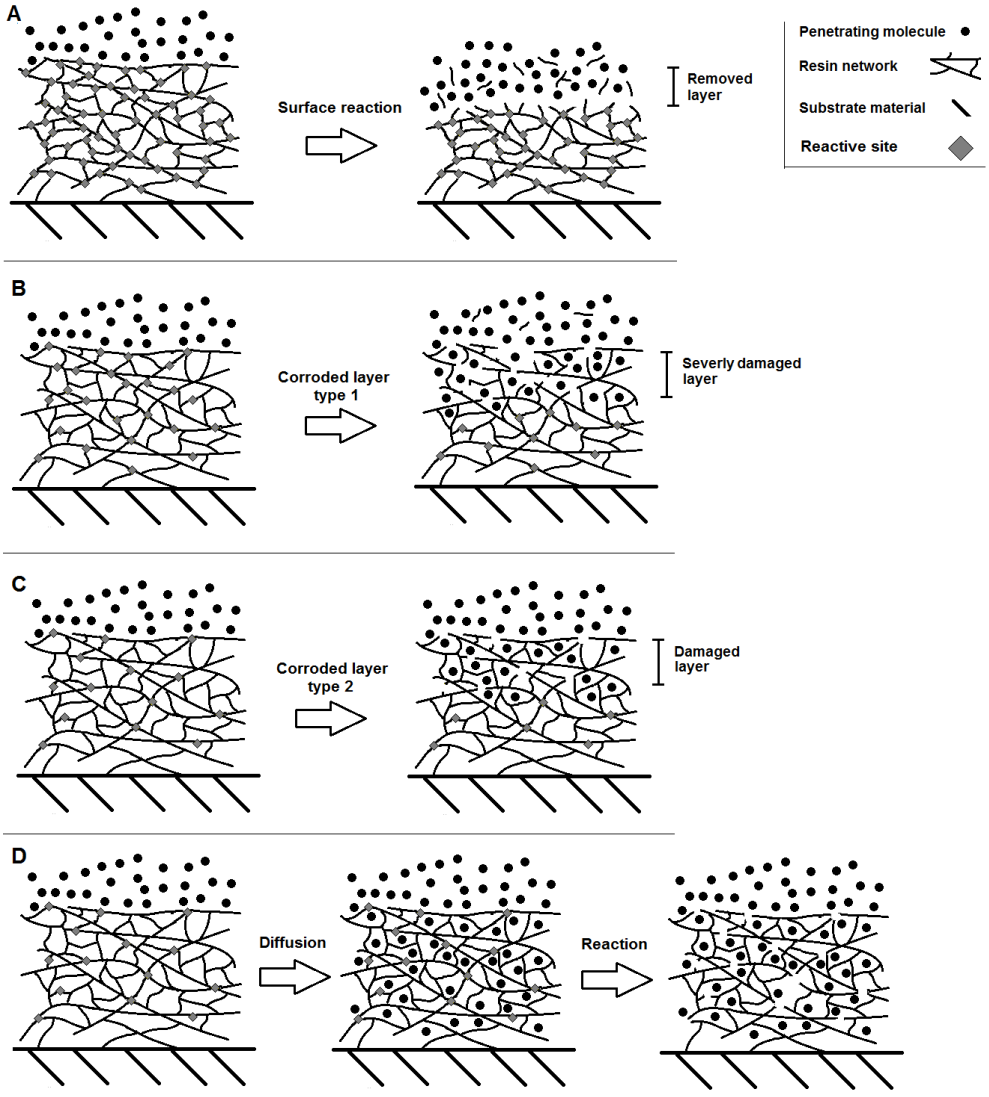

Figure 3.11: The three types of degradation mechanisms of an organic coating immersed in aggressive solutions. A: Surface reaction causes reduction in film thickness. B: Corroded layer type 1 leaves behind a severely weakened network. C: Corroded layer type 2, leaves behind a more intact network that still works as a diffusion barrier. D: Penetration type degradation is molecular diffusion in the presence of a slow reaction. Based on [72].

3.2.3 Commercial resins

Keeping the degradation processes in mind, it is possible to look at the most widely used commercial thermosets and discuss how they, specifically, degrade through chemical reactions in acidic solutions.

According to the Journal of Protective Coatings and Linings' (JPCL's) coatings and linings buying guide, the most common coating systems for acidic environments are made of epoxy (novolac), vinyl ester and polyurethane resins [24], consequently these resins will be covered in the following. See Figs. 2.3, 2.4 and 2.6 for resin formation chemistry.

Epoxy-based coatings have found uses in acidic environments, particularly novolac epoxies are commonly used due to the high cross-linking density compared to regular bisphenol A epoxies [25]. Nevertheless, no work has been found on acid degradation of novolac epoxies, so bisphenol A and F epoxies will serve as examples. The resin chemistry of a cured epoxy can vary greatly, because the epoxy end group can react with a host of chemicals, including itself when heated. Amine-curing systems are most common when a high acid-resistance is desired.
A cured epoxy film contains ether linkages, hydroxyl groups, unreacted epoxy groups or curing agent depending on curing stiochiometry, and a linkage dependent on the chosen curing agent. Fig. 3.12 shows the cross-link chemistry of some curing agents with epoxy.

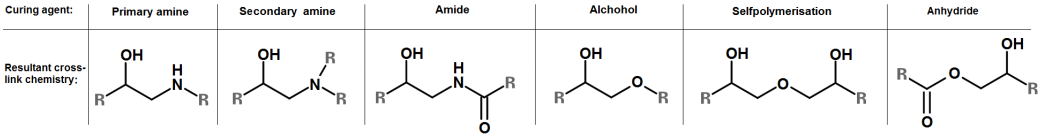

Figure 3.12: Curing agents and the resultant cross-link chemistry by reaction with epoxy groups. Deduced from [59].

Ether linkages are present in the backbone of epoxies and can be susceptible to acid-induced hydrolysis according to [40]. To the authors knowledge, no literature has confirmed this for epoxy resins. The only research available on this topic comes from Bauer [117] who showed that for melamine formaldehyde cross-linked co-polymer coatings, ether bonds can undergo hydrolytic cleavage in the presences of acids. Amide-cured epoxies are vulnerable to degradation in acidic environments, and undergo chemical changes that yield increased concentrations of carbonyl groups as shown by Kotnarowska [115], while the amide linkages themselves have been shown to undergo hydrolytic cleavage for non-epoxy resins according to the reaction scheme shown in Fig. 3.9 [76]. Non-oxidizing acids have also proven to cause increases in cross-linking densities for amide-cured epoxies. Kotnarowska [108, 115] noted an increase in cross-linking density in amide-cured epoxies when exposed to sulfuric acid, generating internal stress followed by blister formation in the coatings.
Amine linkages are not entirely inert either. Kalenda [39] investigated amine-cured epoxies in various acids and it was suggested that the amine bonds in the cured resin were susceptible to acid-induced degradation. Other publications have also noted amine linkages to be susceptible in acidic solutions [71, 97, 118]. Schmitz states that it is prone to hydrolysis, during examinations into Acrylic-melamine degradation in sulfuric acid, followed by conversion to an amine salt [109, 111]. The reaction sequence is reversed for Ono and Hojo [105, 118] who describe the reaction product as an amine salt followed by C-N bond scissoring, shown in Fig. 3.13. In opposition, Sembokuya [95] states that amine-cured epoxies exposed to sulfuric acid do not undergo a significant chemical change.

$$R_3N + HX \longrightarrow (R_3NH^+)X^-$$

Figure 3.13: Production of amine salts from amine linkages and acid reactions in an epoxy network. This salt formation is followed by C-N bond scissoring according to Ono [105]. For which amine types this is valid is not provided.

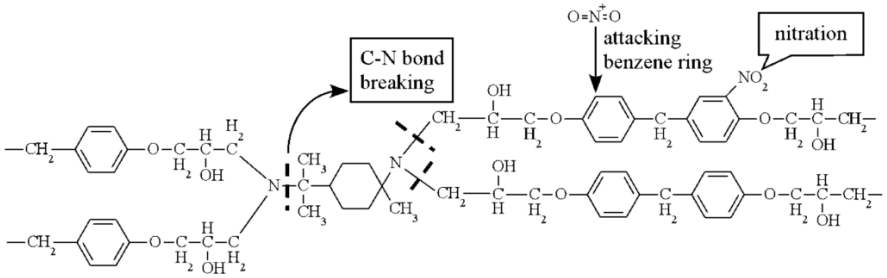

Figure 3.14: Acid-induced corrosion of amine-cured bisphenol F epoxy in oxidizing nitric acid. Reprinted from [119] by permission of Elsevier.

Ono [105] also investigated the behavior of amine-cured bisphenol A in an acidic oxidizing environment, using nitric acid and concluded that the amine and ether bonds were susceptible to cleavage in such an environment. It was observed that this degradation was rapid and highly destructive. Similar work was performed by Dang et al. [119, 120], who studied the degradation of amine cured bisphenol A and F in nitric acid. Dang notes the amine bonds as being susceptible to cleavage and observes a nitration of the benzene rings in both epoxy types, see Fig. 3.14, yet no mention is made of the susceptibility of ether linkages to oxidative cleavage. The scissoring of both C-O in ethers and C-N and C-C bond in tertiary amines by nitric acid is mentioned by Trahanovsky [116].
To summarize, amide-cured epoxies perform poorly in acidic medium because they are susceptible to hydrolysis as well as induced cross-linking. Amine-cured epoxies perform better in acidic environments, but degrade in oxidizing acids due to amine (C-N) and ether (C-O) bond cleavage. The chemical cleavage of the amine bonds by non-oxidizing acids has been described [105], but the reaction must be slow since significant chemical alterations are not easily observed [95].

Vinyl ester resins do not contain amine linkages as the amine-cured epoxies, instead the weak linkages in vinyl esters include ether and ester bonds. The ester bonds would be expected to undergo rapid hydrolysis in acidic conditions as shown in Fig. 3.9, a reaction that would cause chain scissoring and a chemical degradation of the resin network. Hojo and Tsuda [121] observed such a reaction for vinyl ester resins in HCl, but due to sterical effects discussed in Section 3.2.1, the extent of reaction was limited to the surface.
Vinyl esters have high acid-resistance but the formation of micro-cracks when exposed to acidic environments was observed. The cause of these cracks has not been studied in depth, but could be due to induced cross-linking. Fig. 3.15 depicts surface images before and after exposure to a sulfuric acid solution, where the appearance of micro-cracks or crazing is observed [78].

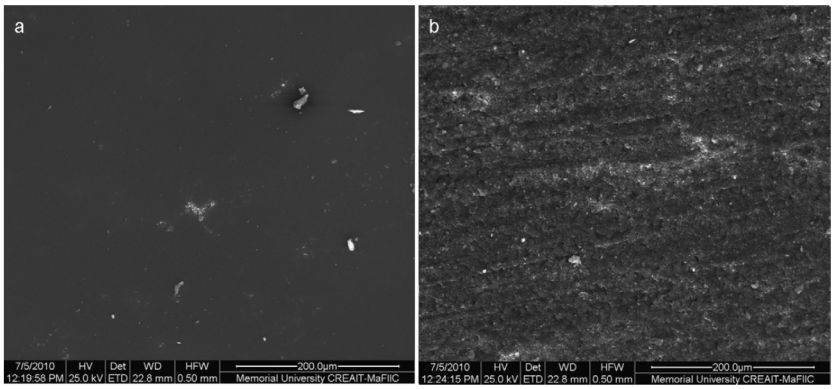

Figure 3.15: Scanning electron microscope image of an epoxy vinyl ester coating (a) unexposed, and (b) exposed to 1 M H_2SO_4 for 4 weeks (temperature was not stated). Reprinted from [78] by permission of Elsevier.

When it comes to acid-induced oxidation reactions, work is rather scarce. The ether groups in vinyl ester are vulnerable bonds shared with epoxies. However, vinyl esters are usable in oxidizing nitric environments [13], likely due to steric hindrance. The ether bond is noted to be cleaved for epoxies in oxidizing environments [105], but no studies have been made to determine the ether bond's part in vinyl ester degradation in oxidizing acid environments.

Polyurethane resins are not as frequently used in acidic environments as epoxies and vinyl esters, but some manufactures still recommend the use of polyurethanes in combination with epoxy coatings [24].
The stability of polyurethanes depends in part on the monomer that provides the alchohol group. If this monomer is a polyester, the resultant resin becomes vulnerable to hydrolysis, due to the ester linkages, specifically for strong acid immersion [122]. If the monomer is a polyether, the polyurethane becomes hydrolytically stable according to Stevenson [123]. Being stable, however, does not necessarily mean inert, the urethane groups themselves have been noted as vulnerable to hydrolytic cleavage in acidic conditions by Hare [40] as shown in Fig. 3.9. Huisman [122] also reported the urethane bond as being susceptible to chemical cleavage in acidic solutions. However, acidic exposure can also induce cross-linking in polyurethanes [123]. A polyether-based polyurethane will form new cross-links in acid, causing a unique case where both formation and cleavage of chemical bonds takes place. The cross-linking is said to occur at the urethane linkages.
Oxidizing nitric acid has been observed by Tanzi [124] to cause chain scissoring in polyether and polycarbonate-based polyurethanes. This was seen through decreasing molecular weight of the polyurethane, though the specific position of this chain scission was not specified.
The chemical degradation of acid resistant resins is a complicated process to generalize as it varies with resin and acid chemistry. It is not a subject of extensive research and potential reaction mechanisms have not been properly mapped. There is room for improvement and research, on the physical and chemical effects of acid exposure to chemically-resistant coating materials. Research, that can improve the understanding of underlying reactions and mechanisms, which in turn allows the formulation of

improved products.

3.3 Mechanical degradation through erosion

Abrasive wear is defined as wear caused by hard particles or hard protuberances forced against, and moving along, a solid surface [125]. It is an issue encountered whenever two surfaces come in contact, and material is mechanically removed from the main body. Erosive wear is a subcategory of abrasive wear, where a free body moving in a medium, is abrading a surface. As a coating material is eroded, or polished, during service, the coating thickness is gradually reduced until it is completely removed. Erosion intensity depends on surface and particle characteristics in the given environmental conditions. Important particle parameters include impingement angle, impact speed, shape, hardness, size, and impact frequency. Important material parameters include hardness, ductility, temperature, erosion media density, presence of turbulent flow, and other effects of erosion media to the mechanical properties of the material, such as softening or hardening of the surface [38, 126–129]. A mathematical breakdown of the erosion phenomena gives an idea of the relative influence of each individual parameter, and is included in Appendix B.

3.3.1 Elasticity and hardness

As Fig. 3.16 shows, brittle and ductile materials behave very different depending on particle impact angles. The elastic modulus of a coating determines these behaviors. For typical abrasive wear, there is a rule of thumb that a surface requires a hardness that is at least 0.5 times the abrasive hardness to have sufficient wear resistance [35]. But as Fig. 3.16 shows for erosion, ductility is also an important factor, as ductile or rubbery materials perform best at high impact angles, while hard and brittle materials have optimal performance at low angles of impact.

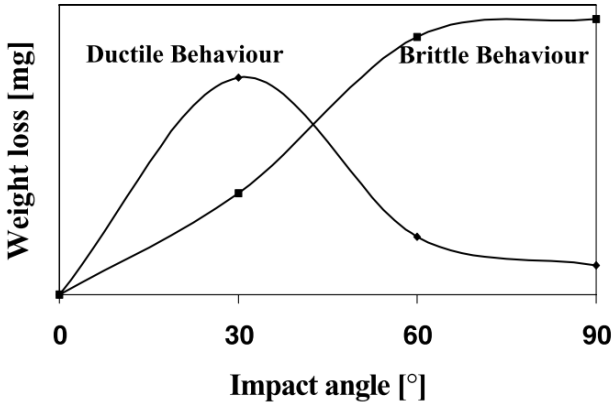

Figure 3.16: Typical erosion behavior of ductile and brittle materials. Brittle materials are more severely eroded when particles impact at high angles on the surface. While ductile materials have poor performance at low impact angles [130].

Fig. 3.17 shows a comparison of low and high elastic modulus material suffering a particle impact, both cases are ideal responses that cause no damage to the material surface. Polymeric materials

are generally not hard enough to resist erosion, but they can have a low elastic modulus, allowing an elastic recovery after particle impact without being damaged. This phenomena is most often observed for elastomers.

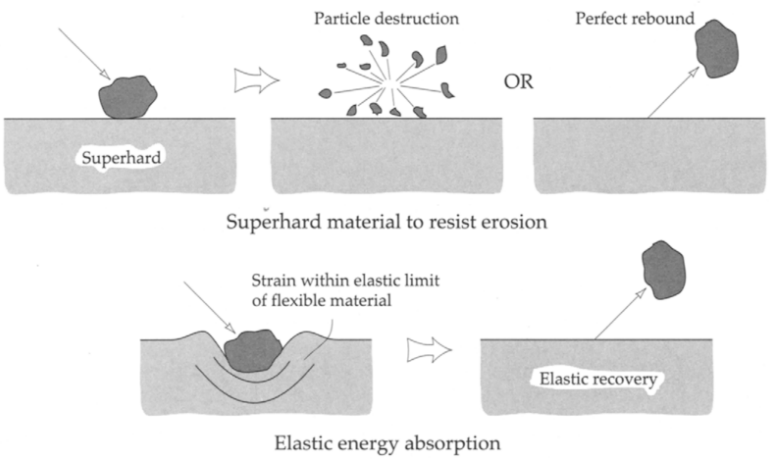

Figure 3.17: Ideal particle impact on high elastic modulus, super hard and tough material, and impact on a low elastic modulus, flexible material [129].

3.3.2 Particles and carrier media

Particle shape is an essential erosive parameter. Sharp-edged particles cause more wear issues than blunt particles, because the sharp corners have very small radii, which are more effective at cutting into a coating and removing surface material than blunt particles. The blunt particles are more likely to cause plastic deformation [129].

The exposure temperature can also affect erosion, as will any environmental change that can alter the mechanical properties of the particles or coating material. Increases in temperature can lead to a softening of organic materials, while decreases in temperature can lead to a material hardening.

Turbulence in the carrier medium can also enhance erosion rates, compared to laminar flow scenarios. This is due to the chaotic flow patterns and eddy formation, which can send particles in collision with the wall surface during turbulence. While laminar flow patterns allow a smooth predictable travel path for the particles parallel a surface.

The carrier media itself can also affect erosion rates. Low viscosity media like gases do not affect a particle trajectory as much as a high viscosity media such as liquids [128, 129]. This phenomena is depicted in Fig. 3.18 and shows how high viscosity media can prevent particle impact, and reduce the angles of impact. This phenomenon is also known as the thin film effect, a theory which states that a particle has to displace a film of molecules at the impact surface, to enable contact and abrade the surface [131]. This provides a cushioning effect that reduces the effective velocity of an incoming particle and reduces the impact angle to favor sliding wear rather than impact. As a rule of thumb, there is only cushioning effect in liquid media.

The last effect of the carrier media occurs if it alters the mechanical properties of the coating material.

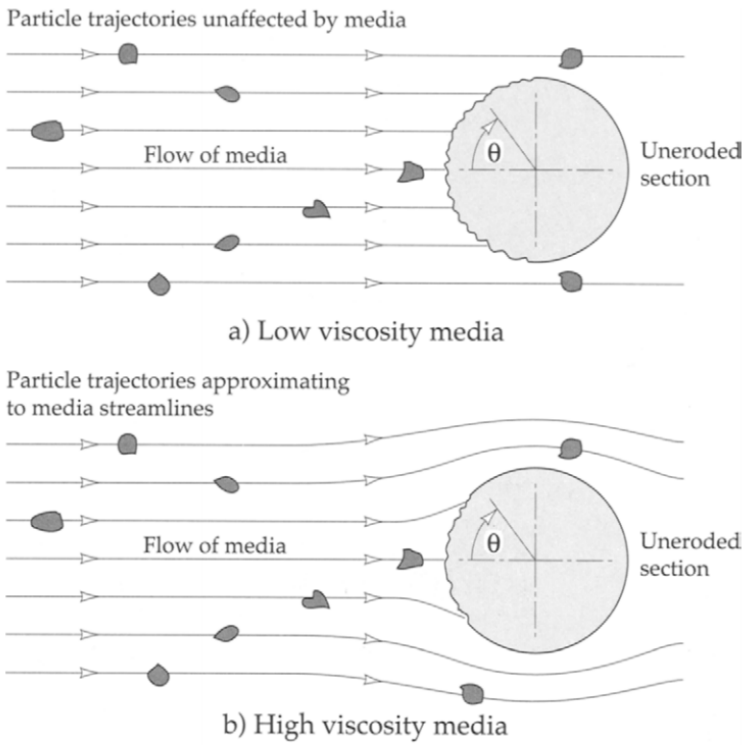

Figure 3.18: Effect on media viscosity on erosive particle trajectories. High viscous media favors low angle impacts and reduces particle impact velocity [129].

This can occur in polymers if the media diffuses into and softens the resin, but also, if reactions occur at the polymer surface, weakening the coating and making it more susceptible to erosion. This phenomena is one of the few cases that have not been studied systematically, but a few examples have been documented. Examples such as an observed reduction in wear resistance of high-density polyethylene (HDEP) by a factor 100, due to effects of 0.01 wt% $FeCl_3$ exposure. With little observable wear resistance change at concentrations below or above said value [132]. Or the incorporation of oxygen and water in elastomers, causing chemical reactions with the rubber and increasing erosion rates [133].

3.3.3 Flow field in a stirred tank reactor

Future discussion requires an understanding and estimation of the flow field in a well stirred tank reactor. Fig. 3.19 shows the liquid flow field, axial and radial velocities, of a flat-bottom tank using a three bladed, pitch blade turbine. From the figure it is visible that flow velocity is relatively low below the impeller and near the tank edge. The vectors at the tank bottom can be used to estimate particle impact angle and magnitude. Stirring intensity of the impeller is estimated to be 0.014 kW/m^3, a factor 100 less than used in the project experiments. The erosive particle impact angle and speed in stirred tanks depend on the flow field which is determined by tank dimensions, impeller type(s), size,

position, presence of baffles, and stirring intensity. Therefore, Fig. 3.19 should only serve as pointer, to what the flow field actually looks like in the set-up constructed for the current project.
Ayranci, I. et al. [134] shows an example of particle off-bottom suspension for an axial pumping impeller, depicted in Fig. 3.20. Particle suspension can be challenging to achieve beneath the center place impeller and at the reactor edge where baffles are shielding. Also Fig. 3.20 should only serve as an example of possible particle sedimentation in a stirred tank reactor.

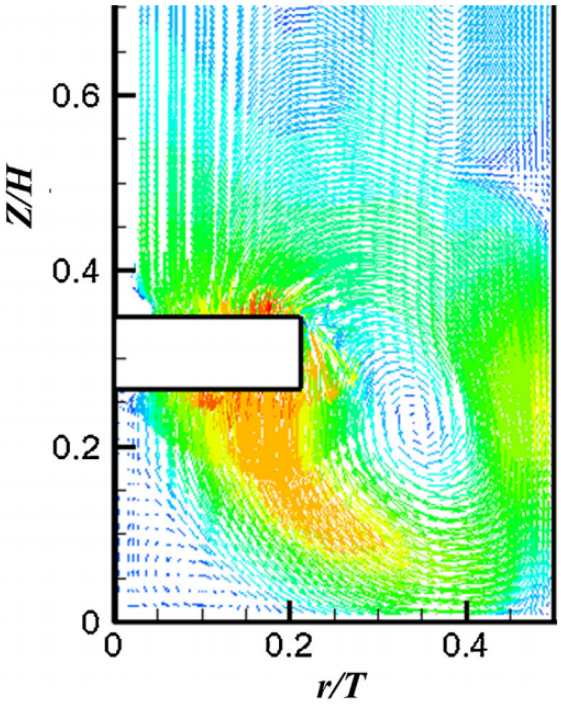

Figure 3.19: CFD simulation of the average flow field for an axial pumping impeller in a CSTR. Impeller type is a 3 bladed pitch blade turbine, sized 0.42 times reactor diameter, central placement, 0.8 times impeller diameter off the bottom. Red, green and blue indicate flow speeds of 0.5, 0.25 and 0 times the tip speed respectively. Z/H and r/T are dimensionless height and diameter respectively [135].

4 Failure analysis

To predict coating lifetime, failure should be measurable and the measurement should be objective. This may seem apparent, but many experimental practices in the coating industry rely on subjective evaluations without considering the underlying cause of failure. But wear, diffusion and chemical change can be monitored in a fashion that allows mathematical predictions of future events.

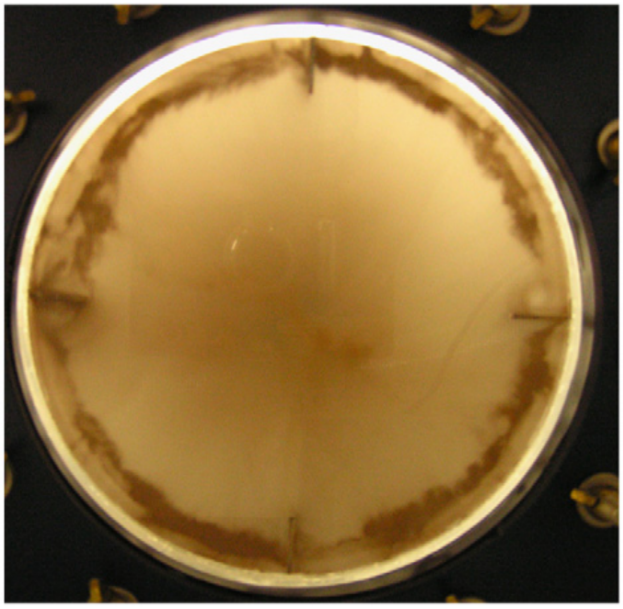

Figure 3.20: Off bottom particle suspension in a CSTR viewed through a transparent container. Impeller type is an A310, sized 0.5 times reactor diameter, central placement, 0.5 times impeller diameter off the bottom, 3 wt% particle load [134].

4.1 Monitoring coating polishing rates

A typical method for determining erosive resistance is by monitoring weight loss of an eroded coating [129, 133]. Weight change was not used in the current project to asses erosion, the weight distortion caused by liquid absorption and the inhomogeneous wear on the sample surface. Gloss measurements were considered, but it was observed that the coating gloss changed immediately after erosion commenced, and then remained constant.
Wood et al. [136] used thickness measurements as a tool for determining polishing rates in pipes, where erosion varies due to differences in particle impact angle and speed. By monitoring these reductions in film thickness, one can observe a thinning rate at any position on a coating sample. Knowing the original thickness, a lifetime estimation can be deduced. DFT (dry film thickness) measurements can be performed on a metallic substrate using a hand held magnetic gauge, with precision down to ± 1 μm. Each measurement takes around 2 seconds, making it an optimal tool for rapid and precise DFT measurements. An Elcometer 355 is used in the current work, see Section 14.1 for more details.
But even film thickness measurements can be deceptive. Liquid absorption in the coating will cause it to swell, yielding an increase in thickness, this is most often observed during the first day of immersion. Solvent diffusion out of a coating will cause the opposite, a collapse and thus a thinning of the coating film, often observed over several days where the thickness is stabilizing. Blister formation on the coating surface will be observed as increasing thickness. Also the surface roughness of the coating is important, as very rough surfaces lead to high measurement uncertainties.
No published literature, except Wood et al. [136], maps polishing rates to monitor erosion for organic

coatings. This is likely because inhomogenous erosion is frequently observed, such as cavities spread out over a surface. For the case of small particle erosion in a stirred tank reactor, the erosion is not severe enough to produce defects in the coating, and DFT is gently reduced during exposure.

4.2 Monitoring diffusion

Monitoring the permeation rate of molecules into and through a coating film determines the ability of a coating to function as a barrier. Three of the most common methods for diffusion analysis include the use of a SEM coupled with EDS, using specialized diffusion cells, or monitoring weight change for immersion experiments.
SEM coupled with EDS can be used to make a qualitative elemental analysis of a coating cross section [7, 95, 97, 137], thus detecting the depth of penetrating elements which are not originally found in the coating. This could for example be a sulfur element analysis as performed by Sembokuya [95] on the cross-section of an amine-cured epoxy, exposed to sulfuric acid, see Fig. 4.1. The penetration depth can be approximated from the image and knowing the immersion time, a plot like the one shown in Fig. 4.2 can be generated.
Alternatively, one of the simplest methods for observing diffusion characteristics is immersion tests followed by weight change analysis. Weight change of a coating provides information relating to both chemical stability and diffusivity [71, 72, 95, 97], but does not necessarily separate the two effects. Therefore, weight change analysis should not be a stand-alone test. Molecular diffusion into a coating causes a weight increase, while leaching of solvents or chemical scissoring of network bonds, can cause a decrease in weight. Fig. 4.3 shows the weight change over time of a glass reinforced amine-cured epoxy resin exposed to a large variety of chemicals at 80 °C. The rapid weight-losses for HNO_3 and H_2O_2 are due to a chemical degradation of the resin in oxidizing environments.
Drying a coating sample after immersion, makes it possible to remove the water content and measure actual changes in weight. For example, if a coating is partly degraded with an increased porosity, the submerged weight will be high, due to the diffusing liquid, while the dry weight might show an overall decrease, see Fig. 4.4.
Another common test set-up is the diffusion cell, often used when diffusion of substances through a coating system is of importance. The principle is to separate a chamber containing the aggressive substance(s) from one containing de-mineralized water using a free coating film, see Fig. 4.5. It is possible to analyze the concentration development of the aggressive substance in the pure water solution as time passes, giving a transient analysis of the diffusion process. A diffusion cell can also measure the mass flow between the two chambers by observing volume increase or decrease in either chamber as shown in Fig. 4.6 [61, 76, 102, 138, 139].

The models shown in Section 3.1.4 utilizes data from these 3 diffusion experiments to deduce diffusion coefficients. But care should always be taken to ensure the applicability of such simple models, since deviations from the model assumptions can be vast.

4.3 Monitoring chemical change

Changes in weight and flexural strength of a coating are not only caused by diffusion and solvation effects, but also of chemical changes in the resin network. IR analysis of a coating surface FTIR, and

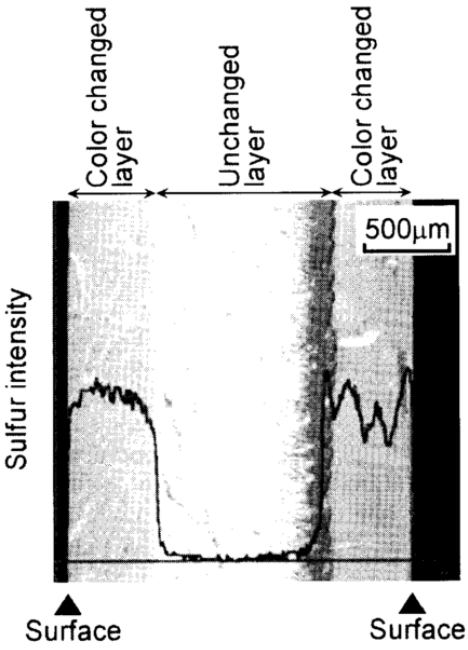

Figure 4.1: Cross-sectional EDS (X-ray) S-element analysis of a free coating film, made of amine-cured epoxy. Immersion in H_2SO_4 for 300 hours at 80 °C. No statement was made on the differences between the two color changed layers [95]. Courtesy of The Society of Materials Science, Japan.

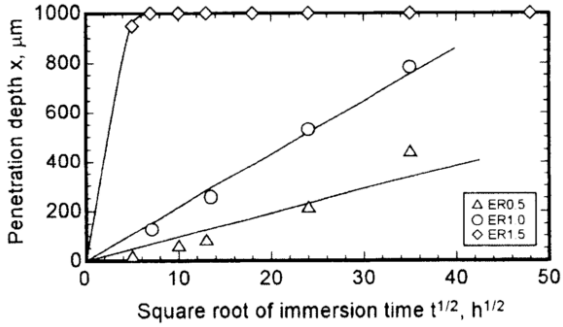

Figure 4.2: Sulfur element penetration depth vs. immersion time of amine-cured epoxies with varying hardener content. Legend refers to: 0.5=0.9 wt%, 1.0=17.9 wt% and 1.5=26.9 wt% hardener at 80 °C [95]. Courtesy of The Society of Materials Science, Japan.

SEM coupled with EDS can also be used to provide information on changes in chemistry within a coating.

A loss in weight during immersion can be caused by unreacted components or solvents diffusing out of the coating, but it can also be due to cleavage of chemical bonds within the film, releasing resin segments over time. But bond scission can occur without a weight loss, if the reaction sites are few and no resin segments are removed. Also, the occurrence of weight loss does not determine the time it takes for reaction to take place because resin segments in cross-linked thermosets can require multiple bond scissions to be completely released. This is shown by Hojo [118] in Fig. 4.4, where a drop in flexural strength, indicating bond cleavage, occurs before the observed weight loss.

FTIR analysis allows the determination of the chemical composition of simple and complex molecules [140]. It is a useful tool in analyzing the chemical degradation, if any, that is occurring within the coating, Fig. 4.7 is an example of this [17, 61, 95, 118, 119]. The figure shows the IR spectra of an amine-cured epoxy before and after immersion in nitric acid and was used to derive the degradation of amine-cured epoxies in oxidizing acids shown previously in Fig. 3.14, Section 3.2.3. The appearance or disappearance of absorption peaks provide indications of new functional groups or the disappearance

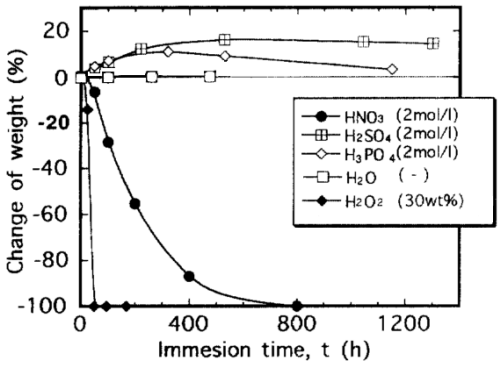

Figure 4.3: Weight change diagram of a glass reinforced amine-cured epoxy resin immersed in various aqueous environments at 80 °C. Reprinted from [72] by permission of Springer.

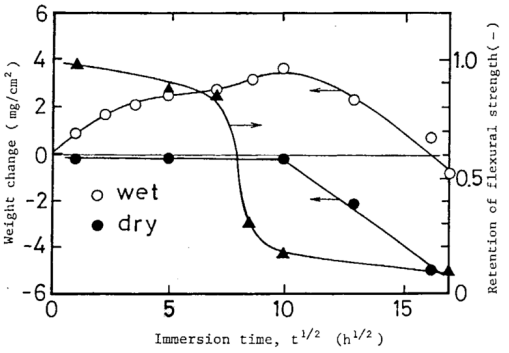

Figure 4.4: The wet and dry weight change of a polyester immersed in boiling water, showing water penetration and subsequent hydrolysis of ester bonds causing weight and flexural strength loss. Reprinted from [118] by permission of Taylor and Francis.

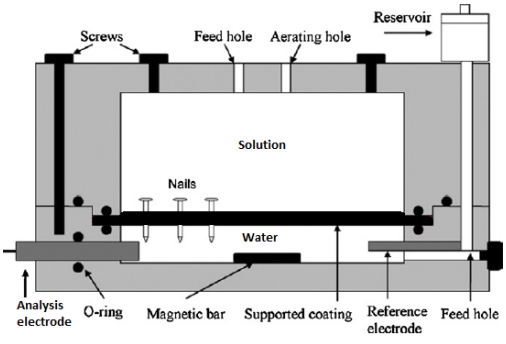

Figure 4.5: An ionic diffusion cell used to monitor the permeation of ionic species across a free coating film or membrane. In this case, the interface diffusion of ionic species along a nail penetrating the film. Reprinted from [107] by permission of Elsevier.

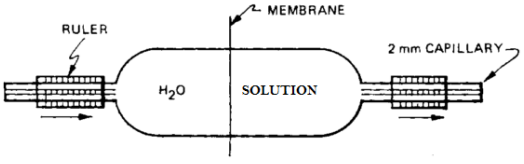

Figure 4.6: Osmotic diffusion cell, measuring the change in volume in either chamber as caused by mass flux through the center membrane. Reprinted from [61] by permission of John Wiley and Sons ©.

of others. Some studies compare IR spectra by scaling the peak intensity of a bond that is known to remain constant during exposure, in order to note the relative change of other peak intensities [141].

5 Summary

Diffusion of ions into organic coatings causes the coating to soften, enables contact between the penetrant and components inside the coating and eventually contact with the substrate. Chemical reactions

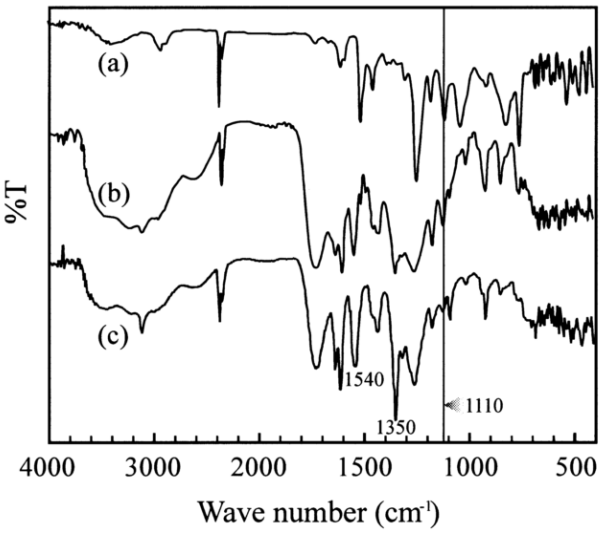

Figure 4.7: IR spectra of a amine-cured epoxy coating before immersion (a), after 150 h (b), and 500 h (c) of immersion in 4 M nitric acid at 80 °C. Wavenumbers at 1350 and 1540 cm^{-1} correspond to nitro and aromatic nitro groups, while the disappearance at 1110 cm^{-1} corresponds to C-N bonds. Reprinted from [119] by permission of Elsevier.

between a penetrant an coating components can cause irreversible failure and weaken the mechanical properties of a coating. Finally, erosive forces can chip away coating material, thinning the coating and wearing it away from the substrate. Physical diffusion, chemical reaction and mechanical erosion are three cornerstones in barrier coating degradation, where each individual mechanism, or a combination of the mechanisms, can lead to coating failure.

Mapping these three degradation mechanisms for any given coating formula would allow better understanding of expected coating performance, and help determine the coating lifetime. This is described in the later parts by monitoring chemical changes in chemically immersed coatings, observing acid diffusion speeds using a diffusion cell set-up, and assessing erosion rates of coatings in a pilot-scale agitated leaching reactor.

Part II

Supporting immersion experiments

Immersion of free films and coated panels was performed to support the later pilot-scale reactor experiments and diffusion cell experiments. Free films were immersed to observe weight change and FTIR analysis was performed on the free films in an attempt to to better understand chemical reactions taking place in the coatings. SEM-EDS analysis was also performed on coating cross-sections to observe sulfur diffusion through coatings samples. Coated panels were immersed to provide DFT change data and to observe visual alterations in the coatings caused by chemical exposure only. This part also provides a description of the coating formulations used in current and later experiments.

List of Abbreviations

FTIR	Fourier-transform infrared spectroscopy
DFT	Dry film thickness
EDS	Energy-dispersive X-ray spectroscopy
IR	Infra-red
JPCL	Journal of Protective Coatings and Linings
NE1	100 % solids novolac epoxy, see Table 6.1
NE2	Novolac epoxy, see Table 6.1
NE3	Novolac epoxy, see Table 6.1
PU	Polyurethane coating, see Table 6.1
SEM	Scanning Electron Microscopy
VE	Vinyl ester coating, see Table 6.1

6 Coatings

Throughout the course of the project a selection of six different coatings were utilized for experimentation. The choice of coatings was based on the resin types that have been mentioned in literature to be resistant to acidic environments. A survey performed by JPCL [24] in 2006, provided such an overview. A total of three types of resins were emphasized in this survey, vinyl ester, novolac epoxy, and polyurethane, with novolac epoxy and 100% solids epoxy being the most recommended. One vinyl ester and one polyurethane, three amine-cured novolac epoxies, where one is 100% solids, and one amide-cured novolac epoxy, were chosen. Table 6.1 shows the coating formulations.

All coating samples were spray applied, either to a substrate, or a slip surface to produce free films. All coatings were allowed to cure for one day at room temperature, followed by post-curing in a heated oven at 60 °C for 2 days.
Coating T_g was determined using differential scanning calorimetry, with a heating rate of 10 °C/min from -90 to 250 °C.
The amide-cured epoxy (NE3) was chosen to observe the effects of chemical reactions in later experiments, but reactions in acidic environments were so fast and destructive that no useful data were obtained. The NE4 coating was only used for preliminary diffusion cell experiments.

Table 6.1: List of coatings with formulations used in the project. Additives in small quantities (<1 wt%) which are not deemed relevant to discussions in the thesis are omitted. R=$Mw_{Eq,\ curing\ agent}/Mw_{Eq,\ resin}$

Coating (code)	R	T_g	Component type	Component description	Weight percentage
Vinyl ester (VE)	NA	145 ± 2	Resin	Epoxy vinyl ester	46.4
			Hardener	Styrene	25.0
			Filler	Glass flakes	22.6
			Pigment	TiO_2	1.9
			Initiator	Cumene hydroperoxide	1.7
Polyurethane (PU)	1.1	25 ± 2	Resin	Styrene acrylate (OH-functional)	37.1
			Hardener	Aromatic polyisocyanate	6.9
			Filler	$BaSO_4$	18.9
			Filler	$CaCO_3$	9.3
			Pigment	TiO_2	12.8
			Pigment	$Zn_3(PO_4)_2$	1.1
			Solvent	Toluene and Xylene	10.6
Novolac epoxy 100% solids (NE1)	0.9	81 ± 2	Resin	Bisphenol F epoxy	40.8
			Hardener	Amine adduct	12.0
			Hardener	Cycloaliphatic amine	5.8
			Filler	Quartz	17.2
			Filler	$BaSO_4$	12.3
			Pigment	TiO_2	4.2
			Reactive dilutent	Butanediol diglycid ether	5.0
Novolac epoxy (NE2)	1.0	45 ± 2	Resin	Bisphenol F epoxy	31.7
			Hardener	Cycloaliphatic amine adduct	16.9
			Hardener	Cycloaliphatic amine	8.5
			Filler	Feldspar (Al/K/Na silicate)	11.0
			Filler	Talc (Magnesium silicate)	11.0
			Pigment	TiO_2	7.7
Novolac epoxy (NE3)	0.8	NA	Resin	Bisphenol F epoxy	33.0
			Hardener	Polyaminoimidazoline	31.9
			Filler	Quartz	13.9
			Filler	$BaSO_4$	9.9
			Pigment	TiO_2	3.5
			Reactive dilutent	Hexandiolglycidylether	4.0
Novolac epoxy (NE4)	0.3	80 ± 2	Resin	Bisphenol-A epoxy	29.4
			Hardener	Aliphatic and diethylamine	2.0
			Filler	Baryte	36.9
			Filler	Muscovite mica (Na/Al silicate)	10.9
			Pigment	Titanium dioxide	3.8
			Solvent	Xylene	9.9
			Solvent	Isobutanol	3.5

7 Set-up, environment and procedure

Immersion experiments were performed on coating free films, and coatings applied to rectangular, 50x100x4 mm^3, stainless steel substrates made of 316 L. The steel substrates were coated on both sides with the chosen coating, and patched up on the sample edges with the NE1. Fig. 7.1 shows the free films and coated steel samples before immersion.
The samples were immersed in two different environments titled "Mild" and "Harsh". The choice of immersion conditions was done to compare results with experiments performed in a pilot-scale leaching reactor, presented in Part III. Mild condition immersion is heated tap water, while Harsh conditions is a low pH, heated mixture of sulfuric acid and copper sulfate, see Table 7.1 for condition overview.

(a) Coated steel.

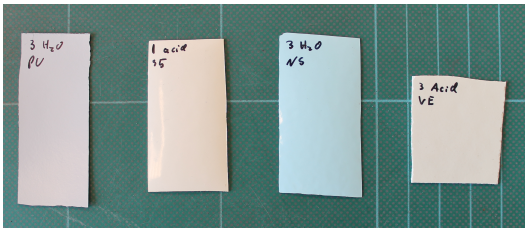

(b) Free film.

Figure 7.1: Coating samples for immersion experiments, from left to right is PU, NE2, NE1 and VE.

Table 7.1: Experimental conditions overview for immersion experiments. All experiments were performed at 75 °C.

Environment:	**Harsh**	**Mild**
H_2SO_4 $[mol/l]$	0.106 ± 10^{-3}	10^{-4}
pH	0.975±0.005	3.9
Cu(II) $[g/l]$	4.68	0

The Mild and Harsh solutions were contained in sealed glass jars placed in a heated oven. The coating

samples were fully immersed inside the jars, ensuring that all sample sides are exposed to the liquid. Each jar contained a VE, PU, NE1 and NE2 coated steel sample, and three free film samples of each coating type.
At every three to four days all coating samples would be removed from the chemical jars, washed with tap water and dried using paper towels. Free coating films would then be weighed on a balance within, 10 min of the drying, to avoid evaporation issues. Film thickness measurements would be performed on the coated steel samples, method and results of these measurements are presented in Part III. After measurement, all coating samples would be re-immersed in their respective environment.
At the termination of the immersion experiment, some samples would be taken for analysis in an FTIR, and some would be used for destructive testing in an electron microscope.

8 Analysis equipment

Overview of the analysis equipment used for analyzing immersion samples.

8.1 FTIR

An FTIR machine can detect chemical bonds on the surface of a material by exposing the surface to IR light at different frequencies, and determining the intensity of the reflected light. The resultant absorption peaks correspond to a frequency of vibration in the sample molecules [140].
A Thermo Scientific Nicolet iS5 was used in this project. The measurement procedure was fairly simple: Before measurement the background was collected and subtracted from the following measurements. The coating sample was then placed on top of a center crystal, while a fixture arm forces the sample to into optimal contact. The measurement took no more than 10 seconds. Three scans were performed on different positions on each sample to ensure repeatability.
To prepare samples for FTIR analysis after immersion in Harsh conditions, coating samples were immersed in de-mineralized water for 32 hours and dried in an oven at 75 °C for 9 hours. This was performed in an attempt to remove sulfur compounds from the surface and provide a spectra that better represents the changes happening inside the resin.

8.2 SEM

An Inspect S. electron microscope was used to gather images of particles (Part III), as well as cross-sections of coatings. SEM uses an electron beam in high vacuum, detecting back-scattered and secondary electrons to gather images with a very high resolution, magnification as well as depth of field. The electron impacts also generate gamma radiation which are unique for the particular element. An EDS detector can read this radiation, allowing an elemental mapping of the image. For more details on SEM and EDS see the book by Goodhew, P. J. [142].

To prepare coating samples for cross-sectional analysis in the SEM, previously immersed free films were shaved using a Microtome Finesse 325. The Microtome used a sharp blade with precision, to cut and expose the coating cross-section as a smooth planar surface. The sample was adjusted so the blade cut parallel to the diffusion front, minimizing any smearing effects which might distort the determination

of penetration depth.

Non-conductive materials such as organic coatings, can be troublesome to image in an SEM due to sample charging. They will charge up during inspection, causing the image to drift and distort, or even burn the resin away if the exposure voltage is too high. To avoid this, the coating samples were coated with a four nm layer gold, by physical vapor deposition using a Quorum Coater.

9 Weight change results

Fig. 9.1 provides the results of weight change measurements performed on immersed free films. The free films had different start weights and surface area. It was found that weight change per surface area gave the same picture as percentage weight changes, therefore only the latter is presented.

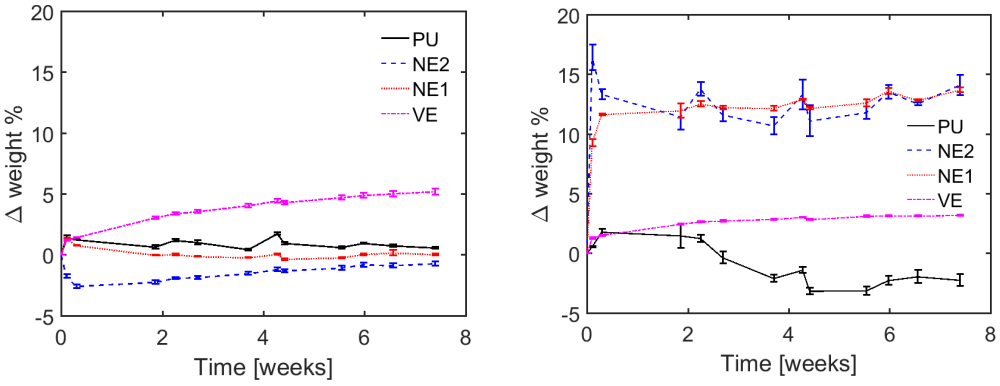

(a) Mild conditions.

(b) Harsh conditions.

Figure 9.1: Weight change of VE, PU, NE1 and NE2 free films immersed in Mild or Harsh conditions for 53 days.

The VE coating did not fully saturate in either condition at the conclusion of the experiment. The weight increase leveled off around five wt% in Mild and three wt% in Harsh. The PU coatings showed an initial weight increase followed by a gradual decrease in both environments. Thus the PU was rapidly saturated followed by a gradual leaching of solvents out of the coating. The weight loss was greater in acidic conditions, likely due to calcium carbonate fillers dissolving and leaching out of the resin. The NE1 showed initial weight increase followed by gradual decrease in Mild conditions. The gradual decrease in weight might be caused by un-reacted components in the film leaching out. In Harsh conditions, the NE1 increased greatly in weight during the first days of immersion, followed by a more gradual weight increase. This indicated a rapid liquid permeation and saturation in Harsh conditions. The NE2 lost mass during the initial stages of Mild condition immersion, followed by a gradual increase in weight. The initial weight loss could be caused by rapid leaching of unreacted components in the film, the following weight increase could be liquid diffusing into the film. In Harsh conditions the NE2 saturated after 17 hours, followed by oscillations in weight. Rapid liquid permeation caused the initial weight increase. Leaching of unreacted components could have caused the weight decrease.

Based on weight change alone it was observed that the NE1 and NE2 performed poorly in Harsh conditions, since both gained a high weight percentage within the first few days of exposure. This showed poor barrier properties as the coatings were unable to keep the sulfuric acid from diffusing into and through the film. NE1 and NE2 performed much better in Mild conditions with little weight uptake. PU and VE showed superior barrier properties in Harsh conditions as the weight increase was much smaller. In Mild conditions, VE had the highest weight uptake while PU performed similar to the NE1.

10 Visual changes

The immersion samples were photographed before immersion and at the conclusion of the experiment. If a coating delaminated or blistered heavily, the experiment was considered finished, since no reliable DFT data could be extracted. Before and after images can be found in Figs. 10.1 and 10.2.
The VE discolored to a more brown hue in both conditions with no delamination blisters occuring. The VE did not fail in either environment. The PU showed slight discoloration in Harsh conditions, but did not fail in either environment. The shorter exposure time was due to an application error in the first PU samples prepared. The NE1 discolored from blue to green in mild conditions, while it discolored to brown and delaminated after 310 hours in Harsh conditions. The NE2 discolored to darker hue in Mild conditions, while it blistered heavily after 17.5 h in Harsh conditions, followed by delamination.

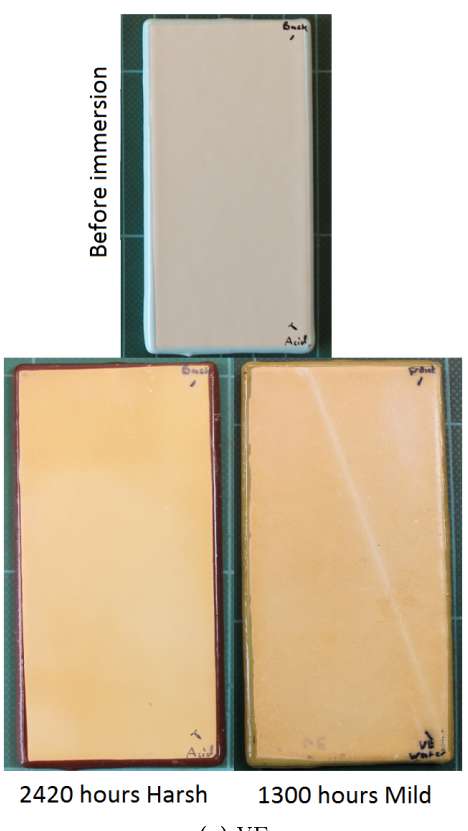

(a) VE

(b) PU

Figure 10.1: Visual changes of VE and PU immersion samples before immersion and at the termination of the experiment in either Harsh or Mild conditions.

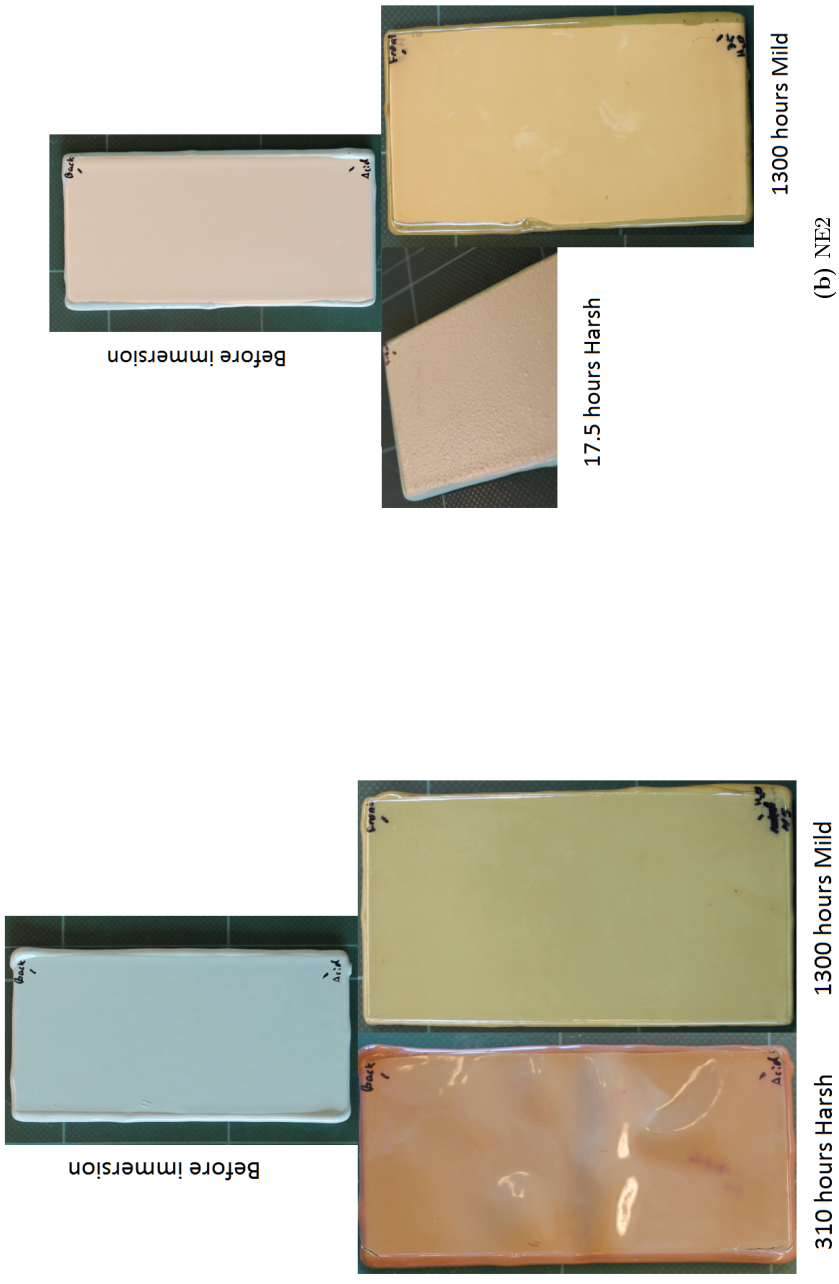

(a) NE1

(b) NE2

Figure 10.2: Visual changes of NE1 and NE2 immersion samples before immersion and at the termination of the experiment in either Harsh or Mild conditions.

11 FTIR analysis

FTIR analysis was performed on the unexposed cured coating, and then again after 53 days immersion in Harsh conditions. Despite the water immersion procedure to remove sulfuric acid ions from the surface, sulfur species were found in the coating samples. This caused obscurities withing the corresponding absorption wavelegnths. The HSO_4^- ion absorbs at 850-870, 1010-1080 and 1180-1190 cm^{-1}, while HSO_4^- absorbs at 1090-1120 cm^{-1}. The amount of -CH_2- groups present in the coating resins is assumed to remain unchanged, so for better comparison all FTIR spectra were scaled after the peak at 1450 cm^{-1}. Table 3.9 on hydrolysis reactions in resin functional groups was used to analyze the changes observed in the absorbance spectra, also plausible chemical changes in fillers and pigments were considered.

11.1 Vinyl ester (VE)

Vinyl ester resins contained ester and ether groups, both of which can hydrolyze causing a reduction in C-O signal and and increase in the O-H signal. This trend was found for O-H signals at 3400 cm^{-1}, ester absorption at 1715 and the C-O signal at 1242 cm^{-1}. Though the O-H absorbance can be caused by water remaining in the film. Signals from sulfur compounds can account for the increases at 1105 and 1037 which covers the remaining C-O signals.
There was evidence that hydrolysis reactions have taken place in the vinyl ester coating to some extent, but he reactions were not severe enough to remove the ester or ether signal, only a slight reduction was observed.

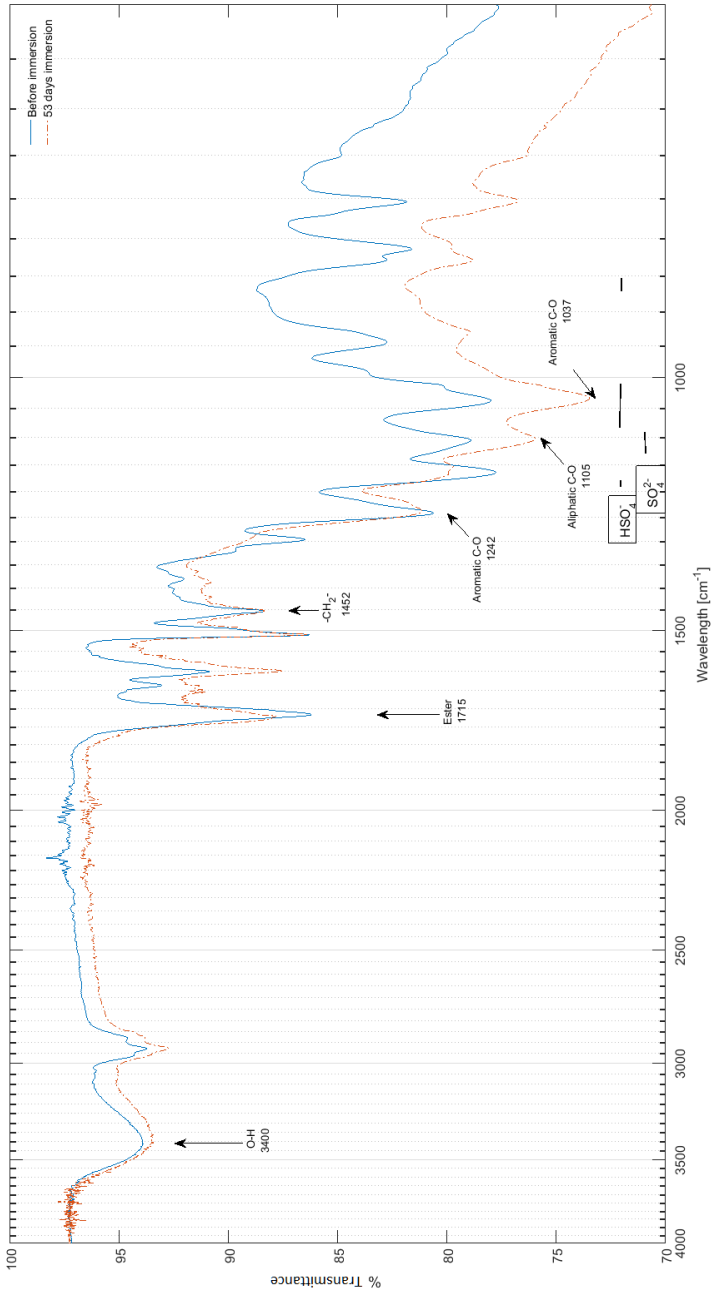

Figure 11.1: FTIR spectra of vinyl ester (VE) coating before and after 53 days immersion in Harsh conditions. The spectra were scaled after the -CH_2- peak.

11.2 Polyurethane (PU)

The polyurethane resin contained urethane linkages, which can be observed in IR as amine and ester bonds. The virgin sample showed evidence of primary, secondary and tertiary amines. Tertiary amines have been reported to hydrolyze to primary amines, and to create tertiary amine salts in sulfuric acid. Thus expected changes due to reactions with the sulfuric acid include: reduction in ester and C-O signal at 1725, 1242, 1105 and 1037 cm^{-1}, reduction in tertiary amines at 1375 cm^{-1}, increase in primary amines at 3400, 1625, 1080 and 800 cm^{-1}, and increase in tertiary amine salts around 2550 cm^{-1}.

This, however, was not entirely the case. Primary and secondary amine salts can account for some absorbance increases at 3000, 1600 and 1525 cm^{-1}. Intensities for regular primary and secondary amines also increased at 1600, 1220, 1160 and 700 cm^{-1}, while tertiary amine signal at 1375 cm^{-1} was reduced. No tertiary amine salt was observed. This could indicate a loss in tertiary amines, a combined loss-creation of secondary amines, and an increase in primary amine to bond scissoring. It could also indicate a production of primary and secondary amine salts as a result of reactions with the sulfuric acid.

With regards to ester hydrolysis, there was an increase in O-H absorption, but there was no reduction C-O related absorbtion spectra. Quite the opposite happened, as the ester frequency 1725 cm^{-1} increased dramatically. Increases in C=O bonds raised this frequency but no reported reaction mechanisms can account for this change.

The signal for calcium carbonate fillers at 1435 and 875 cm^{-1} completely disappeared after acid exposure due to reactions with sulfuric acid. Little evidence of calcium sulfate is found in the exposed sample, thus it was assumed to be dissolved and removed from the coating.

It seems counter-intuitive that reactions with amines are occurring in the film while the ester linkage remain unchanged. A possible reason is that reactions with esters have been sterically hindered, as happens in the vinyl ester, and thus reactions with amines occur at a much faster rate.

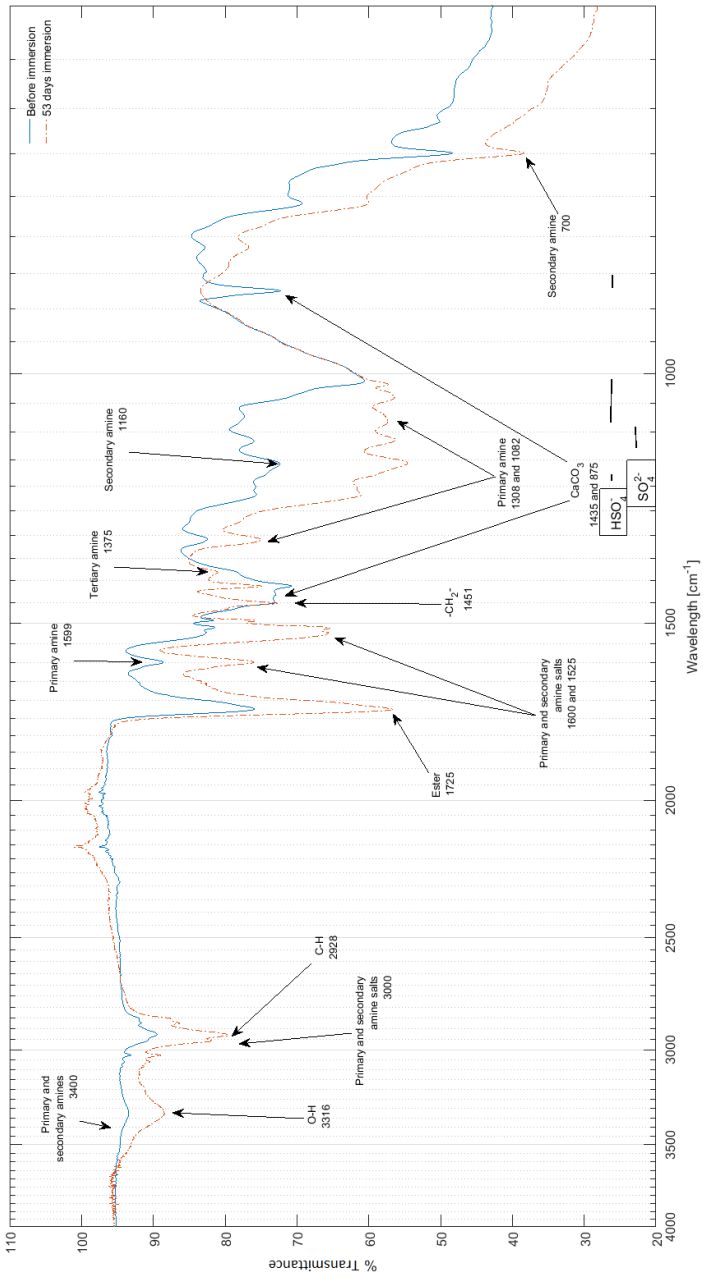

Figure 11.2: FTIR spectra of polyurethane (PU) coating before and after 53 days immersion in Harsh conditions. The spectra were scaled after the $-CH_2-$ peak.

11.3 Novolac 100% solids (NE1)

Amine cured novolac epoxies contained amine and ether linkages. The ether can hydrolyze to alchohols reducing the C-O and increasing the O-H absorbance, while the amines can be reduced in power from tertiary to primary and become salts.
There was significant growth for O-H absorption at 3300, 1080 cm^{-1}, this could be due to ether cleavage or water remaining in the film surface. Furthermore, C-O absorption was reduced at 1240 cm^{-1} as would also occur for ether cleavage, but then it increases greatly at 1030 cm^{-1}, which could be explained by the addition of acid sulfate in the coating. This hinted towards a hydrolysis of ether bonds, but it was not overwhelming evidence.
It is curious that a significant peak rises at 1725 cm^{-1} after acid immersion. This peak accounts for C=O absorption as found in ester bonds. However none of the reaction mechanisms presented in literature can account for the creation of esters, ketones or aldehydes.
All absorption areas for primary amines 3400, 1600, 1310 and 1080 cm^{-1}, increased. However, so did tertiary and secondary amine absorption peaks. It would make sense to observe a reduction in tertiary amines to create the secondary and primary amines. If this was the case, another species would be affecting the tertiary amine absorbance at 1375 cm^{-1}. When it came to the production of amine salts, the absorption peaks were not in agreement. Only the secondary amine salt absorption at 1600 cm^{-1} increased, but the remaining peak at 3100 cm^{-1} did not show. Also, all the expected signal increases for primary salts 3000, 1590 and 1525 cm^{-1}, were not present. Thus no indication of amine salts was found, such as was the case for polyurethane. This did not provide compelling evidence for amine hydrolysis or amine salt production in the coating.
IR spectra did not provide a clear picture of what is happening in the resin in relation to what one would expect based on published literature.

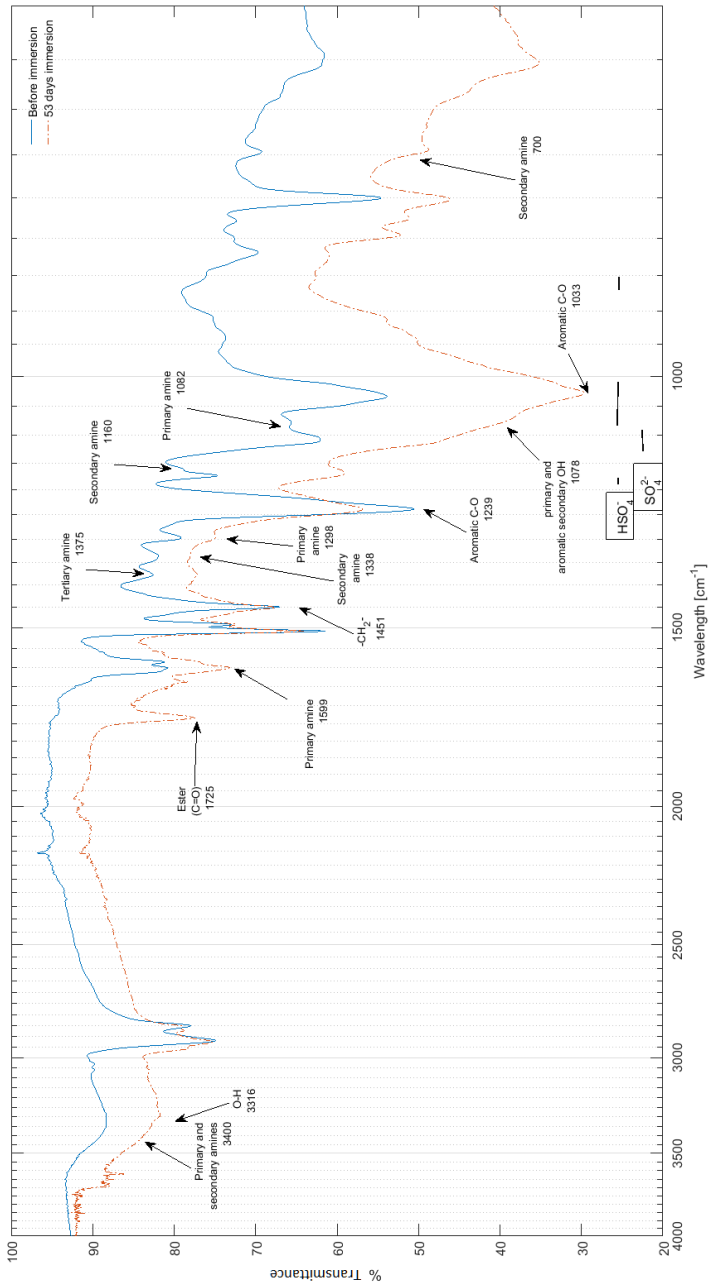

Figure 11.3: FTIR spectra of 100 % solids novolac epoxy (NE1) coating before and after 53 days immersion in Harsh conditions. The spectra were scaled after the -CH_2- peak.

11.4 Novolac epoxy (NE2)

The NE2 resin was made of the same building blocks as NE1. With possible chemical changes including scissoring of ether or amine bonds and the creation of amine salts.
The C-O absorbance at 1240 cm^{-1} was slightly reduced, indicating a reduction of these bonds, while at 1033 cm^{-1} it increased greatly, due to sulfur compounds in the film. The O-H absorption also increased at 3320 cm^{-1}, likely due to water in the film. Similar to the polyurethane and NE1 sample, NE2 showed a peak increase at 1725 cm^{-1} accounting for C=O bonds.
For amines, there was a reduction in the amount of primary amines at 1600, and 1300 cm^{-1} while the sulfur obscured area of 1080 cm^{-1} showed an increase. There was a slight reduction in secondary amines at 1340 cm^{-1} and a great increase at 1160 cm^{-1} which was influenced by sulfur. Tertiary amine absorbance at 1375 cm^{-1} remained unchanged.
There is some evidence towards ether scissoring with a reduction in C-O and an increase in O-H absorption. No reduction in tertiary amines or evidence of amine salts. Only primary and secondary amine absorption wavelengths were reduced.

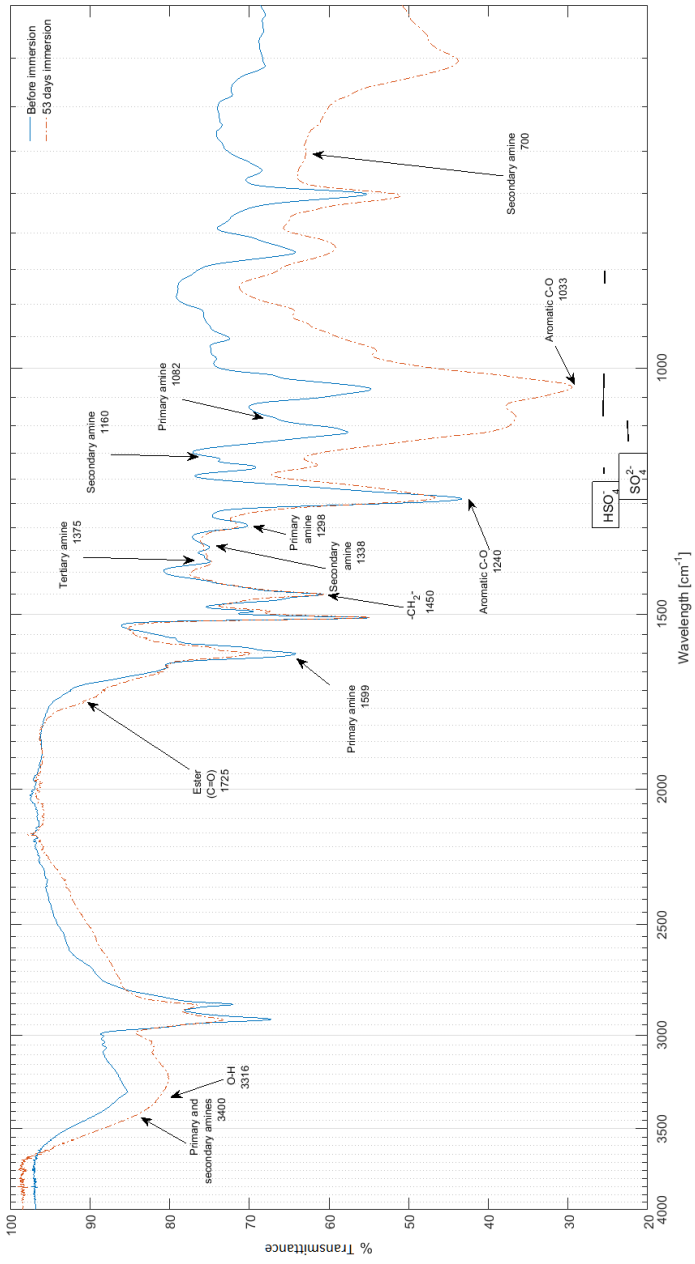

Figure 11.4: FTIR spectra of novolac epoxy (NE2) coating before and after 53 days immersion in Harsh conditions. The spectra were scaled after the -CH_2- peak.

12 Coating cross-section analysis

An attempt was made at determining sulfuric acid penetration depth by observing the S-element signal of free coating film cross-sections using SEM combined with EDS, using free-film samples which were immersed in Harsh conditions up to 53 days. This proved more challenging than expected.
The VE coating showed no detectable S-element front. The PU and NE1 coating contained Barium sulfate filler, which clouded the S-element signal. None of the samples showed an observable front of Cu ions either. It was also attempted to look for the disappearance of Calcium ions in PU, but the search did not prove fruitful. Only the NE2 coating showed a detectable uptake of sulfur. The sulfur diffusion happens so fast in NE2 that only the sample immersed for the shortest amount of time, two hours, was able to show a sulfur diffusion front with a penetration depth of approximately 170 μm, see Fig. 12.1. Another sample was immersed for seven hours and was fully saturated with sulfur. It is noticeable from Fig. 12.1 that cracks are appearing in the film within the sulfur rich regions, denoted degradation zone. This is similar to the corroded layer type 1 or 2 mechanism shown in Fig. 3.11.

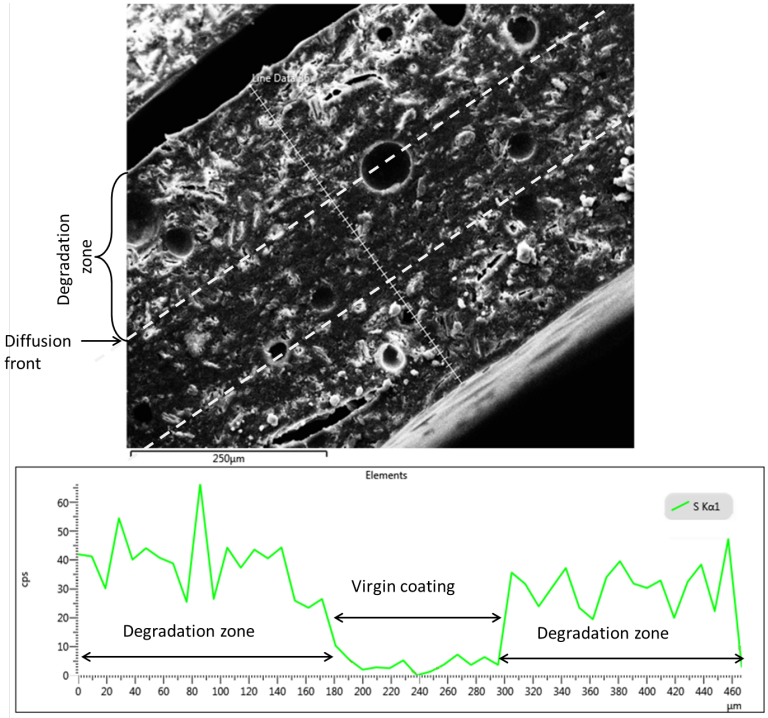

Figure 12.1: SEM image (top) of a cross section of NE2, immersed for two hours in Harsh conditions, the dashed lines represent the sulfur diffusion front. The line-scan (bottom) shows the sulfur intensity across the film.

13 Discussions and conclusions

The weight change, visual observations, FTIR and SEM analysis provided an overview of the barrier properties and chemical resistance of the coatings tested.

The VE had a higher weight uptake in Mild than in Harsh conditions, thus showing a better performance at low pH. The weight uptake in either condition was low and the coating was never fully saturated. Together with no detectable S element in the coating after 53 days it indicated good barrier properties. Only a slight darkening of the samples occurred during immersion, no blisters or delamination. The FTIR showed a slight reduction in ester groups, which might indicate a hydrolysis of this group at the film surface. All in all, excellent barrier properties and high chemical resistance in both environments.

The PU lost weight in Mild conditions, likely due to solvent leaching from the film. This weight drop was increased in Harsh conditions due to the added dissolution of calcium carbonate fillers, as seen in the FTIR spectra. A mild darkening occurred in Harsh conditions while slight sporadic blistering occurred in Mild conditions. FTIR also provided evidence of loss of tertiary amines, and a production of secondary and primary amines and amine salts. Secondary and primary amines are likely produced by cleavage of tertiary amines. Also, an unexplained buildup of C=O bonds was observed. The PU showed decent barrier properties based on weight changes, and exhibited average chemical resistance despite the dissolution of calcium carbonate filler in Harsh conditions.

The NE1 gained weight in Mild conditions followed by a drop, likely due to initial water diffusion followed by a gradual leaching of unreacted components. In Harsh conditions the NE1 barrier properties were greatly reduced as it gained on more than 12% in weight. A weakness to the low pH environment was also seen in immersion panels, where the sample discolors from blue to brown and delaminated after around 13 days. However, the FTIR spectra did not provide a clear picture of what is happening in the resin in relation to what one would expect, based on published literature. The NE1 has excellent barrier properties and chemical resistance in Mild conditions, but poor barrier properties and chemical resistance in Harsh conditions, due to unknown reactions with the environment.

The NE2 starts out loosing weight in Mild conditions, indicating a rapid leaching of unreacted components out of the film, together with liquid diffusing into the film. Performance in Harsh conditions includes heavy blistering after 17.5 hours, and a large weight increase. The SEM image of the coating cross-section verifies a rapid sulfur diffusion and deterioration of the film. This is indicative of a reaction happening between the solution and coating, though predictions of exactly what happens in the film was not clear from FTIR analysis. The NE2 performs similar to NE1, with excellent performance in Mild conditions, but poor barrier properties and chemical resistance in Harsh conditions due to chemical reactions with the environment.

Part III

Simultaneous chemical and erosive exposure in a pilot-scale agitated leaching tank

The initial project aim was to study the use of acid resistant coatings in the mineral industry, to bridge the knowledge gaps by learning more about coating failure mechanisms, and to generate research and results that would be of relevance to the coating end-user. Agitated acid leaching of copper ore was chosen as a case study. It provided an environment in which a coating would be exposed to warm sulfuric acid, and erosive slurry flows simultaneously. The research became focused on investigating the effects of acid exposure on coating polishing rates, and determining coating lifetimes in such conditions.

A pilot-scale replica of an agitated leaching tank was built in collaboration with FLSmidth A/S for coating exposure. The current part provides details of this set-up, analysis equipment, experimental results, coating degradation mechanisms, and lifetime estimations. A compressed version of this part can also be found as a journal article [143].

Nomenclature

d	Diameter [m]
g	Gravitational acceleration [m/s^2]
n	Rotations per unit time [Rot/s]
N_{js}	Minimum stirring required to achieve full particle suspension [Rot/s]
Ne	Power number
P	Effect [W]
r	Radius [m]
Re	Reynolds number
S	Constant determined by impeller and reactor geometry
x	Radial distance $\frac{a}{r_r}$ from reactor center where $0 \leq a \leq r_r$
X	Weight fraction particles

Subscripts

i	Impeller
l	Liquid
p	Particle
r	Reactor

Greek lettering

η	Viscosity [Pa·s]
ν	kinematic viscosity [m^2/s]
ρ	Density [mol/m^3]

List of Abbreviations

CSTR	Continuously stirred tank reactor
DFT	Dry Film Thickness
EDS	Energy-dispersive X-ray spectroscopy
IR	Infra-red
PI	Piping and instrumentation
PSD	Particle size distribution
RPM	Rotations per Minute
SEM	Scanning Electron Microscopy
STP	Standard temperature and pressure (23 °C and 1 atm)
UV	Ultraviolet

14 Analysis equipment

Short description of the analysis equipment used throughout the pilot-scale reactor experiments.

14.1 Inductive magnetic gauge

An inductive magnetic gauge can detect the film thickness of a non-conductive coating on top of a metallic substrate. This is done by inducing a magnetic field and measuring the resultant voltage generated, which a function of distance between the probe and the substrate. Fig. 14.1 shows an image of the Elcometer 355 with coating thickness standards used in the current project.

Figure 14.1: Elcometer 355 magnetic gauge, with coating thickness standards.

Different probes are required depending on the substrate being magnetic or non-magnetic, in the current project stainless steels are used as substrates, which are non-magnetic.
The non-ferrous probe induces Eddy currents in the coating and substrate by exposing them to an alternating magnetic field. The Eddy currents themselves create an opposing magnetic field, which is sensed by the probe by providing a measurable voltage output. When increasing the separation distance between the substrate and the probe, the magnitude of the Eddy currents drop, decreasing the magnitude of the opposing magnetic field and thus the measurable output voltage in the probe.
By performing a two-point calibration, one on the bare substrate and one using a thickness standard, it is possible to accurately measure the thickness of non-conductive coatings on non-ferrous samples. But the Elcometer was not entirely accurate, and would deviate systematically from actual thickness values both above and below the thickness standard used for calibration. However, this deviation was systematic and predictable, therefore a correction factor was included in the data treatment to express the actual thickness values. The details of determining this correction factor is detailed in Appendix C.

14.2 Mastersizer

To rapidly determine a particle size distribution (PSD), the Malvern Mastersizer 3000 was used, shown in Fig. 14.2. The Mastersizer uses the principles of laser defraction to determine the mean spherical

diameter of particles in the range 3500 μm to 0.10 μm.

Figure 14.2: Malvern Mastersizer 3000 with liquid dispersion attachment. Capable of determining PSD using laser defraction.

Proper sampling is essential to obtain a realistic PSD, and this can be a challenge when the particles in question vary between rapidly settling and slow settling particles. Therefore, particle samples are gathered while stirring. Particles are separated from their original solution, by suction filtration, washed with distilled water, and stored dry until analysis.
The particles were suspended in distilled water using a stirring rate of 3000 RPM in the Mastersizer. To determine an accurate PSD of particles below 50 μm the particles refractive index is required. However, the processed particle mass is a mixture, and does not have a uniform refractive index. Instead the a single value of 1.540 is used, which is the refractive index of Chalcopyrite ($CuFeS_2$), the main component in the particulate mixture. This limits the usability of master sizer results to precisely predict the actual PSD, since transparent particles such as quartz are underrepresented, but still allows an observation of net changes in the mixture since Chalcopyrite exists in much greater quantities, see Table 15.1.

14.3 UV absorbance

The Agilent Cary 60 UV-Vis was used to determine the concentration of the clear blue Cu(II) sulfate in leaching solutions. It uses the principles of absorption spectroscopy, sending ultraviolet (UV) light at a given wavelength through a liquid sample, and observing the amount of light absorbed by the specimen.
Cu(II) sulfate was measured using wavelength of 810 nm. To relate the relative absorbance to actual Cu(II) concentrations, a series of standards were prepared, each individual sample with known concentrations of Cu(II) by dissolving copper sulfate pentahydrate ($CuSO_4(H_2O)_5$) in 1.0 M sulfuric acid solution. The resultant curve and linear fit are shown in Appendix D.
Prior to measurement, the machine was zeroed using a 1.0 M solution of sulfuric acid and samples are filtered from all obscuring particles.

15 Agitated leaching process and replication in pilot-scale

Agitated leaching of copper rich minerals was used as the case study for testing coatings in acidic conditions in the mineral industry. It was chosen due to the unique conditions created inside such reactors. These conditions include elevated temperatures (75-80 C°) [144], pH values below 1, and the presence of an erosive particle flow. It is an environment in which all three degradation mechanisms, reaction, diffusion and erosion can be experienced simultaneously. Through talks with FLSmidth specialists in the field, it is know that organic coatings have been implemented in some leaching tanks, also that coating failure is mainly caused by erosive forces, which is most severe on the tank bottom. This section provides an overview of the industrial agitated leaching process and how it was replicated in a pilot-scale set-up for coating experimentation.

15.1 Agitated leaching process

Agitated leaching is a hydrometallurgical process that takes place after mineral rich ore has been liberated through crushing and grinding, and the mineral-containing particles have been separated from the bulk by flotation. The feed to agitated leaching tanks includes a copper concentrate from flotation separation, a sulfuric acid solution, and air. The product is a depleted particle mass, and a pregnant liquid containing the clear blue copper sulfate. Fig. 15.1 shows a series of industrial scale leaching tanks, while Fig. 15.2 provides a cross-sectional description of a single leaching reactor. After the leaching process, the particle mass is separated in a thickener, and the dissolved copper is removed using liquid-liquid extraction. Finally pure solid copper sheets are produced from the copper-containing liquid in an electrowinning process [18, 145].

Figure 15.1: A series of industrial scale agitated leaching tanks for processing mineral ore, located in Cochrane, Ontario, Canada. Courtesy and copyright Fournier Indsutries. Observe the truck in the bottom right hand corner for scale.

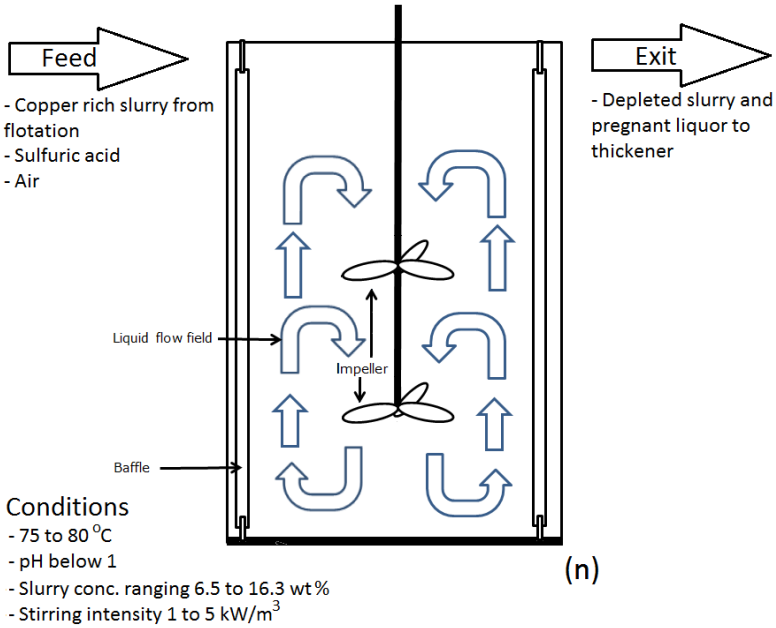

Figure 15.2: Overview of a typical leaching reactor. Multiple leaching reactors are placed in series, each reaching individual equilibrium conditions. The number of reactors required depends on the feed and reactor design decisions, and is denoted "n". Flow field estimated from [146].

Agitated leaching is an important step in mineral recovery, and is taking the place of heap leaching processes, where the leaching agent is sprayed over a heap of mineral containing ore, and autoclave leaching performed at high temperature and pressure [144]. Copper sulfide minerals, which are challenging to process, can be leached rapidly in the agitated leaching process, because elevated temperatures and stirring helps to remove the passivating film that forms on the minerals and slows the dissolution reaction [147]. Leaching of chalcopyrite occurs mainly via Eqn. 8, where Cu(II) is the desired product [148]. The reaction is possible at low pH and high electrochemical potential, as shown in a Pourbaix diagram Fig. 15.3 for chalcopyrite, top left corner.

$$CuFeS_2 + 4Fe^{3+} \longrightarrow Cu^{2+} + 5Fe^{2+} + 2S^{\circ} \tag{8}$$

Agitated leaching reactors are typically placed in series, as shown in Fig. 15.1, with each tank at its own equilibrium conditions. The tanks can range in size from 28 to 1000 m^3 (3 to 10 m in diameter) depending on the feed volume. The stirring intensity in a tank is above the requirement for full particle suspension, and is typically around 1 to 5 kW/m^3 [148]. A dual impeller system is used for stirring, a Lightnin A310 above a Lightnin A315. Baffles are present to prevent vortexing and air is bubbled through, to provide oxygen for controlling the electrochemical potential of the solution. The solids load in these reactors will also vary depending on copper mineral content. When the copper purity is 21 wt%, a 6.5 wt% solids in the reactor is needed, while 7.6 wt% copper purity requires 16.3 wt% solids in the reactor [144]. The particles themselves change over time as they are being leached, the solids

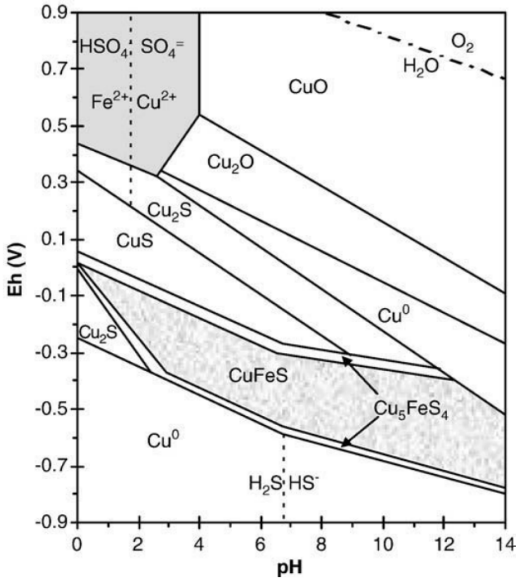

Figure 15.3: Pourbaix diagram of chalcopyrite in water, with the desired leaching product Cu(II) available in the top left corner [149].

weight fraction is decreased depending on the copper purity of the ore, the leaching takes around 6 hours to complete for more modern operations [148]. Solids feed to agitated leaching reactors consists of an up-concentrated mixture of calcopyrite, with zinc and iron sulfides and oxides, and insoluble quartz.

15.2 Pilot-scale replication

With no similar work published on the subject and no pre-existing set-up to use, the entire construction was designed and build from scratch. The only existing knowledge of coating performance was that failure was typically caused by wear in the tank bottom. Without a firm literature basis for ruling out the effects of chemical exposure on coating wear rate, and knowing temperature can have great effects, both factors had to be included. The pilot-scale reactor was aimed at replicating the most important process conditions for coating experimentation. This included the acidic chemicals, elevated temperatures and erosive conditions, while leaving out the air bubble injection used to promote leaching.

Chemical exposure and erosive conditions are challenging to replicate. For erosive conditions, the flow field inside the agitated leaching reactor needs to be the same to provide the same particle impact efficiency, impingement angle and speed. Furthermore, the erosive particles themselves need to have the same shape, relative hardness, density, concentration and PSD as in practice, to be representative of leaching operations. For chemical exposure, the pilot-scale reactor had to keep constant pH and Cu(II) concentrations to replicate conditions in a single tank. This was a challenging as the chalcopyrite would leach and alter the solution chemistry. Investigations into changes in erosive particles and chemical

environment were performed throughout reactor experiments and can be found in Appendix E.

15.2.1 Erosive environment

To emulate the same erosive conditions in terms of particle hardness, shape, PSD, density, and composition, the same copper concentrate was used for pilot-scale experiments, as in industrial processes. However, a pre-leaching was performed on the particles to decrease the effects of chalcopyrite leaching. This was deemed necessary when comparing experiments using an acidic and a more neutral liquid solution, presented later on.
Pre-leaching was performed by mixing the copper concentrate particles with 0.15 M sulfuric acid, with agitation, at STP, for 24 h. It was deemed necessary after small-scale leaching experiments in stirred Erlenmeyer flasks revealed, that the majority of the erosive particles are leached withing the first 13 h of exposure to sulfuric acid.
Fig. 15.4 shows the result of two small-scale experiments that were carried out to investigate the weight loss of particles. The particles were dried in an oven at 100 °C overnight to determine initial dry weight. In both experiments 20 wt% dry particles were immersed in 0.15 M H_2SO_4 with stirring. One experiment was performed at ambient temperature while the other was heated to 45±3 °C. The particle weight loss was measured by filtering the slurry after exposure, and drying the resulting particle cake at 70 °C for 24 h, before weight measurement. It was found that weight loss of particles plateaued after around 13 h exposure, and that heating sped up this procedure, but did not change the plateau. Since the pre-leaching lasted 24 h, the main particle mass loss occurred during this procedure.

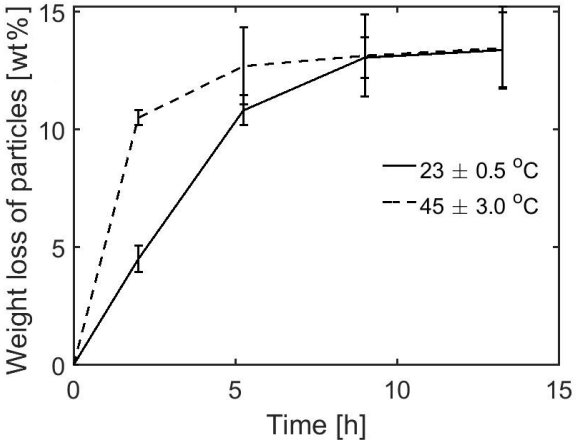

Figure 15.4: Weight change of erosive particles in 0.15 M H_2SO_4

Fig. 15.5 shows the shape of pre-leached particles, and Table 15.1 describes their relative composition. The pre-leached copper concentrate consisted mainly of chalcopyrite, with lesser amounts of zinc, iron, silicon and aluminum species. The shape was mostly chipped with medium sphericity, and the mean spherical diameter was 17.1 μm.

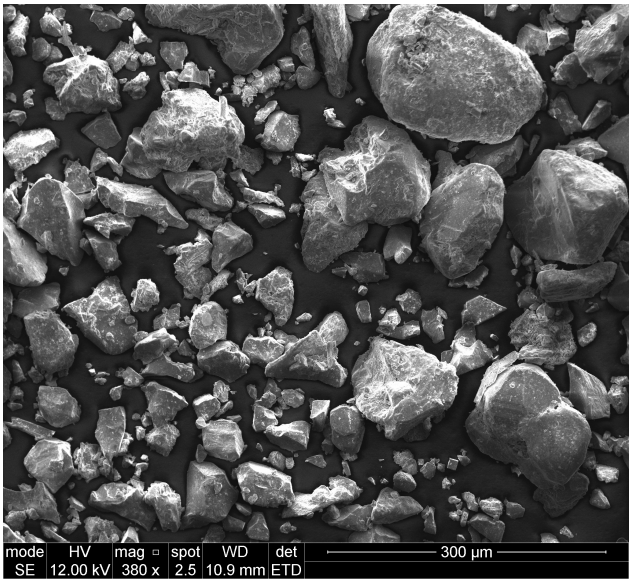

Figure 15.5: Copper concentrate particles after pre-leaching.

Table 15.1: Elemental composition of the feed particles used as erosives in the pilot-scale leaching reactor. With plausible mineral compositions and corresponding weight percentage. Obtained by EDS analysis in an SEM. Weight % values below 1.0 have been omitted.

Element	Fe	S	Cu	O	Zn	Si
Weight %	27.5	26.5	24.0	15.7	4.1	1.1
Suggested compositions	$CuFeS_2$	FeS_2	SiO_2	ZnO		
Weight %	84.9	5.3	2.9	6.3		

The particle concentration used for experimentation was 18 wt% after the pre-leaching, which is slightly higher than the maximum reported literature values of 16.3 wt%. This is due to an expected loss of particles throughout the experiment caused by leaching, sampling and reactor cleaning.

15.2.2 Chemical environment

In the agitated leaching process of copper, sulfuric acid is used to adjust the slurry pH below 1.0. The same was done in the pilot-scale reactor, where pH was monitored and adjusted using either concentrated sulfuric acid or sodium hydroxide pellets to fit the experimental parameters.
Full-scale reactors bubble air into the tank to promote the leaching kinetics. It was chosen not to do this in the pilot-scale leaching reactor, as it was desired to maintain a constant weight fraction of particles and not speed up the leaching process.

15.2.3 Downscaling of an industrial leaching reactor

The pilot-scale set-up was made to mimic the conditions inside an agitated leaching reactor and allow the user to remove and insert coating samples for continuous analysis. The relative sizes of the tank, impeller and baffles are the same as what one would observe in a full-scale agitated leaching reactor. Fig. 15.6 shows some of these sizes relative to the impeller diameter, which is 130 mm for the pilot-scale reactor.

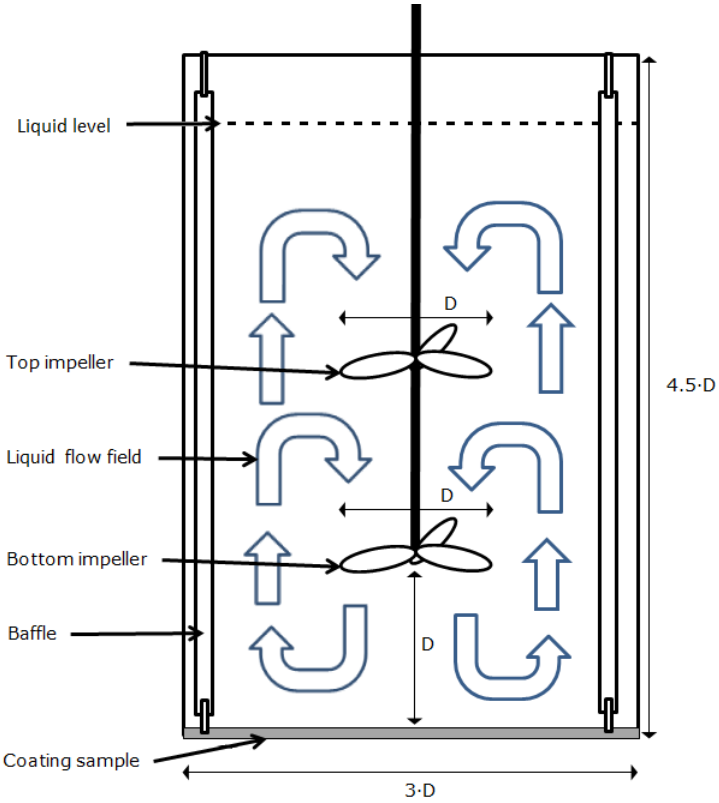

Figure 15.6: Cross-sectional diagram of the leaching reactor. The liquid flow fields are caused by the axial pumping impellers, as described in reference [146]. Relative dimensions are given with respect to the impeller diameter D=130 mm. The reactor is filled to 90% capacity.

The impellers used were specialized for suspending particles by pumping the slurry axially towards the reactor bottom. The top impeller is a Lightnin A310, the bottom impeller is a Lightnin A315, same as used in industrial processes. Radial flow is also present, but vortexing is avoided by the presence of baffles. A stirring intensity of 3.7 kW/m^3 was chosen for this study, corresponding to a mixing speed of 1000 RPM. This provides turbulent flow in the pilot reactor, same as full-scale leaching reactors. Table 15.2 shows a comparison of mixing conditions of a full-scale and the pilot-scale tank.

Table 15.2: Comparison of mixing conditions in a pilot-scale reactor with a tank diameter of 0.4 m and a small full-scale reactor with a tank diameter of 3 m, both with a stirring intensity of 3.7 kW/m^3.

Scale (volume)	Impeller diameter [m]	Impeller tip speed [m/s]	Re of tank[a]	Suspension, RPM [min^{-1}] [a]	RPM [min^{-1}] at 3.7 kW/m^3 [a]
Pilot-scale (68 l)	0.13	6.8	$8.4 \cdot 10^5$	360	1000
Full-scale (28600 l)	1.05	12.7	$1.3 \cdot 10^7$	60	230

[a] The power contribution of each impeller used to derive these values, were calculated separately using equations for single impeller systems [150, 151].

The stirring required for full particle suspension is calculated via the Zwietering's correlation [151], in Eqn. 9. The Renaults number for the tank is found via Eqn. 10. The power distribution on the two impellers are estimated by Eqn. 11 [150].

$$N_{js} = \frac{S\nu d_p^{0.2}(g\Delta\rho/\rho_l)^{0.45}X^{0.13}}{d_i^{0.85}} \tag{9}$$

$$Re = \frac{\rho n d_r^2}{\eta} \tag{10}$$

$$Ne = \frac{P}{\rho d_r^5 n^3} \tag{11}$$

15.3 The pilot-scale set-up

With the geometric ratios, mixing, erosion and chemical conditions in check, it was possible to construct a set-up capable replicating the conditions inside an industrial leaching tank, while allowing safe insertion and removal of coating samples. Fig. 15.7 shows the set-up with raised and lowered lid.
During experimentation the set-up was in closed position, with the reactor containing the warm acidic slurry and the coating samples. When the coating samples needed to be analyzed, the acidic slurry was transported to the storage tank and the reactor was washed internally to remove trace acids. The wash water was flushed to the dump tank. The lid was then raised and the reactor moved to the open position, allowing access to the coating samples inside. The entire set-up was placed inside a fume-hood, on top of a plastic bath to contain acidic vapors and liquid spills.
A detailed PI diagram can be found in Fig. 15.8.

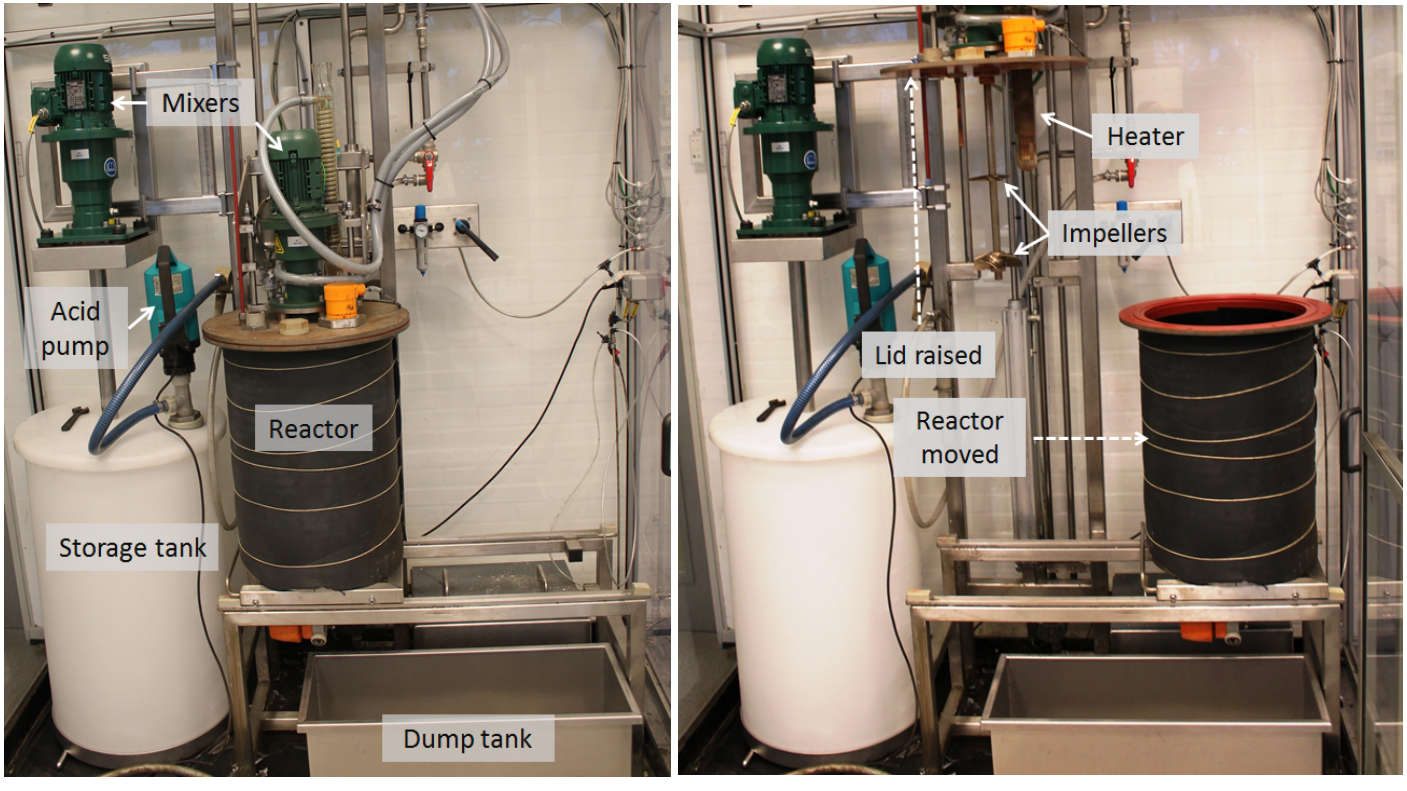

(a) Closed lid position.

(b) Open lid position.

Figure 15.7: The pilot-scale set-up. Experiments are run in the closed position. The lid can be lifted via a pneumatic crane, and the reactor can be moved to the side, allowing access to the samples inside. The set-up is placed inside a fume-hood.

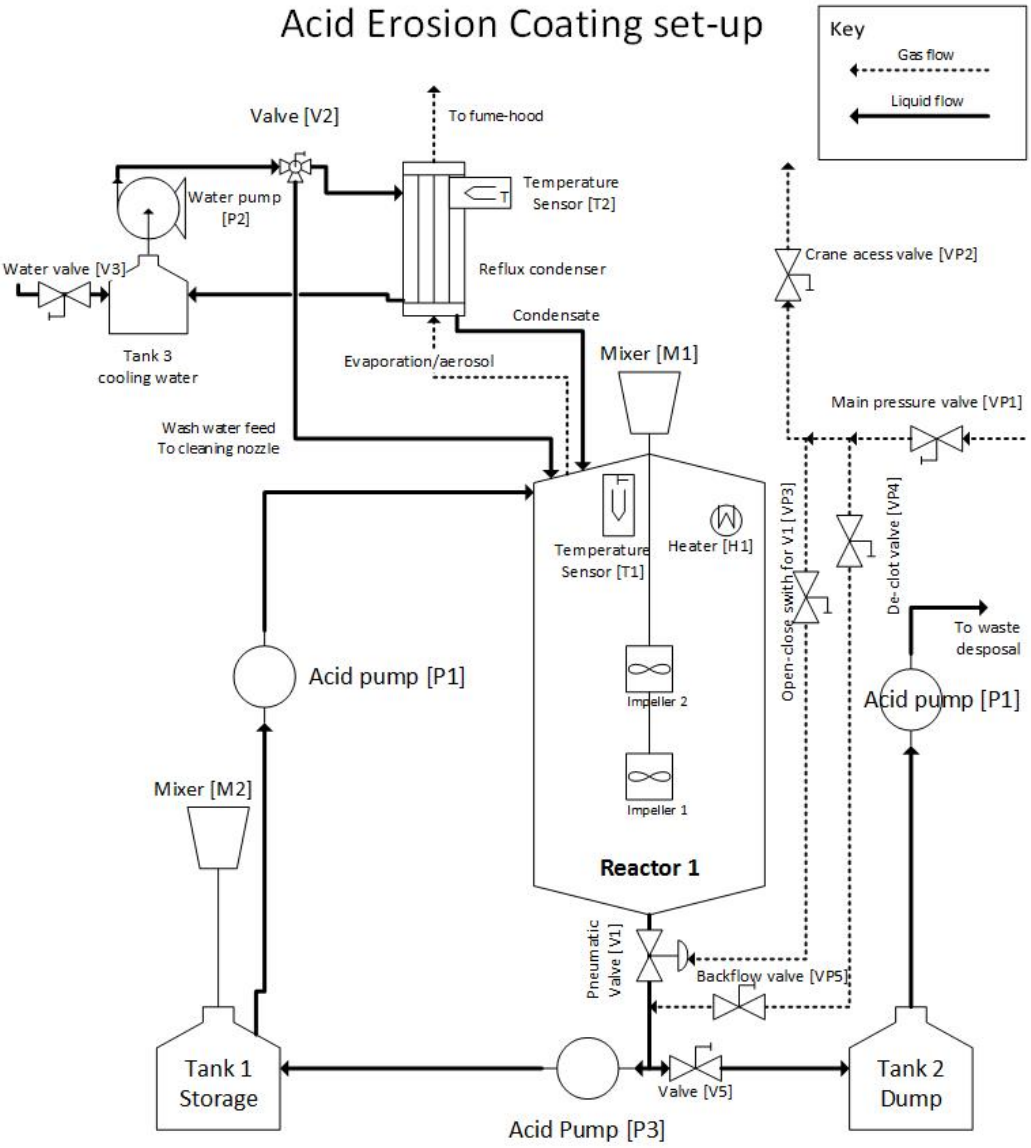

Figure 15.8: Pipe and instrument diagram of the pilot-scale leaching set-up.

15.4 Samples and DFT measurement

Coating sample substrates for the reactor were quarter circles with a side length of 200 mm and a thickness of 4 mm, made of an acid resistant stainless steel type 316 L. The coatings were spray applied on both sides to the substrate, and brush applied on sample edges. The coated samples were inserted into the bottom of the reactor as seen in Fig. 15.9, and fastened using the baffles and a threaded center piece. A total of four different samples were run simultaneously.

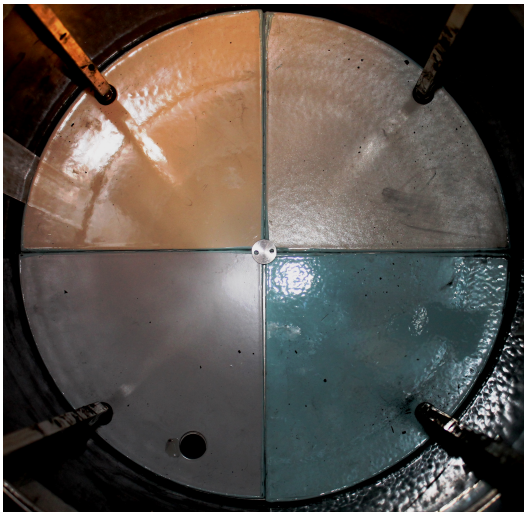

Figure 15.9: Four different coating samples inside the reactor. Each sample can be removed and re-inserted into the reactor when empty.

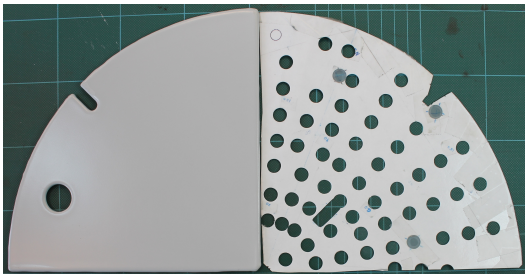

Figure 15.10: Reactor sample shown along side the guiding DFT measurement template.

An Elcometer 355 with a non-ferrous probe is used for DFT measurement of the reactor samples for each consecutive measurement campaign. A template was used to ensure DFT measurements were performed on the same places on the coating samples, shown in Fig 15.10. Using this template allowed tracking of DFT changes in specific locations, throughout an experiment. The template was made to allow detection of systematic differences in DFT change, for both radial and tangential directions on the sample.

16 Experimental conditions and procedure

Two experimental series were performed, one using harsh conditions mimicking those found in industrial leaching tanks, and and one with milder conditions at elevated pH. Table 16.1 provides an overview of the "Harsh" and "Mild" conditions.
Before experiment start, DFT readings were performed and photographs were taken of all coating samples. The reactor was filled with the desired solution and pre-leached particles were added to the liquid, where after the slurry was heated to 75 °C. The slurry was then pumped into the storage tank, the reactor lid was opened and coating samples were inserted. The reactor lid was closed and the

Table 16.1: Reactor experimental conditions overview. All experiments were performed at 75 °C, with a stirring intensity of 3.7 [kW/m^3] (1000 RPM), and a particle load of 18±2 wt%. Harsh conditions are meant to imitate the chemical environment in a real life leaching reactor. Mild conditions are meant as experiments without the stress of low pH exposure.

Condition	**Harsh**	**Mild**
H_2SO_4 [mol/l]	0.1±0.038	$5 \cdot 10^{-3} \pm 4.9 \cdot 10^{-3}$
pH	1.03±0.17	3.5±1.5
Cu(II) [g/l]	8.4±6.3	0.88 ± 0.88

slurry was pumped back into the reactor to start the experiment. After a given time interval, usually seven days, a measurement campaign was performed. This involved emptying the reactor slurry into the storage tank, and washing the reactor insides with tap water. The coating samples were removed from the reactor and dried using paper towels, followed by DFT measurement and photographs. The samples were then re-inserted into the reactor and the lid was closed. The reactor was filled with the slurry from the storage tank and the mixer was turned on to continue the experiment. For a very detailed description of the set-up, including reactor filling, washing, and emptying procedure, the set-up control box, and materials selection see Appendix F.

17 Reactor results

This section shows the experimental results from the pilot-scale reactor: The observed DFT changes of coating reactor samples, compared with DFT changes of immersion samples described in Section 7.

17.1 Coating failure

Fig. 17.1 shows the reactor samples after experimentation. Coatings NE2 and NE3 were unable to stay intact long enough to gather useful data. Under Mild conditions blisters were found on NE2 obscuring erosion effects, while in Harsh conditions NE2 delaminated rapidly. NE3 degraded and delaminated within the first day in both conditions. The NE1 coating delaminated after around 15 days under Harsh conditions, so DFT data could be obtained until the failure occurred. The turbulent liquid flow stripped the reactor samples of all coating after failure.

17.2 Mild condition erosion

DFT changes for immersion experiments represent the change caused by chemical exposure alone, while reactor experiments include both chemical and erosive effects. The difference between erosive and immersion DFT changes, if any, is a result of coating wear. Potential water erosion was also investigated, and found to be negligible, shown in Appendix G.
In Fig. 17.2, DFT changes of the PU, NE1 and VE coatings in immersion and reactor experiments under Mild conditions are shown. Note that each point represents the average thickness change relative to the virgin coating, across the entire sample. Large uncertainties in reactor samples are caused by an inhomogeneous erosion, discussed in Section 17.4.

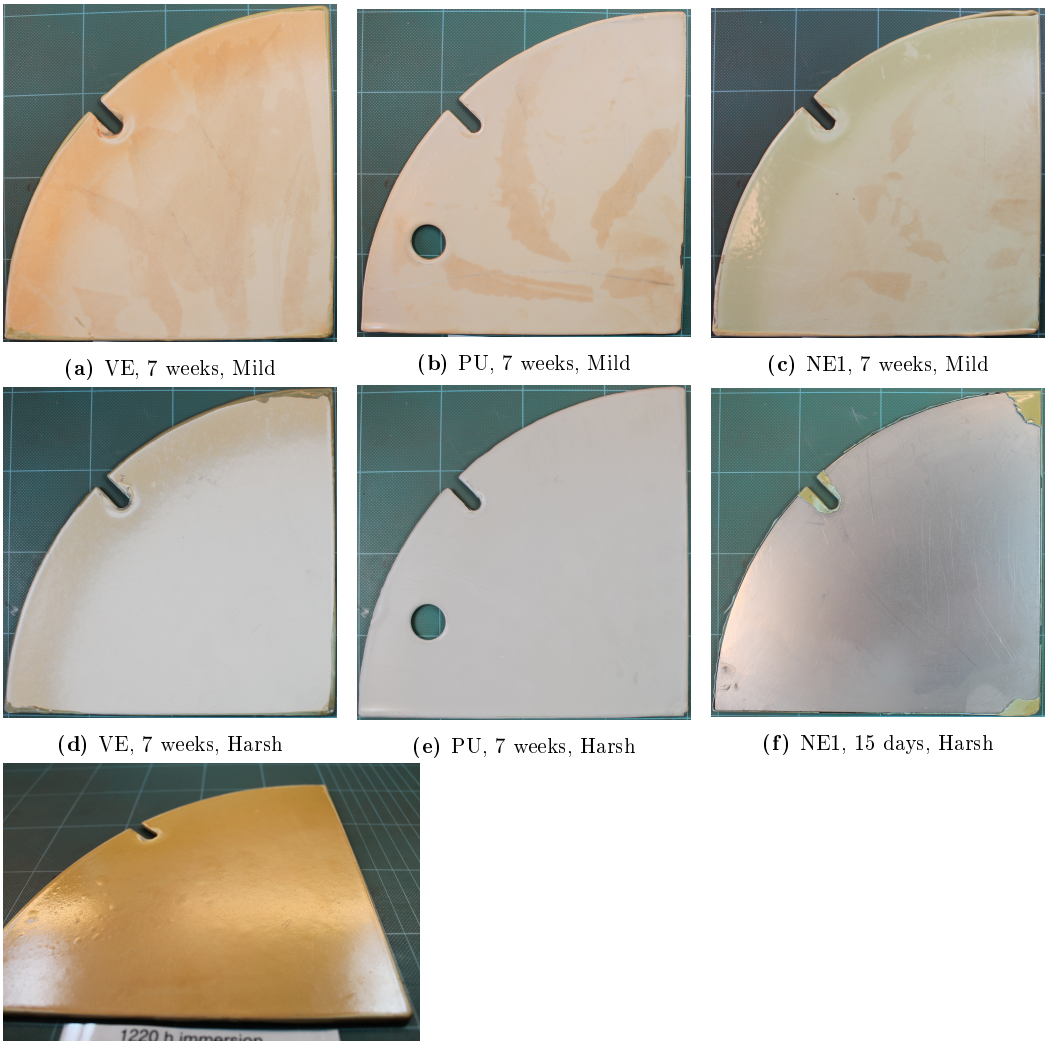

(a) VE, 7 weeks, Mild

(b) PU, 7 weeks, Mild

(c) NE1, 7 weeks, Mild

(d) VE, 7 weeks, Harsh

(e) PU, 7 weeks, Harsh

(f) NE1, 15 days, Harsh

(g) NE2, 7 weeks, Mild

Figure 17.1: Coating samples after use in the pilot-scale reactor in either Mild and Harsh conditions.

The PU immersion sample swelled due to chemical diffusion into the film, while the reactor sample, after the initial swelling, decreased steadily in thickness due to erosive forces. Both immersion and reactor PU samples showed localized blistering after 13.5 days of exposure. The immersed NE1 sample initially swelled, then contracted, reaching a steady thickness after around 25 days. A similar trend was seen for the reactor sample, with the exception that the thickness reduction continued even after 25 days (3.6 weeks). Both the VE immersion and reactor samples rapidly swelled. The immersion sample stopped swelling and maintained its thickness, while the reactor sample thickness steadily decreased as time passed. In Mild conditions, coating performance in descending order is as follows:

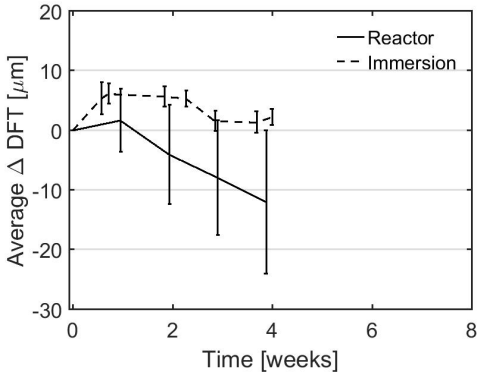

(a) Polyurethane (PU)

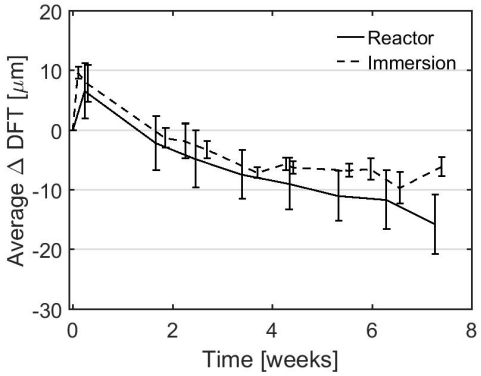

(b) Novolac epoxy (NE1)

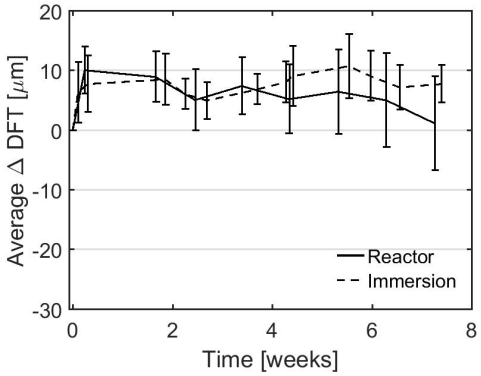

(c) Vinyl ester (VE)

Figure 17.2: DFT changes of coatings during immersion and reactor experiments in Mild conditions.

VE>NE1>>PU>>NE2>NE3.

17.3 Harsh condition erosion

Fig. 17.3 shows DFT changes from immersion and reactor experiments in Harsh conditions.
The PU immersion sample kept gaining thickness, while the reactor sample was worn down by particle impacts. The continued PU swelling in the Harsh conditions affected the perceived polishing rate. Both immersion and reactor NE1 samples delaminated between 14 and 18 days of exposure time, after very significant swelling. For the reactor sample, the swelling rate was much greater than the polishing rate as observed by the rise in thickness. Nevertheless, erosion occurred as seen by the gap between the reactor and immersion sample DFT. The VE immersion sample swelled and maintained its thickness, while the reactor sample swelled only slightly initially, followed by a steady loss in thickness. In Harsh conditions, coating performance in descending order was as follows: VE>>PU>>NE1>>NE2=NE3. The performance of NE1 dropped radically in Harsh conditions because it was unable to handle the low pH conditions more than 15 days.

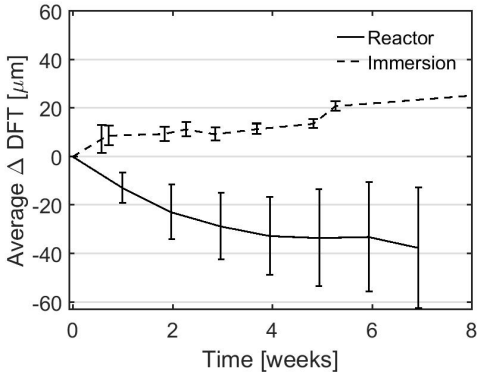

(a) Polyurethane (PU)

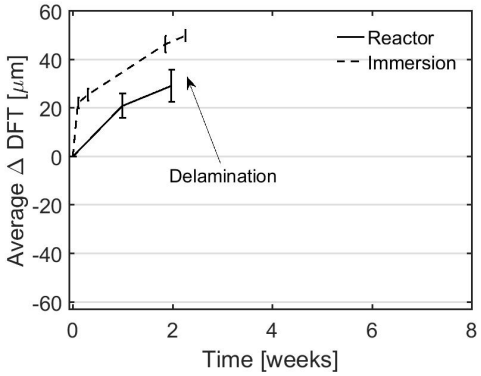

(b) Novolac epoxy (NE1)

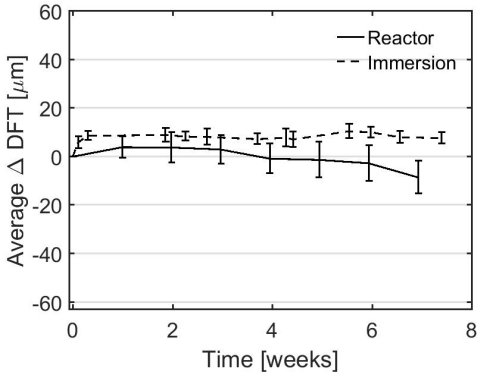

(c) Vinyl ester (VE)

Figure 17.3: DFT changes of coatings during immersion and reactor experiments in Harsh conditions. NE1 delaminated between 400 and 500 h for both reactor and immersion experiments.

Immersed samples had a tendency to rapidly swell and maintain their thickness, but in some cases, like NE1 in Mild conditions, the coating contracted instead, or, like PU in Harsh conditions, the swelling continued. Coating thickness changes in the reactor experiments, become a function of their chemical swelling and contracting behavior and magnitude, combined with particle polishing rates. It is therefore necessary to map the thickness change behavior of coating products in immersed conditions, to properly evaluate the rate of polishing caused by erosion.

17.4 Position dependent polishing rates

Particle impact angle and speed vary with radial distance from a center-placed impeller in a stirred tank as shown in Section 3.3.3 [134, 135]. It was therefore investigated whether this had a significant effect on coating polishing rates. Fig. 17.4 shows the polishing rates of the coating samples for Mild and Harsh conditions for different positions on the reactor bottom. x is the radial position on the

coating sample, defined as distance from reactor center divided by reactor radius. With $x = 0$ being right beneath the impeller and $x = 1$ representing the edge of the reactor. Values in Fig. 17.4 are calculated as the difference between immersion and reactor DFT at the termination of the reactor experiment. As an example, a polishing rate of 0 μm/week means zero difference between immersion and erosion experiments and thus no significant erosion. It should be noted that localized blistering for PU in Mild conditions caused DFT values to spike in four specific points, these values have been omitted from Fig. 17.4a because they do not represent the actual polishing rates.

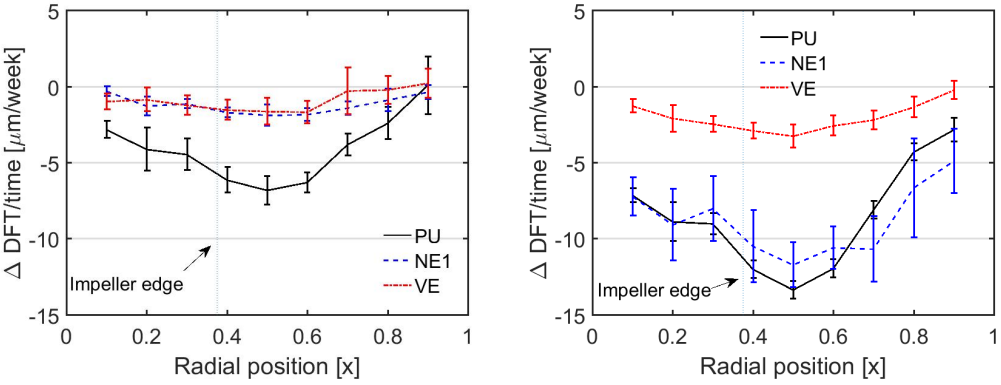

(a) Mild conditions. **(b)** Harsh conditions.

Figure 17.4: Polishing rates of all coating types in Mild and Harsh conditions as a function of radial distance from reactor center (x=0). Polishing rates are calculated from differences in data from immersion and reactor experiments at the end of the reactor experiment.

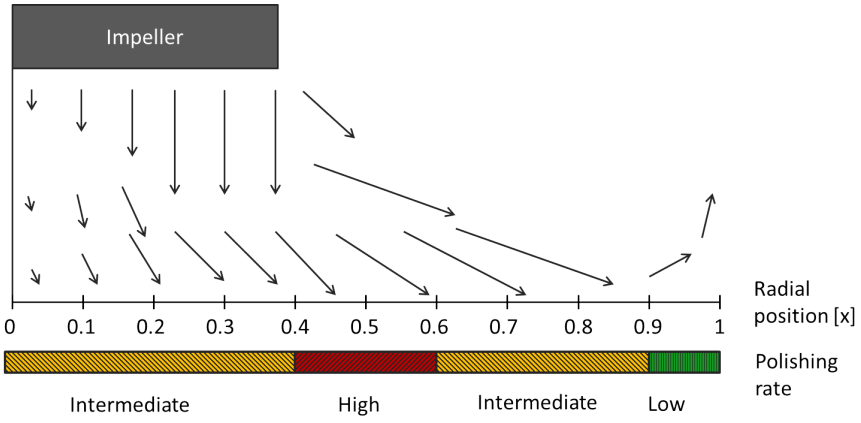

Figure 17.5: Flow-field vectors on the bottom of the tank as described in reference [135], and the relative polishing rates found in Fig. 17.4. Position $x = 0$ corresponds to the reactor center, and $x = 1$ to the reactor wall.

It can be seen that polishing rates vary with radial position for every coating in both environments. This has been highlighted in Fig. 17.5. Neither the steepest particle impact angle ($0 \leq x \leq 0.4$), nor the highest flow speed ($0.6 \leq x \leq 0.8$) caused the greatest amount of coating damage. Instead an intermediate speed and impact angle caused the highest polishing rate, more precisely for $0.4 \leq x \leq 0.6$. The polishing rate was less severe towards the reactor edge, $x = 1$, and beneath the impeller $x = 0$. In Mild conditions, near zero erosion was observed near the reactor edge, $x = 0.9$, where liquid flow is obstructed by baffles, while in Harsh conditions polishing rates were two to seven times smaller in this region compared to the high erosion area.

The area with the highest polishing rate will be removed first, and therefore determines the coating erosion lifetime. Based solely on the highest polishing rate at the termination of the experiment, ignoring failure by all other means, a 1000 μm coating would have lifetimes as provided in Table 17.1. The vinyl ester resin with glass flakes and titanium dioxide pigments, was superior to all other tested coatings in both environments.

Table 17.1: The highest observed polishing rate with extrapolated lifetime of a 1000 μm coating in both Mild and Harsh conditions. Pencil gauge hardness (ASTM D3363) of dry coating samples prior to exposure is also shown.

		Mild conditions		Harsh conditions	
Coating (code)	Pencil gouge hardness	Polishing rate [μm/week]	Estimated lifetime [years]	Polishing rate [μm/week]	Estimated lifetime [years]
Vinyl ester (VE)	6H	1.7 ± 0.7	11.5 ± 5.0	3.2 ± 0.6	5.9 ± 1.1
Novolac epoxy 100% solids (NE1)	2H	1.9 ± 0.7	10.2 ± 3.9	11.7 ± 1.50	1.6 ± 0.2
Polyurethane (PU)	H	6.2 ± 0.8	3.1 ± 0.4	13.4 ± 0.6	1.4 ± 0.1

17.5 Time dependent polishing

The reactor experiments were run using a single batch of slurry, due to the difficulties in running continuous mode. This caused the particles and chemical environment to change over the course of the experiments. Details regarding the environment, particle shape and size distribution are given in Appendix E, with the overall conclusions that: The erosive conditions in the Mild experiment did not change much. A continuous particle leaching in Harsh conditions yielded a particle mass loss of approximately 13% over the first 5 weeks, causing the erosive condition to become milder as time passed.

It can be seen from Fig. 17.6, that polishing rates were relatively time-independent after the first two weeks in Mild conditions, while it varied continuously with time in Harsh conditions. This corresponds with the observation of constant erosive conditions in the Mild experiment, and gradually reduced erosive conditions in the Harsh experiment due to chalcopyrite dissolution. The PU in Mild conditions was experimented on from the 4 to the 7 week mark.

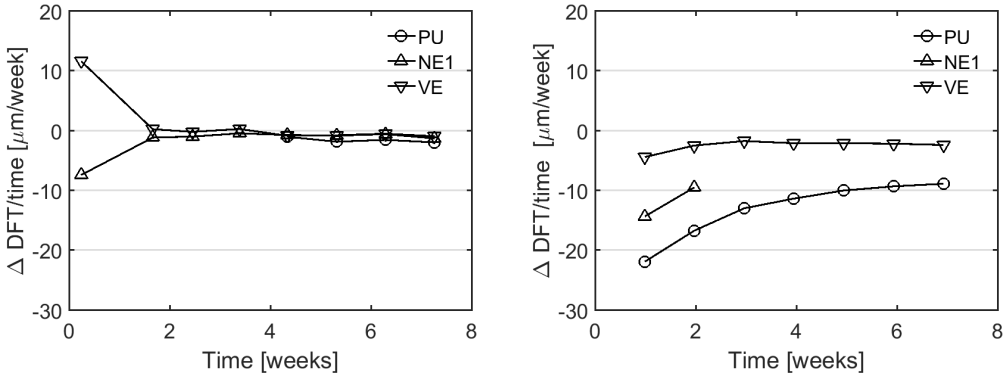

(a) Mild conditions.

(b) Harsh conditions.

Figure 17.6: Average polishing rates of PU, NE1 and VE coatings over the course of the experiments. Polishing rates are calculated from the differences in immersion and reactor DFT at the given points in time.

17.6 Repeatability

Through continuous changes to the set-up and samples and due to the long experimental time, it was not possible to conduct repetitions of experiments. However, the large quantity of measurements on each coating sample, serves as a replacement. Due to the rapid failure of NE2 and NE3 in Harsh conditions, it was possible to insert two separate samples of VE, to compare their relative performance, shown in Fig. 17.7. The average DFT changes are the same, within the range of uncertainty. The similarities are even more evident when one looks at DFT change as a function of the radial position, where the two samples have the same values, within the measurement uncertainty, for each radial position.

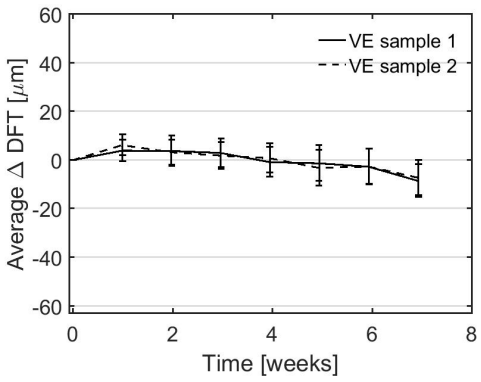

(a) Average DFT change on the entire sample.

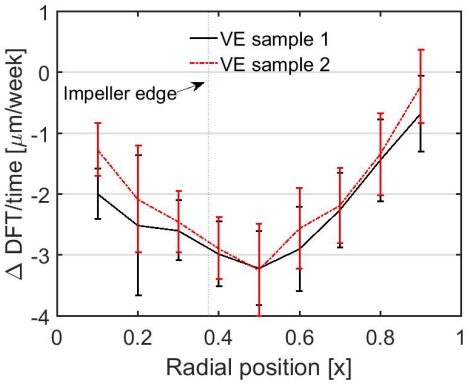

(b) DFT change based on each given radial position.

Figure 17.7: Comparison of DFT change on two VE samples in Harsh conditions.

18 Discussion

This section provides a short discussion in the effects of coating T_g, hardness, chemical reactions with the environment, and presents a mechanism for coating failure in an agitated leaching tank.

18.1 T_g and hardness effects

Table 18.1 provides a comparison of the hardness in the erosive copper concentrate with the inorganic fillers present in the coating formulations. It can be seen that the calcopyrite is fairly soft, and is only harder than baryte, talc and calcium carbonate. The pyrite and quartz are harder, or match hardness, with the majority of coating fillers, but are present in smaller quantities. The softness of calcopyrite helps reduce the erosive severity in the leaching tank.

Coating hardness is a key property when it comes to erosion resistance [152], however, for the selected coatings, hardness had little to no effect on the polishing rates. The hardness difference 6H to 2H, for VE and NE1 respectively, did not result in a big difference in the Mild condition polishing rate (see Table 17.1). The difference from 2H to H, for NE1 and PU respectively, was therefore not the cause of PU's relatively high polishing rate in Mild conditions. The T_g of PU, on the other hand, can account for this difference. Operating above a coating's T_g can cause a deterioration of mechanical properties. The high temperature environment will alter the hardness properties, because the resin is softened. The T_g of PU was 25 °C, and was below the experimental temperature of 75 °C, while the NE1 and VE T_g were above this threshold.

Table 18.1: Mohs hardness and weight percent content, of inorganic erosives, fillers and pigments [153, 154].

Inorganic name	Mohs hardness	Designation and weight %
Chalcopyrite	3.5-4	Erosive, 84.4
Zinc oxide	4.5	Erosive, 6.3
Pyrite	6-6.5	Erosive, 5.3
Quartz	7	Erosive, 2.9
Glass-flake	5.5	VE, 22.6
Titanium dioxide	5.5-6.5	VE, 2.0
		NE1, 4.3
		PU, 12.8
Quartz	7	NE1, 17.2
Baryte	2.5-3.5	NE1, 12.3
		PU, 18.9
Calcium carbonate	3	PU, 9.3

18.2 Chemical reaction effects

It is evident when comparing the polishing rates in Mild and Harsh condition exposures that the added stress of low pH exposure decreases the erosion resistance of all selected coatings. The performance of NE1 coating in particular, was worsened in Harsh conditions. Weight change experiments of immersed free films revealed a rapid weight increase, within the first day of exposure, see Fig. 9.1b. NE1 looses its barrier properties in Harsh conditions resulting in a fast acid diffusion compared to PU and VE. It is likely, that reactions between the coating and sulfuric acid caused this loss in coating barrier properties. This chemical degradation increased the polishing rate of NE1 by a factor of six, despite NE1 having a T_g above the experimental conditions and a hardness that proved sufficient in Mild conditions.

The polishing rate of PU was also drastically increased by acid exposure, likely due to the removal of limestone fillers. VE polishing rates were low compared to the NE1 and PU, however its value almost doubled with the addition of acid exposure. This indicates that the VE is not entirely inert, but some chemical interactions are occurring in acid to weaken either the resin, the fillers, or perhaps the resin-filler interface.

18.3 Polishing and reaction mechanism

A suggested mechanism for simultaneous polishing, liquid diffusion, and reaction is visualized in Fig. 18.1. Molecules diffuse into the coating surface and change the mechanical properties by softening, swelling, and/or reacting with the coating. Erosive particles continuously polish away the mechanically compromised surface, enabling further ionic diffusion. The mechanism bears similarity to erosion/corrosion effects commonly found in metals, where mechanical properties of a surface layer are altered due to chemical reactions with the environment, making it more vulnerable to erosion [35].

Liquid diffusion into a coating can create a degradation zone, such as Hojo describes as Corroded layer type 1 and 2, depicted in Fig. 3.11. The thickness of this zone depends on the diffusion front

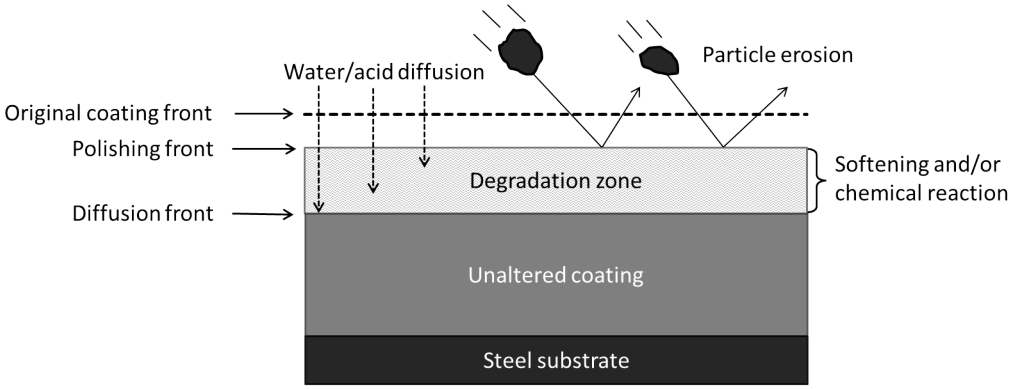

Figure 18.1: Proposed erosion/corrosion mechanism for organic coatings. Liquid diffuses into the film thereby softening and/or reacting with the coating; This affects the polishing rate.

and the polishing front. Methods for determining polishing rates are described in the current part, while diffusion rates of an acid through a coating can be found using diffusion cells. Diffusion cells are described in Part IV, where diffusion coefficients for VE, PU and NE1, are also provided.
The mechanical properties of a coating can be altered in the degradation zone. The coating is softened by the penetrant, reducing the coating's T_g. Reactions may also occur in this zone, the severity of which can have a significant influence on the mechanical properties, and thereby the polishing rate. So, the polishing rate is enhanced by acid diffusion, and the acid diffusion can be accelerated by the removal of coating surface layers.
A visual example of the degradation zone is seen previously in Fig. 12.1, which shows a cross-sectional image of a free NE2 film immersed in Harsh conditions. The sulfuric acid diffusion front is visible through the sulfur element signal, and leaves behind a visibly damaged degradation zone.

19 Conclusions

In the study of coating wear in the pilot-scale agitated leaching tank, coating film thickness change was found to be a function of physical interactions with the environment such as swelling or film contraction, as well as mechanical erosion.
The ability to monitor polishing rates on a large amount of individual points on a coating sample, led to the discovery of a high variance of these rates, on the reactor samples along the radial position. The highest polishing rates were found below the tip of the axial pumping impeller for all coating types, whereas the lowest polishing rates were found near the reactor wall. Positional dependencies were caused by differences in particle speed and impact angle.
The mechanical properties of coatings determine their erosive resistance, and the immersion environment influences these properties. Increasing the sulfuric acid concentration in a chemical slurry increased the polishing rates of the organic coatings. Polishing rates of the VE and PU coatings were doubled in the Harsh acidic slurry compared to the more neutral, Mild, slurry. The NE1 polishing rates were increased by a factor of six. The cause of this increase can be speculated to be due to chemical reactions between the acid and coating resin, fillers, and/or resin-filler interfaces, leading to a

change in the mechanical properties of the coating surface. This change caused the surface to be more susceptible to erosion from the impacting particles.

For the coatings tested, the VE showed best performance in all conditions. NE1 performed well in the neutral slurry, but deteriorated in the acidic slurry. The other epoxies, NE2 and NE3, failed rapidly in both conditions. The PU showed poor erosion resistance in both environments because conditions were above the glass transition temperature of the coating. The VE was determined to have a lifetime of approximately six years per 1000 μm applied thickness in the acidic slurry conditions representing the agitated leaching environment, making it applicable in industrial operations.

Organic thermoset coatings can be used as protective coatings in agitated leaching tanks. However, to explore the viability of protective coatings, one has to assess factors like erosion resistance in the same environment as the intended use, because chemical exposure, and other environmental factors such as temperature, can have a significant effect on polishing rates.

Part IV

Evaluation of coating barrier properties using diffusion cells

Coating failure in an agitated leaching tank is not solely caused by coating polishing rates and reactions with the liquid media. Acid diffusion into and through coating films is another important degradation mechanism to map, before one can make conclusions on actual coating performance in the agitated leaching environment.

The current part provides a description of the diffusion cells that were designed and constructed to evaluate barrier properties of the selected coatings, together with a mathematical model developed to simulate the results. A compact version of this part can also be found as a journal article [155].

Nomenclature

A	Effective diffusion area [m^2]
α	Plasticization power [l/mol]
C	Concentration [mol/l]
D	Diffusion coefficient [m^2/s]
D_0	Zero concentration diffusion coefficient [m^2/s]
F	Ion flux [$mol/m^2 \cdot s$]
l_0	Coating thickness [m]
t	Time [s]
V	Volume [m^3]
l	Position in the coating film [m]

Subscripts

B	Breakthrough
D	Donor chamber
degraded	Acid-exposed
dry	Dry
i	Initial
lag	Time lag
sat	Saturated
R	Receiver chamber
SS	Steady state
T	Transient state
virgin	Non-acid-exposed

20 Diffusion cell concept

Effective barrier coatings are expected to have lifetimes of 15 years or more [11]. Therefore, testing with conventional immersion, where the time to failure is recorded, is a challenge. A simple principle for monitoring ionic diffusion is the diffusion cell, consisting of two chambers separated by a free coating film, as shown in Fig. 20.1. In such a set-up, chemicals diffuse from the Donor chamber, through the coating film and into the Receiver chamber, where the concentration change is monitored using an ion selective probe.

In the past, a range of liquid diffusion cells have been used to monitor ion permeation through organic coatings. Studies include investigations into the effects of formulation parameters on ionic diffusion rates [156, 157], estimation of the ionic flux through coatings [138] or along interfaces [107], and diffusion mechanisms [76]. Diffusion cells have also been used to estimate diffusion coefficients of ions through protective coatings [107, 138, 157]. For an overview of permeation studies in barrier coatings see the review paper by Pajarito and Kubouchi [102].

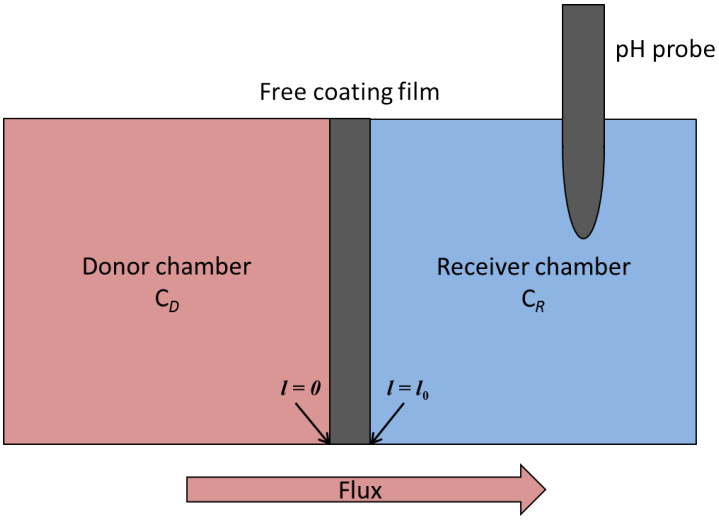

Figure 20.1: Basic diffusion cell concept. A free coating film of thickness l_0 separates the two chambers. Solute molecules diffuse from the Donor to the Receiver chamber.

A diffusion cell can be used to map the barrier properties of protective coatings, and, due to its simplicity, the concept is also useful in an industrial perspective. However, a thorough understanding of diffusion mechanisms in these cells is lacking, and the effects of chemical reactions within a coating film are poorly understood. In the current project, a diffusion cell with the simplest design possible was constructed. Breakthrough times and steady state flux data were measured, and, using a mathematical model, acid diffusion coefficients were estimated for selected coatings. The model was also used as a tool to investigate diffusion mechanisms and predict acid diffusion lifetimes.

21 Previous diffusion cell designs

Past work using liquid diffusion cells includes a variety of different designs. However, they all share the concept presented in Fig. 20.1, with the exceptions of Allen [61], who relied on volume changes, and Romhild et al. [82] who only used an acid filled Donor chamber, and monitored the cell weight loss as chemicals permeated the coating and evaporated. The most common designs are described in Table 21.1. References to gas diffusion cells were not relevant for this work and were omitted.
Most diffusion cell designs use ion-selective probes that can measure the ionic flux in the Receiver chamber. The Na^+, Cl^-, and H^+ ions have been tracked in past work, but probes are available that can be used to detect many other types of ions. Some cell designs use stirring in the Donor and/or Receiver chambers to ensure a homogeneous concentration, but this feature has the disadvantage that the cell design becomes more complex [107, 138, 156, 157]. Liquid volumes in the chambers can change throughout an experiment and therefore aerating holes are present in some cells to ensure a constant atmospheric pressure. However, this also increases the evaporation rate of volatile chemicals [107, 138, 157]. The volume of the Donor chamber, for some designs [107, 138], is larger than that of the Receiving chamber. This is done to promote a constant concentration in the Donor chamber, but it also increases the size of the cell. Heating is typically not used, but it can be required to simulate certain industrial conditions or to accelerate diffusion rates [76].

Table 21.1: Overview of selected liquid diffusion cell designs. The Donor to Receiving chamber volume ratio is provided as V_D/V_R.

Cell type	Measurement	Coating type	Substrate	Stirring	V_D/V_R	Pressure conditions	Heating	Reference (year)
Ionic	Ion flux (H^+)	Polyamide	None	None	1.0	Closed chambers	Both chambers	[76] (2006)
Osmotic	Volume change	Vinyl ester	None	None	1.0	NA	None	[61] (1979)
Ionic	Ion flux (Cl^+)	Waterborne	Kraft paper	Receiver chamber	2.7	Open Donor chamber	None	[138] (2006)
Ionic	Ion flux (H^+)	Polyvinyl alcohol and polyethylene glycol	None	Both chambers	1.0	Open Donor chamber	None	[157] (2005)
Ionic	Ion flux (Na^+)	Epoxy	Kraft paper	Receiver chamber	2.8	Open Donor chamber	None	[107] (2010)
Ionic	Ion flux (H^+)	Polyvinyl alcohol and epoxy	None	Both chambers	1.0	Closed chambers	None	[156] (2004)
Single chamber	Weight change	Vinyl ester and liquid crystal polymers	None	None	-	Closed chamber	Yes	[82] (2005)

22 New diffusion cell design

Important design criteria for the acid diffusion cell of this work were: Simple to produce and upscale to an array of cells, compact design, and the cell material should be chemically inert and transparent. The cell was constructed using Plexiglas, poly(methyl methacrylate). This material is inert to the acid concentrations of importance (down to pH≈0), and is transparent, allowing observation of changes in the coating sample or liquid levels in the cell during experimentation.
The major design differences between the current and previous diffusion cell designs are the lack of aerating holes and stirring, and the possibility of heating. No aerating holes were used; cell chambers were equilibrated with the atmospheric pressure during a pH measurement, where rubber stoppers blocking the feed holes were removed. Moggridge et al. [101] observed that stirring was insignificant in either chamber of an ionic diffusion cell and therefore stirring was not used in the current cell. The Donor chamber volume was made 2.8 times larger than the Receiving chamber, causing a near constant Donor chamber concentration during experimentation. Rather than integrating heating in the cell design, it was established by inserting the entire cell into an oven.

23 Diffusion cell details

The new cell is shown in Fig. 23.1 with a schematic view in Fig. 23.2. Cell dimensions are 150x80x80 mm^3. The liquid volume in the Donor and Receiver chamber are 92.1 cm^3 and 33.1 cm^3, respectively. The coating film used for experimentation is placed between the two chambers, and the connections are sealed with O-rings inserted into each chamber wall as shown in Fig. 23.2. The chambers can be assembled using screws and bolts through holes in the flanges, creating a tight seal between O-ring and coating film. The effective coating surface area for diffusion is 9.1 cm^2.
A single feeding hole is placed in the Donor chamber for filling and emptying liquid, while two feeding holes are present in the Receiver chamber. The two access holes for the Receiver chamber were made to avoid overflow when inserting the pH probe. A total of eight diffusion cells were constructed and used for experimentation.

24 Experimental conditions

Two types of experiments were performed in the current work. The first type, referred to as "Preliminary" conditions, were used as an investigation into the effects of water saturation. These experiments were performed at ambient temperatures with the NE4 coating type. The second type of experiment is referred to as "Harsh" conditions, and is a replication of the chemical environment and temperature in the agitated leaching tank, the VE, PU, NE1, and NE2 coatings were experimented in this conditions. Table 24.1 provides an overview of the experimental conditions and chemicals applied.

25 Experimental procedure

For all experiments, the procedure was the same. Before inserting and fastening the free coating film in the diffusion cell, the dry film thickness was measured using an Elcometer 355. The experimental liquids and assembled cell were heated separately to the required temperature, whereafter the Receiver

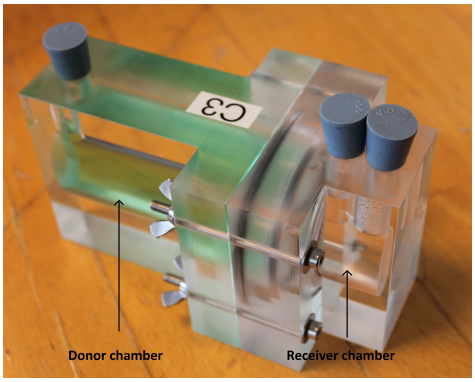

Figure 23.1: Ionic diffusion cell with rubber stoppers in the access holes.

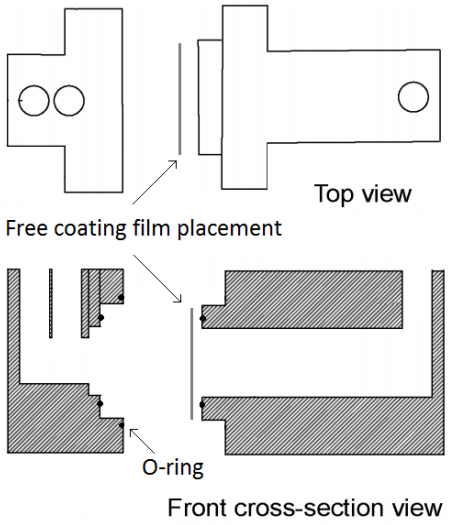

Figure 23.2: Schematic cross section view of the diffusion cell.

Table 24.1: Chemical environments in the Donor chamber. Harsh conditions simulate the chemical environment in an industrial leaching reactor. The Receiver chamber contained demineralized water in all experiments.

Condition	Preliminary	Harsh
H_2SO_4 [mol/l]	1.08	0.13
pH	-0.03	0.9
Cu(II) [g/l]	0	4.1
Temperature [°C]	20.0±1.0	68.5±2.5

and Donor chambers were filled with liquid, while ensuring the coating was in full contact with liquids on both sides.

pH measurements were done through one of the holes in the Receiver chamber using a Pt1000 probe with a 913 pH meter from Methrohm. The measurement intervals were based on the observed diffusion rate of acid through the individual coatings. Before conducting a pH measurement, the liquid level in the Receiver chamber was noted. If the level had dropped, due to diffusion or evaporation, it was refilled with distilled water, ensuring a consistent volume. The pH probe was left in the Receiver chamber until the reading stabilized, typically after 30 seconds, and temperature readings were performed simultaneously. The pH probe was calibrated each week using buffered standards at pH 7.0 and 4.0. An experiment was terminated when the concentration curve reached a steady state, typically achieved between pH 1.0 and 2.0.

26 Mathematical modeling

A model capable of simulating the transient H^+ (H_3O^+) concentration change in the Receiver cell is now described. The underlying model assumptions are given below.

- The Donor chamber has a constant H^+ concentration
- Chamber liquid volumes remain constant
- Liquid temperatures are constant
- The only H^+ ion transport resistance is in the coating (i.e. the Receiver and Donor chambers are well mixed)
- No H^+ ions are consumed or produced in the coating film
- The coating has a constant thickness, equal to the dry film thickness
- The H^+ diffusion coefficient can vary in the coating with H^+ concentration
- The diffusion area remains constant
- The coating is non-porous
- The initial H^+ concentration in the film corresponds to a pH of 7
- The H^+ diffusion rate is not affected by liquid absorption in the coating
- H_2SO_4 is fully dissociated to HSO_4^- and H^+
- HSO_4^- dissociation to SO_4^{2-} and H^+ is considered negligible
- The diffusion coefficients of HSO_4^- and H^+ are assumed equal, whereby the charge balance is fulfilled throughout the coating
- The liquid solutions are considered ideal, i.e. activity coefficients of unity

The validity of these assumptions is addressed in a later section.

26.1 Mass balance

The ionic transport over the coating film is described by a mass balance for H^+ ions.

$$\frac{\partial C}{\partial t} = \frac{\partial}{\partial l}\left(D_{H^+}(C)\frac{\partial C}{\partial l}\right) \tag{12}$$

with initial and boundary conditions:

$$C(l, t = 0) = C_i \tag{13}$$

$$C(l = 0, t) = C_D \tag{14}$$

where C is the H^+ concentration in the coating. The transient mass balance for H^+ in the Receiver chamber is given by

$$\left.\frac{dC_R}{dt}\right|_{l_0} = \frac{A}{V_R} \cdot F_R \tag{15}$$

with

$$C(l = l_0, t = 0) = C_{R0} \tag{16}$$

where F_R is the flux into the Receiver chamber at $l = l_0$ given by

$$F_R = -D_{H^+}(C)\left.\frac{\partial C}{\partial l}\right|_{l_0} \tag{17}$$

The diffusion coefficient is taken to be an exponential function of penetrant concentration [82]

$$D_{H^+}(C) = D_0 \exp(\alpha C) \tag{18}$$

where D_0 and α are the so-called zero-concentration diffusion and plasticization power respectively [158]. Later in the investigation D_{H^+} was found to vary also with time. This time-dependency was simplified by assuming a three-step time variation of D_0: one value before acid breakthrough, one value during a transient phase, and one for the final steady state phase (discussed in detail later).
The model was discretized using methods detailed in [159], and numerically solved using MATLAB. The MATLAB code used is included in Appendix H. A dimensionless version of this model is included in Appendix I, where the effect of H^+ concentration increase in the Receiver chamber on H^+ flux rates is shown.

26.2 Estimation of model parameters

Table 26.1 provides an overview of the model input and adjustable parameters. The D_0 and α fitting procedure was through trial and error; a set of parameter values were examined for their ability to fit the experimental data.

Table 26.1: Model input parameters. D_0 and α are adjustable parameters.

Parameter	Value
C_D	0.13 and 1.08 [mol/l]
C_i	10^{-7} [mol/l]
C_{R0}	10^{-5} to 10^{-7} [mol/l]
l_0	114 to 788 μm
D_0 and α	Best fit, see Table 29.1

27 Experimental results

Two types of experiments were performed using the diffusion cells. The Preliminary experiments at ambient temperature using the NE4 coating, and the Harsh experiments at elevated temperature using the VE, PU, NE1 and NE2 coatings.

27.1 Preliminary conditions

To observe the effect of water saturation, pre-saturated coatings were evaluated against dry samples. Pre-saturation was done by immersing NE4 free films in demineralized water for seven days at 21 °C, and comparing results with dry, non-presaturated NE4 films. Complete saturation was found after two days of immersion at 21 °C (not shown), using weight change experiments on films with thickness of 98 to 127 μm.
The pre-saturated NE4 films had issues with crack formations in some of the films. NE4S 1, had a crack near the O-ring, as shown in Fig. 27.1a. This was discovered after five days, and the crack was moved out of the O-ring area, whereafter the demineralized water in the Receiver chamber was replaced to continue the experiment. As the examples show in Fig. 27.1, the NE4 coating films showed a slight discoloration in the acid exposed area, and some deformation of the film occurred.

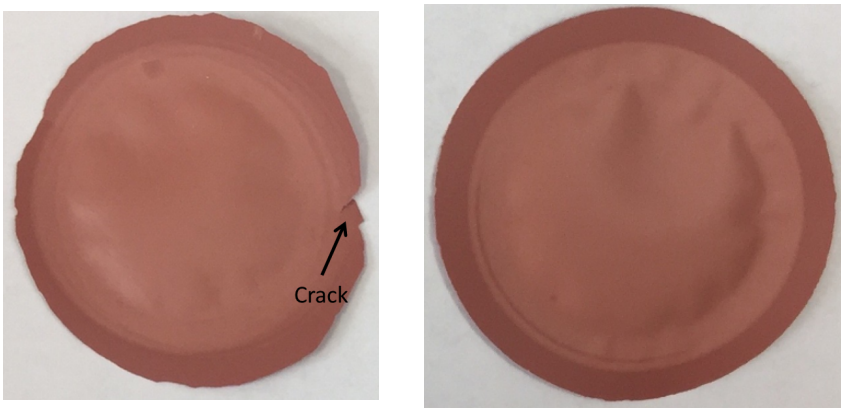

(a) Presaturated sample.

(b) Non-presaturated sample.

Figure 27.1: Example of NE4 coating samples after experimentation in the diffusion cell. The surface in view was the side facing the acidic Donor chamber.

The diffusion cell results are shown in Figs. 27.2a and 27.2b, which depict the measured pH values with the corresponding H^+ concentration for saturated and dry coatings respectively.

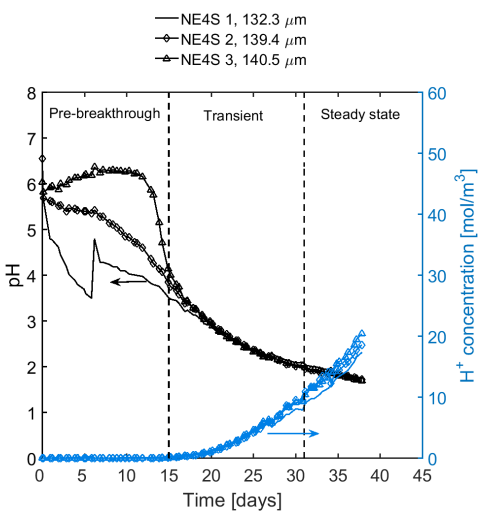

(a) Presaturated coatings.

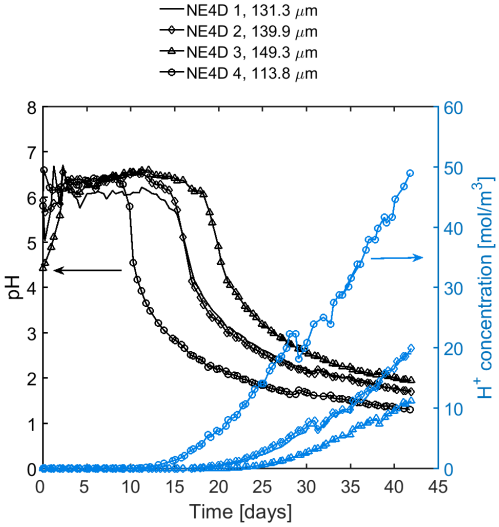

(b) Initially dry coatings.

Figure 27.2: Transient concentration and pH profiles for H^+ ions in the diffusion cell Receiver chamber. Diffusion was through presaturated and non-presaturated NE4 free films. Coating thickness is provided next to the sample name.

Acid breakthrough time was chosen to be the time it takes for the pH in the Receiver chamber to drop below 4.0. A transient state of the acid flux follows acid breakthrough, whereafter the acid flux reaches a steady state where the concentration-time curve exhibits an approximate linear slope.
The pre-saturated samples have different pH curves before acid breakthrough, most likely due to micro-crack formation in sample 1 and 2 as discussed earlier, but they converge in the transient and steady state period. Only NE4S 3 shows an expected trend from start to finish. The results for dry NE4 coatings are more consistent; acid breakthrough time is smaller for the thinner coatings and the H^+ concentration increase is transient after breakthrough, reaching a steady state after around 35 days. The small initial variation in pH values in the pre-breakthrough period for the dry coatings, Fig 27.2b, is caused by the lack of ions in the demineralized water in the Receiver chamber. A discussion on the effects of water saturation on acid diffusion is provided in a later section.

27.2 Harsh conditions

In the Harsh conditions experiments, the NE1 (T_g=81 °C) and NE2 (T_g=45 °C) coatings experienced severe discoloration and blistering respectively, as shown in Fig. 27.3. The NE2 also developed cracks along the O-ring sealing. The PU coating discolored slightly but provided a more effective acid barrier than NE1 and NE2, even though it was operated above its dry T_g of 25 °C. The VE (T_g=145 °C) coating film did not bend like NE1, NE2 and PU throughout the diffusion experiment, but the glass flake fillers became exposed at the surface facing the Donor chamber, and detached when touched.

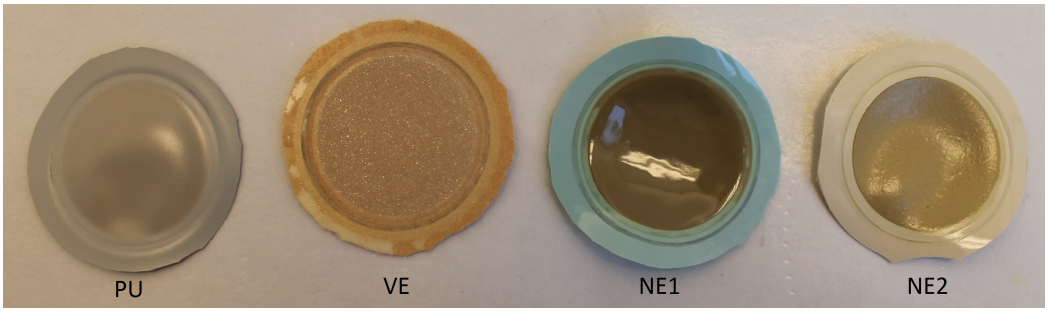

Figure 27.3: PU, VE, NE1, and NE2 free films after use in a diffusion cell under Harsh conditions. The surface in view was the side facing the acidic Donor chamber.

Diffusion cell results from the Harsh condition experiments are shown in Fig. 27.4. Note the difference in time scale on the x-axis, as the coating performance was very widespread. Note also that the initial pH value in the diffusion cells varied between 4.5 and 7. This is likely caused by the coating leaching slightly acidic (unknown) residual compounds, when contacted with the demineralized water.
The NE1 and NE2 reached a steady state H^+ flux rapidly after acid breakthrough, almost skipping the transient state that was seen for NE4 in Fig. 27.2. The PU showed all the expected trends of a functional barrier coating, with a transient period separating the H^+ flux rate between breakthrough time and steady state. The VE coating thickness was noticeably larger than the other coatings, due to application difficulties, and it showed no sign of acid breakthrough during the 118 day long experiment.

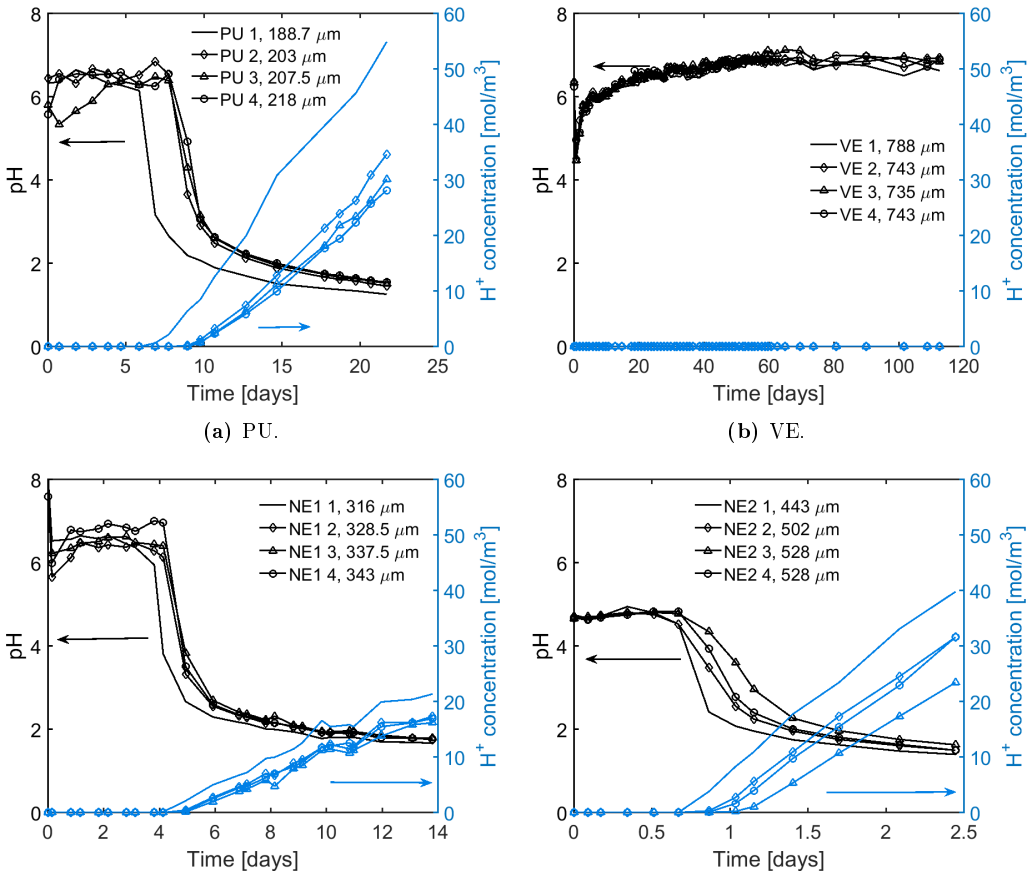

(a) PU. **(b)** VE. **(c)** NE1. **(d)** NE2.

Figure 27.4: Transient concentration and pH profiles for H^+ ions in the diffusion cell Receiver chamber for Harsh conditions. The samples for the individual coatings varied slightly in thickness. Note the time scale differences in the figures.

28 Mathematical modeling of diffusion data

To validate the mathematical model, the experimental data were simulated. The NE4D 3 coating was used as a case study, because it showed acid breakthrough, an intermediate transient concentration curve and finally, reached steady state flux conditions.

28.1 Constant diffusion coefficients

As shown in Fig. 28.1, the experimental data could not be simulated using a constant acid diffusion coefficient. The model could either predict the acid breakthrough time, or the following steady state acid flux, but not both.

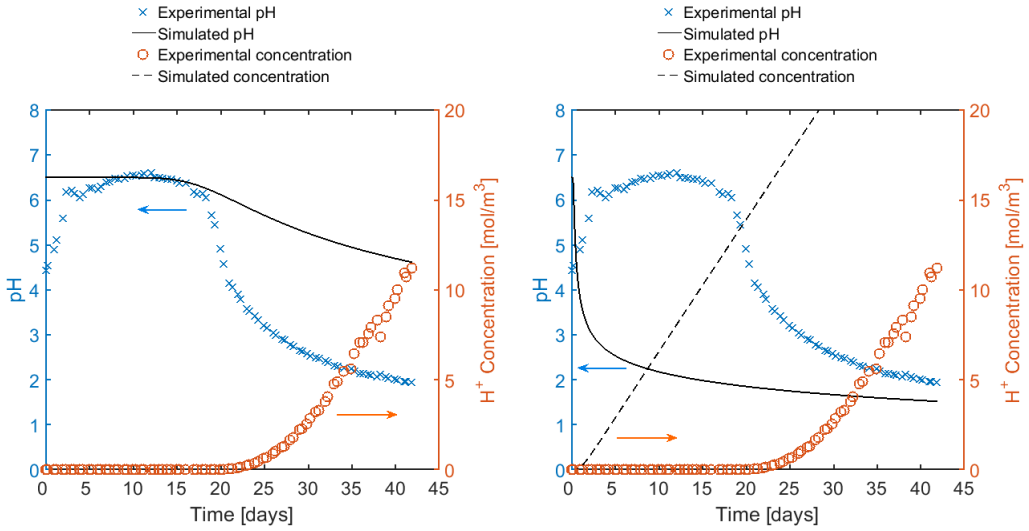

(a) $D_{H^+} = 0.5 \cdot 10^{-15}$ m^2/s. **(b)** $D_{H^+} = 35.0 \cdot 10^{-15}$ m^2/s.

Figure 28.1: Comparison of model simulations with experimental data for NE4D 3 (constant diffusion coefficient).

28.2 Concentration and time-dependency

To improve model simulations, it was attempted to use a concentration-dependent diffusion coefficient. This succeeded in a better simulation of the pH drop after acid breakthrough. However, it still suffered from the problem discussed in the previous paragraph.

It was found that the diffusion coefficient required to simulate the acid breakthrough-time would be a factor of 18 to 190 times smaller than the value required to simulate the steady state flux. Therefore, it was assumed that the diffusion coefficient was a function of both concentration and time:

$$D_{H^+} = f(C, t) \tag{19}$$

The time-dependency was simplified by assuming that the pre-exponential factor, D_0, changed at the time of acid breakthrough, t_B, and after reaching the steady state flux, t_{SS}. A three-step time-dependency was implemented by applying one value of D_0 before acid breakthrough (denoted with the subscript B), another value during the transient phase (subscript T) and a final value for the steady state flux (subscript SS). The plastization power, α, was assumed constant at all times.

Fig. 28.2 shows an example where the three sets of D_0 values have been used in the three distinct time intervals. Note the that the D_{0B} is 32 times smaller than the D_{0SS}. In Fig. 28.3, the simulated H^+ concentration profiles inside the coating film are shown, where the acid front reaches the full thickness of the film at the point of acid breakthrough of 20.5 days.

It was observed that when using three D_0 values, the breakthrough time and the steady state curve could be simulated very well. However, for the transient period some deviation between simulations

and experimental data is seen. To accurately represent this part, a continuous variation of the diffusion coefficient over time is required, rather than the simplified three-step simulation.

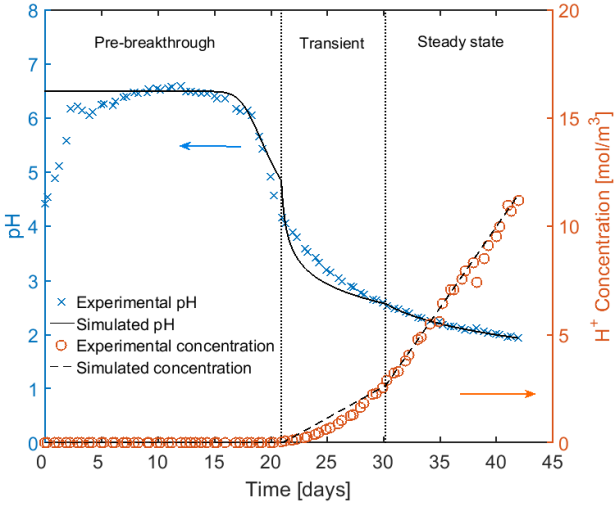

Figure 28.2: Comparison of experimental data and simulations of transient pH and concentration profiles for NE4D 3. The simulation used a diffusion coefficient which is concentration dependent, and has a three-step time variation. $D_{0B} = 0.096 \cdot 10^{-15}$ m^2/s for the pre-breakthrough time, $D_{0T} = 1.1 \cdot 10^{-15}$ m^2/s in the transient state, and $D_{0SS} = 2.8 \cdot 10^{-15}$ m^2/s in the steady state. $\alpha = 0.005$ for all values of time.

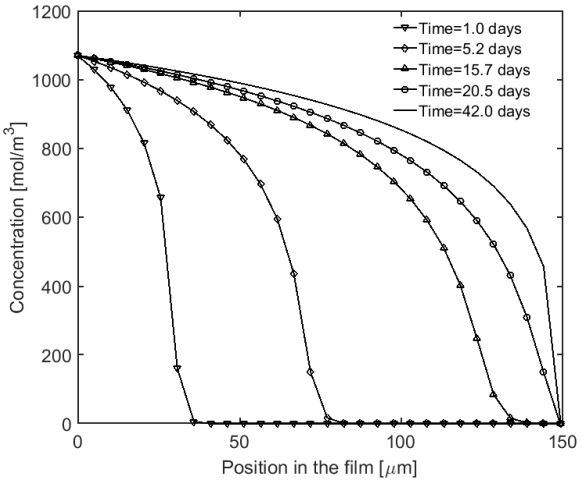

Figure 28.3: Simulated H^+ concentration profiles inside the coating film.

29 Discussion

The experimental and modeling results enable an investigation into the diffusion phenomena occurring in the coating films in the diffusion cells, as well as a comparison of barrier properties and estimations of coating lifetimes. Diffusion mechanisms and the resultant diffusion coefficients are presented and discussed in this section.

29.1 Coating barrier properties

Table 29.1 provides an overview of the pre acid-breakthrough D_{0B}, the transient state D_{0T}, and the post breakthrough constants D_{0SS}, as well as the α values, derived using the concentration and three-step time-dependent diffusion coefficient model. The data fitting figures using these values can be found in Appendix J. No acid permeated the VE samples, and diffusion coefficients could not be accurately determined for this coating type. In the literature, no studies on diffusion coefficients for VE type coatings in warm sulfuric acid have been provided.

Table 29.1: Diffusion coefficients overview for all experiments conducted using diffusion cells. The coefficients shown are derived using the concentration and time-dependent model.

Conditions	Coating code	Sample nr.	Coating thickness [μm]	α [l/mol]	$D_{0B} \cdot 10^{-15}$ [m^2/s]	$D_{0T} \cdot 10^{-15}$ [m^2/s]	$D_{0SS} \cdot 10^{-15}$ [m^2/s]
Preliminary	NE4D	1	131.3	0.005	0.091	1.3	3.2
Dry		2	139.9	0.005	0.105	1.4	3.4
(21 ± 1 °C)		3	149.3	0.005	0.096	1.1	2.8
		4	113.8	0.005	0.105	1.6	3.9
Saturated	NE4S	1	132.3	0.005	0.16	1.3	3.0
(21 ± 1 °C)		2	139.4	0.005	0.17	1.2	3.5
		3	141.5	0.005	0.12	1.4	3.7
Harsh	PU	1	188.7	0.03	1.2	210	230
(68.5 ± 2.5 °C)		2	203.0	0.03	1.1	170	180
		3	207.5	0.03	1.1	140	170
		4	218.0	0.03	1.1	140	170
	VE	1	788.0	0.03[a]	1.0[a]	NA	NA
		2	743.0	0.03[a]	0.9[a]	NA	NA
		3	735.0	0.03[a]	0.9[a]	NA	NA
		4	743.0	0.03[a]	0.9[a]	NA	NA
	NE1	1	316.0	0.03	6.0	290	290
		2	328.5	0.03	5.5	260	260
		3	337.5	0.03	5.5	250	250
		4	343.5	0.03	5.5	250	250
	NE2	1	443.0	0.03	80	3500	3500
		2	502.0	0.03	110	3500	3500
		3	528.0	0.03	100	1500	3300
		4	528.0	0.03	100	1500	3800

[a] These are the largest possible values assuming acid penetration occurred right at the termination of the experiment. No acid breakthrough was observed and the actual D_{0B} is expected to be much lower.

29.2 Comparison with immersion experiment

In Section 12, a cross-sectional SEM image was shown of an NE2 free film, immersed in Harsh conditions. A sulfur element analysis across the sample, revealed that the sulfuric acid had permeated approximately 170 μm into the 465 μm thick film on both sides after two hours. Fig. 29.1 shows the observed S-element fronts along side the simulated H^+ concentration profile after two hours. The simulation was performed using the average α and D_{0B} values for NE2 in Table 29.1, and using $C = C_D$ for both the right and left side boundary conditions. The H^+ concentration curves give a reasonable estimate of the placement of the perceived sulfuric acid front. However, the S-element signal indicates a flat concentration profile followed by a sudden drop at the acid diffusion front, while the simulated profile has a gradual drop. It is likely that the S-element observed in the film is a solid sulforous reaction product, caused by a rapid reaction with the sulfuric acid.

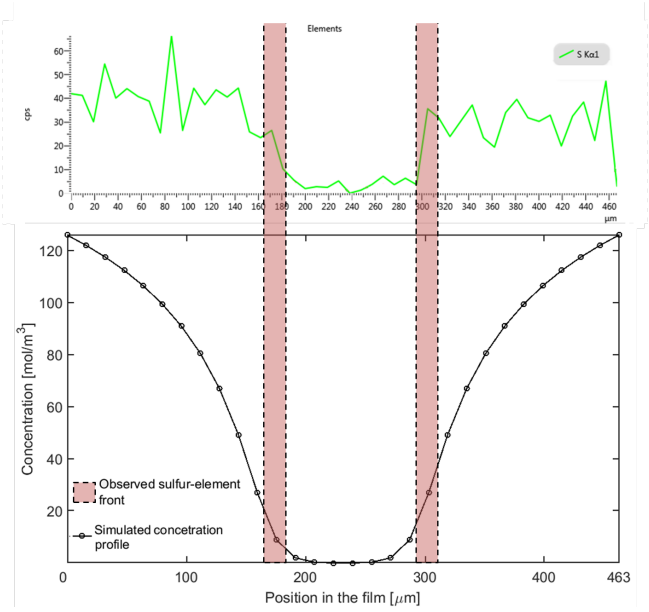

Figure 29.1: Simulated H^+ concentration curved compared to observe S-element diffusion front. The simulation was performed using $C(l = 0) = C(l = l_0) = C_D$ as boundary conditions, $\alpha = 0.005$, $D_{0B} = 97.5 \cdot 10^{-15}$ at $t = 2$ hours.

29.3 Coating performance and lifetime estimation

To put the results into perspective, a 1000 μm coating film is considered. The coating lifetime is defined to end when the simulated pH in the Receiver chamber drops from an initial value of 7 to 4. Using the average D_{0B} and α values shown in Table 29.1, this yields the lifetimes shown in Table 29.2.

Table 29.2: Coating properties and estimated lifetimes based on a 1000 μm film, using average D_{0B} and α values from Table 29.1.

Condition	Coating code	XLD [mEq/l][a]	Density [kg/m^3]	PVC [wt%]	Lifetime [days]
Preliminary	NE4 (Dry)	4.49	1.30	37.0	914±65
(21 ± 1 °C)	NE4 (Saturated)	4.49	1.30	37.0	619±120
Harsh	PU	2.13	1.76	26.4	278±13
(68.5 ± 2.5 °C)	VE	NA	1.25	13.1	>337±18[b]
	NE1	7.79	1.39	15.7	56±3
	NE2	6.38	1.29	16.1	3.2±0.5

[a] Milimol crosslinks per liter dry coating. Theoretical value, assuming full conversion of limiting reactant.

[b] Very conservative estimate, assuming acid breakthrough at the termination of the experiment. The lifetime could be much longer.

The large difference in expected lifetime of NE4 coatings, compared to the rest, is likely due to the distinctive temperatures used during experimentation. Elevated temperatures will increase the diffusion coefficient according to an Arrhenius relationship [90].
As seen in Table 29.2, no correlation was found between expected lifetime and cross-link density (XLD), density, pigment volume concentration (PVC) or dry T_g of the coating samples.
In descending order of performance, the coating barrier properties were as follows:
VE>>PU>NE1>>NE2.

29.4 Coating degradation and diffusion mechanisms

The difference between the breakthrough and the steady state diffusion coefficient values indicates that a change is happening inside the coatings, causing a faster acid diffusion once the acid has permeated the film. It is likely that the presence of acid induces changes in the coating film, causing a reduction in the coating barrier properties behind the acid front, such as depicted in Fig. 3.11 where ionic diffusion, followed by reactions with the resin, created a corroded layer, which could reduce the coating barrier properties. In Section 3.2, the amine linkage found in all NE coatings, the ester bonds in VE, and urethane linkages found in PU, were all reported as vulnerable to acid-induced hydrolysis. However, if these bonds were hydrolyzed in the present work, the coating barrier properties would also diminish after acid permeation had occurred, and a steady state flux should never be reached. Furthermore, FTIR scans in Section 11 provided no evidence of hydrolysis reactions. Only dissolution of limestone filler in the PU coating was observed by the disappearance of the $CaCO_3$ absorption peak.
For PU, the dissolution of limestone filler (initially 9.3 wt%) could provide an accessible pathway for acid diffusion. For the NE coatings, the resin-filler or resin-pigment interfaces could provide transport paths for the diffusing acid, enabling a faster diffusion rate.
Stress-cracking inside the coating film could also account for the increased diffusion coefficient. This phenomenon was observed using scanning electron microscopy inside the NE2 coating in Fig. 12.1; it was most likely caused by rapid acid permeation yielding high coating weight increase ($\approx$ 13%) under Harsh acidic conditions.

If the barrier properties were reduced through acid-filler interactions or stress-cracking, then once the

acid permeated the entire film, a degraded coating would remain. The movement of the acid front before breakthrough, corresponding to the D_{0B} values in Table 29.1, can be expressed by a virgin diffusion coefficient, D_{virgin}. After acid breakthrough, corresponding to the D_{0T} and D_{0SS} values, the acid flux would be a result of the degraded diffusion coefficient, $D_{degraded}$, which was found to be around one to two orders of magnitude larger than the virgin coefficient. Fig. 29.2 provides a depiction of the expected mechanisms.

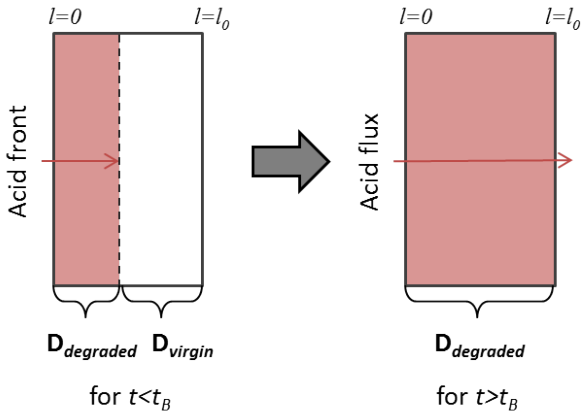

Figure 29.2: Time-dependent diffusion phenomena of coating films in the diffusion cell. The D_{virgin} diffusion coefficient value is related to the movement of the acid front only. The $D_{degraded}$ diffusion coefficient value represents acid diffusion through the degraded coating, behind the acid front. The $D_{degraded}$ determines the steady state diffusion once the acid breakthrough time, t_B, is reached.

29.5 Water saturation effects

Diffusion cell experiments differ from industrial applications due to the lack of a substrate, which, in the cell, is replaced with distilled water. This causes a diffusion of water from the Receiver to the Donor chamber during experimentation. The Preliminary experiments can be used to examine the effect of water saturation.

Table 29.1 shows no significant difference between the D_{0SS} and D_{0T} values for the dry and saturated Preliminary experiments. However, the saturated D_{0B} values are on average 33.8% higher than the dry. This indicates that pre-saturation of coatings in water speeds up the breakthrough time, but not the steady state diffusion rate. This makes sense, given that the steady state ionic diffusion always occurs through a water-saturated film, regardless of the coating pre-treatment.

The coating pre-saturation provided time for water to penetrate and plasticize the film, lowering the T_g [160], thereby allowing a faster acid diffusion rate and yielding a shorter breakthrough time. A similar T_g reduction must therefore also occur for dry coatings, due to diffusion of demineralized water in the opposite direction. This ultimately causes D_{B0} values estimated using the diffusion cell, to be somewhat higher than for situations where a substrate is present.

29.6 Combined diffusion cell mechanism

Based on the degradation mechanism shown in Fig. 29.2, and the observations made regarding the effects of water saturation, a combined mechanism to describe the diffusion phenomena in diffusion cells, observed for reactive acidic substances, can be suggested. The mechanisms are illustrated in Fig. 29.3. The figure depicts the diffusion phenomena observed in the diffusion cell for pre-saturated coating films and dry films, compared with the expected diffusion mechanism for industrial situations where a coating is applied to a substrate.

For pre-saturated coatings in the diffusion cell, the acid front is continuously moving through a virgin pre-saturated film, while a flux of water is occurring in the opposite direction. When the acid front reaches the Receiver chamber, the observed concentration change is determined by the acid flux through a fully degraded coating.

For dry coatings in the diffusion cell, three diffusion fronts are initially present in the film. From the Donor to the Receiver chamber, an acid front is moving through the non-saturated coating, while a water front is moving ahead of the acid front. In the opposite direction a water front is moving, reducing the T_g of the affected area. When $t = t_f$ the acid and water fronts meet, and the acid front rate is changed, yielding a new diffusion coefficient which is around 34% larger than the dry value. This also allows a water flux from the Receiver to the Donor chamber. Finally when $t = t_B$ the acid front has reached the Receiver chamber, and the acid flux is occurring through a degraded coating film.

In practice, acid and water will not diffuse as a vertical concentration front, more likely they will have a concentration gradient through the coating film. The plasticization and T_g reduction will occur over time within the water saturated area, and coating degradation will likely develop gradually within the acid exposed area.

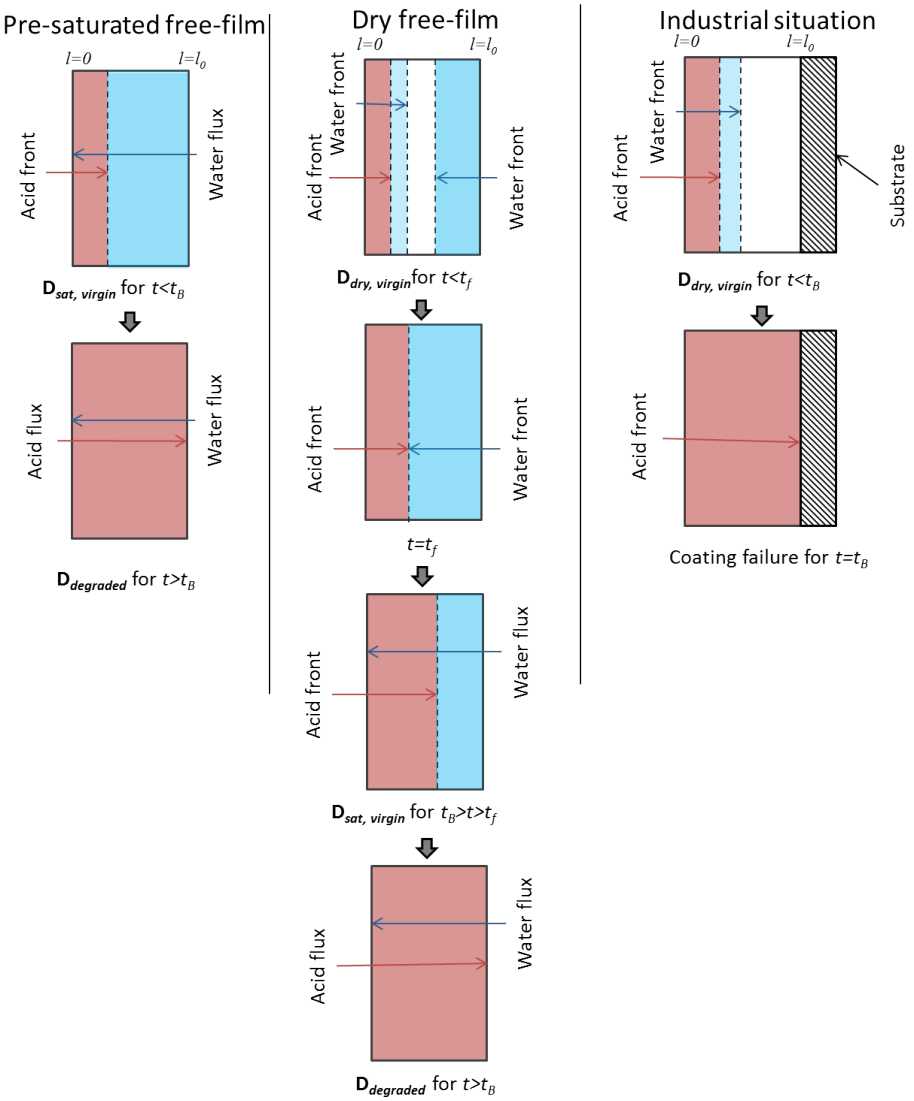

Figure 29.3: Diffusion phenomena of pre-saturated and dry coating films in the diffusion cell with a comparison to a real-life situation. The diffusion coefficients depicted are for acid diffusion only. D_{sat} and D_{dry} are the diffusion coefficients of acid in saturated and dry coating respectively. t_f represents the time it takes for the water and acid diffusion fronts to meet. The D_{virgin} diffusion coefficient presents the movement of the acid front before the acid breakthrough time t_B. The $D_{degraded}$ diffusion coefficient represents acid diffusion behind the acid front, and determines the acid flux through a coating after t_B.

30 Validation of model assumptions

Not all the model assumptions were verified in the previous discussion, the following readdresses the most important ones.

- The H^+ diffusion in water was assumed to be much higher than inside the coating. The H_2SO_4 diffusion coefficient in water is around 10^{-9} m^2/s [161] compared to an approximate value of 10^{-14} m^2/s through coatings, i.e. five magnitudes lower.
- The coating thickness was considered constant. However, the films will to some extent swell or contract causing up to a 9% change in thickness, as seen in the immersion experiments.
- It was assumed that no H^+ ions are produced or consumed inside the coating due to acid-coating reaction. This assumption could not be verified.
- Electric potential gradients were neglected and the H^+ and HSO_4^- counter-ions were assumed to diffuse together. This is a crude assumption, especially in the pre-breakthrough period, where the ionic strength is low inside the coating film.
- It was assumed that HSO_4^- ions do not dissociate to H^+ and SO_4^{2-}. This too is a crude assumption because the pKa value of the equilibrium is approximately 2 at 25 °C [162].

In the light of the other simplifying model assumptions and the experimental uncertainty, these added complexities are not expected to improve simulations at the present stage.

31 Conclusions

The new acid diffusion cell was a useful tool for analyzing coating barrier properties and estimating coating lifetime. The battery of cells used allowed a relatively fast mapping and performance comparison of a series of coating products. The cell results also provided insight into the various diffusion mechanisms. As a barrier to sulfuric acid diffusion in conditions similar to agitated leaching conditions, the vinyl ester is the optimal candidate. Of the coatings tested, the barrier performance in descending order are: vinyl ester >> polyurethane > 100% solids amine-cured novolac epoxy >> amine-cured novolac epoxy.
It was possible to model the diffusion behavior (breakthrough time and steady state acid flux) using a concentration and three-step time-dependent diffusion coefficient. The acid diffusion rate was greatly increased after acid breakthrough, due to a degradation of coating barrier properties, most likely caused by reactions with the diffusing acid at the resin-filler interface, or stress-cracking in the film. Water saturation of the coating film was found to decrease acid breakthrough time.
The model accuracy may be improved by including the effects of water saturation, film swelling, electric potential gradients and HSO_4^- dissociation. The nature of the acid-induced reduction of coating barrier properties, e.g. chemical reaction or cracking, needs to be better understood before it can be properly included in the model.

Part V
Combined polishing and acid diffusion

The immersion, diffusion cell and pilot-scale agitated leaching experiments performed and described in the previous parts can be used to map the relative performance of the selected experimental coatings. This part provides an overview of coating performance, effective lifetime predictions, and the synergy between the various degradation mechanisms which are seen in an agitated leaching reactor.

Nomenclature

D	Diffusion coefficient [m^2/s]
l_0	Coating thickness [m]
p	Polishing rate [m/s]
t	Time [s]

Subscripts

B	Breakthrough
d	Diffusion
p	Polishing

32 Coating performance

Using the coating immersion, diffusion cell, pilot-scale experiments, and the literature review, it was possible to map the performance of the selected coatings. A summary for each coating in the Harsh agitated leaching environment is given in Table 32.1 below.

Table 32.1: Coating performance in the Harsh agitated leaching environment. 1:Very poor, 2:Poor, 3:Good, 4:Very good.

	NE1	NE2	NE3	PU	VE
Chemical inertness	2	1	1	3	4
Barrier properties	1	1	NA[a]	3	4[b]
Erosive resistance	2	NA[a]	NA[a]	2	4

[a] Coating was compromised too fast to obtain any useful data
[b] No acid permeation was observed in diffusion cell experiments

The novolac epoxy type coatings were generally very susceptible to chemical degradation in the sulfuric acid environment. The NE1 and NE2 had a high weight gain in immersion experiments and showed discoloration followed by blistering or delamination after several days of exposure. The NE3 coating broke apart after a few hours and no further experimentation was performed using this coating. FTIR analysis showed no evidence of chemical reactions in the film, while literature suggests the amine-linkages found in the resin network could be vulnerable. It is likely that the filler-resin and pigment-resin interface gets disrupted by the sulfuric acid, and/or stress-cracking is caused by the high weight uptake. The low acid resistance was accompanied by poor acid barrier properties as shown through experiments with the diffusion cells, and poor erosive resistance in the agitated leaching reactor, where NE1 was the only epoxy coating to last long enough for any data to be gathered. The NE coatings are very poor choices for the agitated leaching reactor conditions.

The polyurethane had limestone fillers which dissolve in acidic conditions and urethane linkages which are noted in the literature to be vulnerable to acid hydrolysis, and yet the appearance of the PU coating was unaffected by acid exposure. The limestone filler was shown to dissolve by FTIR analysis and weight loss in immersion experiments, while no evidence was discovered regarding the breakage of urethane groups. The barrier properties of PU were better than the NE type coatings but still too poor for continuous immersion. The PU's low T_g caused relatively high polishing rates in agitated leaching environment. Therefore, the current PU was a poor choice for the agitated leaching reactor, but it could find use in secondary exposure areas.

The vinyl ester coating showed a high degree of chemical inertness, with low weight gain in immersion experiments, accompanied by a slight darkening. The ester groups in the VE network can be hydrolyzed in acid, but literature says this reaction is hindered by sterical effects. Acid exposure did, however, increase the coating polishing rates, though it remained very low. Diffusion cell experiments showed good barrier properties, so good that the experiment had to be terminated before acid permeation was observed. The VE is suitable for the agitated leaching environment and similar acidic environments, though further experimentation is required to accurately predict the barrier properties.

33 Lifetime optimization

To optimize coating lifetime in the agitated leaching environment, the first priority is to ensure that the cured resin, fillers and resin-filler interfaces are chemically inert. Chemical degradation has been found to severely diminish both, coating barrier properties and wear resistance. The coating T_g should always be above the operational temperature, as coating softening also reduces barrier properties and wear resistance. The effects of chemical degradation shrouded the effects of other parameters such as cross-link density, density, pigment/volume concentration, and hardness, on ionic diffusion and polishing rates. However, literature discussed in Section 3.1 suggests that increasing the cross-link density, the amount of crystalline regions in a resin, and using barrier fillers reduce molecular permeation speeds. While literature in Section 3.3 suggests that for polishing rates, a high coating coating hardness, relative to the erosive particle, is desirable in low impact angle regions, while a more rubbery/ductile nature is wanted in high impact angle regions of the reactor.

34 Polishing effects on acid diffusion

Coating failure due to acid diffusion was the dominant, lifetime determining, mechanism for NE1, NE2, PU, and VE in an agitated leaching tank. Even the delamination failures observed for NE1 and NE2 after 15 days and 17.5 hours respectively, were found to occur after the simulated acid front permeated the film, which was 12 days and 16.8 hours respectively. However, diffusion cell experiments neglected the effects of polishing. When the coating is continuously polished while acid is diffusing through, the effective coating thickness is reduced, which in turn decreases the time of acid breakthrough.
The lifetime of a 1000 μm coating film was previously determined, based on coating polishing rates, and acid diffusion rates, separately. An effective lifetime of coatings exposed to both degradation mechanisms, would be the time it takes for the acid concentration to reach a critical concentration on the substrate-side of a film which is simultaneously being worn down. However, the addition of polishing rates in the model developed for acid diffusion, was too extensive to be included in the current project. Instead, the relative importance of polishing and diffusion resistance is estimated by comparing the time constants for each phenomena.

The time constants for acid diffusion and coating polishing in the leaching reactor environment, are given in Eqn. 20 and 21 respectively, while the ratio of the two is given in Eqn. 22.

$$t_d = \frac{l_0^2}{D_B} \tag{20}$$

$$t_p = \frac{l_0}{p} \tag{21}$$

$$\frac{t_d}{t_p} = \frac{l_0 \cdot p}{D_B} \tag{22}$$

An approximate D_B value can be found using Eqn. 7, presented in Section 3.1.4, with the experimental breakthrough time and coating thickness determined using the diffusion cells. Note that D_B is an experimentally estimated constant, and does not vary with acid concentration such as the previous model work. An extensive list of D_B values for all coating samples is given in Appendix K. The

p values are the maximum polishing rates observed from "Harsh" environment experiments, in the agitated leaching reactor. Table 34.1 shows the p and mean D_B values for PU, NE1 and VE.

Table 34.1: Experimentally estimated rate parameters for determining the relative effects of acid diffusion and coating polishing.

	NE1	PU	VE
$p \cdot 10^{-10}$ [m/s]	1.94 ± 0.24	2.22 ± 0.01	0.53 ± 0.01
$\overline{D}_B \cdot 10^{-14}$ [m^2/s]	26.8 ± 1.2	5.8 ± 0.5	5.8 ± 0.4^a

[a] Very conservative estimate

The relationship of the time constants, shown in Eqn. 22, is a crude estimate of the relative time it takes for the diffusion and polishing fronts to reach a given coating thickness. When $t_d/t_p > 1$, the diffusion resistance is larger than the polishing resistance. The polishing front will reach the full coating thickness faster than the diffusion front, and coating performance is best improved by increasing the polishing resistance. When $t_d/t_p < 1$ the opposite is true. Fig. 34.1 provides a depiction of those phenomena, where $t_d/t_p = 1$ divides the graph into an polishing dominant and diffusion dominant section, with the slope being the p/D_B relationship. Fig. 34.1 also shows the time-constant ratio for the PU, NE1, and VE coatings, using the values in Table 34.1. It can be seen that for all coatings, until a thickness of around 2500 μm, polishing resistance is dominant, and improvements of coating performance should be focused on increasing diffusion barrier properties. The significance of polishing rates in the effective lifetime determination, increases the better barrier properties a coating has.

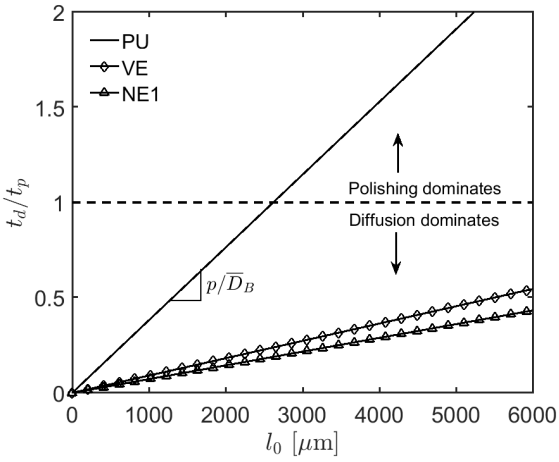

Figure 34.1: Ratio of diffusion and polishing time constants as a function of coating thickness for PU, VE, and NE1. The relative importance of the polishing and diffusion phenomena are indicated by the separating line at $t_d/t_p = 1$. Note that the $\overline{D}_B$ value used for VE is an overestimate of the actual value.

35 Combined mechanisms

The diffusion, polishing, and chemical reaction mechanisms, are coupled. The results presented in the previous Parts show how these degradation mechanisms influence each other, the following is a summary of this:

Ionic diffusion enables chemical reactions. Hojo et al. [72] theorized a mechanism for the relationship between diffusion and reaction, presented in Fig. 3.11, where diffusion is said to enable reactions to occur inside a coating film. This was also observed in the current study for an amine-cured novolac epoxy, where sulfuric acid diffusion left a visually degraded coating film, shown in Fig. 12.1.

Chemical reactions influence ionic diffusion. This too was included in Hojo's degradation mechanisms, where chemical reactions would damage the coatings barrier properties by chain scissoring the resin network. Such a phenomena was observed during the diffusion cell experiments, where the acid-permeated coating films had reduced barrier properties, compared to what they had before acid saturation. Fig. 29.2 describes the observed phenomena.

Combined diffusion/reaction affects the polishing rate. The experiments in Mild and Harsh conditions in the pilot-scale leaching reactor, showed how the low pH environment would increase the coating polishing rates. As depicted in Fig. 18.1, the degradation zone, created by ionic diffusion and reactions in the resin, alters the mechanical properties of the coating surface and thus its erosive resistance.

Erosive wear speeds up ionic diffusion. Finally, the continued polishing of a coating film enables ionic diffusion to occur faster, as the effective coating thickness is reduced.

Part VI
Conclusions

This thesis investigated chemical, physical, and erosive degradation of organic coatings, using immersion experiments, diffusion cells, and a pilot-scale leaching reactor to map the influence of the individual degradation mechanisms, and determine coating lifetime in agitated leaching reactors.
Three types of resins were used for experimentation, each type being to some degree recommended for acidic environments. The poorest performance was from amine-cured novolac epoxies that experienced blistering, discoloration, high weight gain, poor barrier properties, and rapid delamination in warm sulfuric acid. The performance in acidic-erosive environments was equally poor, due to these chemical interactions with the acid. Polyurethane showed higher resistance to the acid, with a lesser discoloration, slight weight loss, and improved barrier properties. However, its performance in the acidic and erosive environment was as poor as the novolac epoxies, in part due to to the chemical interactions with the acid, and partly because of its low glass transition temperature. The vinyl ester coating was far superior to the novolac epoxies and the polyurethane, with little discoloration, low weight gain, excellent barrier properties, and with no deformations in the warm acid. Its resistance to acidic-erosion was also higher than the other coating types.
Chemical degradation was the most significant factor in influencing coating lifetime. Coatings that were susceptible to reactions with sulfuric acid, like the amine and amide-cured novolac epoxies and polyurethane, would have reduced barrier properties and greatly diminished erosive resistance in the acidic environment compared to the vinyl ester, which was relatively inert.

Diffusion cells were constructed and used to monitor the diffusion of H^+ ions through thin barrier coatings, and the data were used to predict the performance of thicker films. Despite their simple design, the cells proved useful for determination of coating barrier properties and investigating diffusion mechanisms. Water saturation was found to decrease the time required for acid breakthrough, by lowering of the coating glass transition temperature. Therefore, due to the diffusion of demineralized water into the coating, the diffusion cell would simulate an ionic breakthrough time which is slightly shorter than in industrial situations. It was also found that to model experimental results, a concentration and three-step time dependency of the diffusion coefficient was required. Degradation of the coating barrier properties, due to sulfuric acid exposure, proved a significant factor. The diffusion coefficient had to be increased after acid breakthrough by a factor of 18 to 190, to simulate both the breakthrough time and the subsequent steady state flux.

A pilot-scale agitated leaching reactor was constructed to evaluate coating performance in full scale reactors, and to determine the effects of simultaneous acidic and erosive exposure. Dry film thickness change was used to monitor coating polishing rates and estimate erosion lifetime. The polishing rates were found to vary on the coating samples, placed on the reactor bottom, due to variations in particle impact angle and speed. Coating erosion was also found to be influenced by the chemical environment, as acidic conditions were able to increase polishing rates by a factor of two to six, compared to more neutral erosive environments. The enhanced polishing rates were closely linked to the chemical susceptibility of the coating in question.

The immersion, diffusion cell, and pilot-scale reactor experiments were combined to estimate the coating lifetime inside an agitated leaching reactor. Reactions with sulfuric acid, causing delamination were found to be the dominant failure mechanism for amine-cured novolac epoxies, they would fail after around two weeks into exposure. Acid diffusion was the dominant mechanism for the polyurethane and vinyl ester, and the coating polishing rates in agitated leaching reactors would increase the diffusion rate. It was initially hypothesized that protective organic coatings could fail via three main mechanisms: reaction, diffusion, and erosion. It was discovered through the literature study and experiments, that rather than viewing the mechanisms separately, coating failure is more likely to occur by a combination of the three. The coupled phenomena are as follows:

- Ionic diffusion enables chemical reactions in the coating.
- Chemical reactions can enhance ionic diffusion.
- The combined diffusion/reaction can reduce a coating's erosion resistance.
- Erosive wear increases ionic diffusion rates.

As an example, consider a 1000 μm thick polyurethane coating for use in an agitated leaching reactor. Acid immersion experiments would show a durable coating, with little discoloration and no deformation. Erosive experiments in the pilot-scale reactor, without the low pH environment would result in a lifetime of 1100 days, but adding acid to the slurry would reduce the lifetime to 500 days. However, diffusion cell experiments would indicate an even lower lifetime, of 278 days. Finally, adding the effect of acid-slurry erosion further decreases the coating lifetime, as the effective thickness is reduced, but improvements in coating diffusion barrier properties were found to be the most significant factor. It is therefore necessary to investigate all the plausible degradation mechanisms before evaluating a coating's usability, but it is also required to evaluate the synergies between the mechanisms to provide an accurate mapping of coating performance.

Future work

This section provides suggestions for future work beyond experimenting with new coating formulations or using different environmental conditions with the pilot-scale agitated leaching reactor and diffusion cell set-ups.

A degradation of the epoxy novolac coatings was observed in sulfuric acid, through severe reductions in coating barrier properties, erosive resistance, and internal crack formation. This degradation was not observed in warm water erosion or immersion experiments. It was suggested that the disruption of physical bonds between resin and fillers by the permeating acid, and stress-cracking from rapid volume increase, were the main causes of epoxy failure. However, further investigations are required to enlighten the chemical degradation mechanisms, causing the amine-cured novolac epoxies to have high weight uptake and diminished resistances in warm sulfuric acid.
In a similar case, the vinyl ester was found to have diminished erosion resistance in sulfuric acid, even though it performed well in the diffusion and immersion experiments. Investigations into possible chemical interactions with the sulfuric acid could show the reason behind this, and help formulate coating solutions for simultaneous chemical and erosive exposure.

A diffusion model was developed to evaluate and compare the coating barrier properties, this model was based on a series of simplifying assumptions since the diffusion mechanism is not thoroughly understood. Some of these assumptions can be included to develop a model which has a closer proximity to reality. The effects of water saturation could be included, by knowing the speed of demineralized water diffusion and the impact of water saturation on the acid diffusion coefficient. The effects of coating swelling and coating erosion could be included by including moving fronts. The simplifying assumptions such as neglected potential gradients, no second sulfuric acid dissociation, and ideal liquids could also be included. Finally the effects of chemical interactions inside the resin could be added, once more knowledge has been acquired on the subject.

Finally, to draw a comparison between industrial-scale and pilot-scale coating's performance, the results acquired using the pilot-scale agitated leaching reactor need to be verified in full-scale. Full-scale operations may include factors that where not considered in the present work, such as extended downtime or environmental fluctuations, which could add new failure mechanisms. Furthermore, the coating polishing rates in full-scale operations need to be mapped to ensure that the erosive conditions used in the present work are comparable.

References

[1] Møller, VB, Dam-Johansen, K, Frankær, SM, Kiil, S, "Acid resistant organic coatings for the chemical industry: a review", J. Coat. Techol. Res. 14 (2) 279–306 (2017)

[2] Allahverdi, ALI, Škvára, F, "Acidic corrosion of hydrated cement based materials part 1.- Mechanism of the phenomenon", Ceramics 44 (3) 114–120 (2000)

[3] Policastro, S, Martin, F, Natishan, P, Moran, P, "Corrosion and corrosion control", in: Kirk-Othmer Encyclopedia of Chemical Technology, pp. 1–31, John Wiley and Sons (2011)

[4] Harvey, C, "Delta air lines flying high with containment coatings", Coatings Pro Magazine (2014)

[5] Silva, M, "Cold bonding eliminates tank's through-wall corrosion", Coatings Pro Magazine (2014)

[6] Moukwa, M, Barkey, T, "The performance of thermoset polymers in mineral and organic acid service", J. Prot. Coat. Linings 13 (7) 58–69 (1996)

[7] Banna, MH, Shirokoff, J, Molgaard, J, "Effects of two aqueous acidic solutions on glass reinforced vinyl ester resins tubes", Canadian Metallurgical Quarterly 51 (1) 91–100 (2012)

[8] Kelley, D, "How to reduce construction and maintenance costs in metal extraction and refining processes", in: SME Annual Meeting and Exhibit, pp. 326–329 (2010)

[9] Hare, CH, "Corrosion control of steel by organic coatings", in: Uhlig's Corrosion Handbook, pp. 971–983, John Wiley and Sons (2011)

[10] Khaladkar, PR, "Using plastics, elastomers, and composites for corrosion control", in: Uhlig's Corrosion Handbook, pp. 915–970, John Wiley and Sons (2011)

[11] Hag, N, Harrison, P, "Experience with the use of Derakane vinyl ester-based GRP in flue gas desulphurization plants", Anti-Corros. Method Mater. 43 (2) 15–19 (1996)

[12] Shing, CK, Wu, CML, Chen, JWJ, Yuen, CS, Ricky, YC, "A review on protection of concrete for sewage installations and an accelerated test on protection systems", Hong Kong Inst. Eng. Transactions 19 (3) 8–16 (2011)

[13] Reichhold Inc., "FRP material selection guide: An engineer's guide to FRP technology", Tech. rep., Reichhold Inc. (2009)

[14] Hare, CH, "Chemically induced degradation", J. Prot. Coat. Linings 16 (12) 17–25 (1999)

[15] Cooper, CD, "Air pollution control", in: Kirk-Othmer Encyclopedia of Chemical Technology, John Wiley and Sons (2007)

[16] Ragnar, M, Henriksson, G, Lindstrom, ME, Wimby, M, Blechschmidt, J, Heinemann, S, "Pulp", in: Ullmann's Encyclopedia of Industrial Chemistry, Wiley-VCH (2014)

[17] Compère, C, Hechler, J, Cole, K, "Behavior of phenolic-coated steel in concentrated sulfuric acid", Prog. Org. Coat. 20 (2) 187–198 (1992)

[18] Duby, P, "Metallurgy", in: Kirk-Othmer Encyclopedia of Chemical Technology, John Wiley and Sons (2005)

[19] De Belie, N, Monteny, J, Beeldens, a, Vincke, E, Van Gemert, D, Verstraete, W, "Experimental research and prediction of the effect of chemical and biogenic sulfuric acid on different types of commercially produced concrete sewer pipes", Cement Concrete Res. 34 (12) 2223–36 (2004)

[20] Hacias, K, "Metal surface treatments, pickling", in: Kirk-Othmer Encyclopedia of Chemical Technology, pp. 1–3, John Wiley and Sons (2000)

[21] Taylor, AW, "Fertilizers", in: Kirk-Othmer Encyclopedia of Chemical Technology, pp. 111–128, John Wiley and Sons (2004)

[22] Dittmar, H, Drach, M, Vosskamp, R, Trenkel, ME, Gutser, R, Steffens, G, "Fertilizers, 2. types", in: Ullmann's Encyclopedia of Industrial Chemistry, pp. 200–246, Wiley-VCH (2009)

[23] Bayer, O, "Polyurethane", Angewandte Chemie 59 (9) 257–288 (1947)

[24] Staff., J, "Coating systems for concrete in severe service: A brief discussion", J. Prot. Coat. Linings 23 (1) 50–57 (2006)

[25] Watkins, MJ, "Epoxy resins in coatings", in: Paint and Coating Testing Manual, 15th edn, pp. 87–92, ASTM (2012)

[26] Gannon, JA, "History and development of epoxy resins", High Perfor. Poly.: Orig. Devel. pp. 299–307 (1986)

[27] Kelley, D, Graham, J, Johnson, T, "Different FRP resin chemistries for different chemical environments", Tech. rep., Ashland Perfomance Materials (2010)

[28] Thomson, B, Campion, RP, "Testing of polymeric materials for corrosion control", in: Uhlig's Corrosion Handbook, pp. 1107–16, John Wiley and Sons (2011)

[29] Sonawala, SP, Spontak, RJ, "Degradation kinetics of glass-reinforced polyesters in chemical environments. Part 1 Aqueous solutions", J. Mater. Sci. 31 (18) 4757–65 (1996)

[30] Marais, S, Metayer, M, Nguyen, TQ, Labbe, M, Saiter, JM, "Diffusion and permeation of water through unsaturated polyester resins - influence of resin curing", European Poly. J. 36 (3) 453–462 (2000)

[31] Miller, WA, Schlanger, LM, Baumgaertner, ER, "Fluoroplastics", Managing Corros. Plastics 5 98–102 (1983)

[32] Koga, A, Yamabe, T, Sato, H, Uchida, K, Nakayama, J, Yamabe, J, Nishimura, S, "A visualizing study of blister initiation behavior by gas decompression", Trib. Online 8 (1) 68–75 (2013)

[33] Byrappa, K, "Hydrothermal processing", in: Kirk-Othmer Encyclopedia of Chemical Technology, John Wiley and Sons (2005)

[34] Takadoum, J, "Tribology", in: Kirk-Othmer Encyclopedia of Chemical Technology, pp. 1–18, John Wiley and Sons (2012)

[35] Møller, P, Nielsen, LP, Advanced surface technology: volume 1, Moeller and Nielsen (2013)

[36] Zhang, S, Dam-Johansen, K, Nørkjær, S, Bernad, PL, Kiil, S, "Erosion of wind turbine blade coatings - Design and analysis of jet-based laboratory equipment for performance evaluation", Prog. Org. Coat. 78 103–115 (2015)

[37] Wicks, ZW, Jones, FN, "Coatings", in: Kirk-Othmer Encyclopedia of Chemical Technology, pp. 1–88, John Wiley and Sons (2013)

[38] Mallinson, JH, "Abrasion of fiber-reinforced plastics in corrosive environments", Chem. Eng. 89 (11) 143–144 (1982)

[39] Kalenda, P, "Diffusion of acids into epoxy resin compositions", Appl. Poly. Sci. 45 (12) 2235–38 (1992)

[40] Hare, CH, "Chemically induced degradation of coatings: Part II", J. Prot. Coat. Linings 17 (1) 63–75 (2000)

[41] Møller, P, Nielsen, LP, Advanced surface technology: volume 2, Moeller and Nielsen (2013)

[42] Lawrence, GCK, "New developments in reinforced corrosion-resistant thermosetting plastic lining materials", Australasian Corros. Eng. 19 (4) 25–28 (1975)

[43] Campbell, JL, "Metals resist hot sulfuric acid", Ind. Eng. Chem. 53 (11) 125–126 (1961)

[44] Schweitzer, PA, Fundamentals of metallic corrosion, vol. 825, Taylor and Francis Group (2006)

[45] MetalPrices.com, "MetalPrices.com", URL `www.metalprices.com`, [accessed 16-10-2015] (2015)

[46] Infomine.com, "Infomine.com", URL `www.infomine.com`, [accessed 16-10-2015] (2015)

[47] Hall, GR, "Improved corrosion protection for flue gas systems utilizing a dual liner concept", Energy in the 90's pp. 100–108 (1991)

[48] Hall, GR, Sauereisen, CK, "Restoration of a brick chimney with a dual lining system and polymer concrete", Mater. Performance 45 (11) 34–38 (2006)

[49] Sergent, JE, "Ceramic materials", in: Ceramic Interconnect Technology Handbook, pp. 163–197, Taylor and Francis Group (2007)

[50] Morrell, R, "Ceramics, structural", in: Kirk-Othmer Encyclopedia of Chemical Technology, John Wiley and Sons (2011)

[51] Bennett, JP, "Corrosion resistance of ceramic materials to hydrochloric acid", Tech. rep., Bureau of mines (1983)

[52] Leigh, HD, "Refractories", in: Kirk-Othmer Encyclopedia of Chemical Technology, John Wiley and Sons (2000)

[53] Regester, RF, "Behavior of fiber reinforced plastic materials in chemical service", Corrosion 25 (4) 157–167 (1969)

[54] Morton, M, "Elastomers, synthetic, survey", in: Kirk-Othmer Encyclopedia of Chemical Technology, pp. 1–20, John Wiley and Sons (2009)

[55] ASTM Commitee D01, "D16 - Standard terminology for paint, related coatings, materials, and applications", Tech. rep., ASTM (2015)

[56] ASTM Commitee J01, "G193 - Standard terminology and acronyms relating to corrosion", Tech. rep., ASTM (2013)

[57] Praw, M, "Polyurethane coatings: A brief overview", J. Prot. Coat. Linings 30 (8) 34–39 (2013)

[58] Stevens, MP, Polymer chemistry: An introduction, Addison-Wesley (1975)

[59] Pham, HQ, Marks, MJ, "Epoxy resins", in: Ullmann's Encyclopedia of Industrial Chemistry, pp. 155–244, Wiley-VCH (2005)

[60] Hall, GR, "Understanding the basics of chemical-resistant polyesters and vinyl esters", J. Prot. Coat. Linings 30 (11) 34–45 (2013)

[61] Allen, RC, "Some corrosion mechanisms in attack of resin and resin-glass laminates", Poly. Eng. Sci. 19 (5) 329–336 (1979)

[62] Mills, CC, Day, FB, "Application of thermoplastics for corrosion control", Managing Corros. Plast. 5 1–12 (1983)

[63] Gahleitner, M, Paulik, C, "Polypropylene", in: Ullmann's Enclyclopedia of Industrial Chemistry, pp. 1–44, Wiley-VCH (2014)

[64] Jeremic, D, "Polyethylene", in: Ullmann's Enclyclopedia of Industrial Chemistry, pp. 1–42, Wiley-VCH (2014)

[65] Hintzer, K, Zipplies, T, Carlson, DP, Schmeigel, W, "Fluoropolymers, organic", in: Ullmann's Enclyclopedia of Industrial Chemistry, pp. 1–55, Wiley-VCH (2013)

[66] Chapman, FM, "Fluoropolymer linings for corrosion protection of chemical process equipment", Managing Corros. Plastics 5 121–127 (1983)

[67] Chandrasekaran, VC, Rubber as a construction material for corrosion protection: A comprehensive guide for process equipment designers, Scrivener Publishing LLC (2010)

[68] Webb, RN, Shaffer, TD, Tsou, AH, "Butyl rubber", in: Kirk-Othmer Encyclopedia of Chemical Technology, John Wiley and Sons (2003)

[69] Visakh, P, Sabu, T, Arup, KC, Mathew, AP, Advances in elastomers I, vol. 11, Springer (2013)

[70] Ashland Inc., "Design engineers depend on FRP for corrosion challenges in chemical processing", Tech. rep., Ashland Inc. (2015)

[71] Tsuda, K, "Behavior and mechanisms of degradation of thermosetting plastics in liquid environments", J. Japan Petroleum Inst. 50 (5) 240–248 (2007)

[72] Hojo, H, Tsuda, K, Kubouchi, M, Kim, DS, "Corrosion of plastics and composites in chemical environments", Met. Mater. 4 (6) 1191–97 (1998)

[73] Abeysinghe, H, Edwards, W, Pritchard, G, Swampillai, G, "Degradation of crosslinked resins in water and electrolyte solutions", Poly. 23 (12) 1785–90 (1982)

[74] Sobrinho, LL, Ferreira, M, Bastian, FL, "The effects of water absorption on an ester vinyl resin system", Mater. Res. 12 (3) 353–361 (2009)

[75] Sonawala, SP, Spontak, RJ, "Degradation kinetics of glass-reinforced polyesters in chemical environments. Part 2 Organic solvents", J. Mater. Sci. 31 (18) 4757–65 (1996)

[76] Abastari, Sakai, T, Sembokuya, H, Kubouchi, M, Tsuda, K, "The reciprocal influence between ion transport and degradation of PA66 in acid solution", Polym. Degrad. Stabil. 91 (11) 2595–604 (2006)

[77] Kootsookos, A, Burchill, PJ, "The effect of the degree of cure on the corrosion resistance of vinyl ester/glass fibre composites", Composites Part A: Appl. Sci. Manuf. 35 (4) 501–508 (2004)

[78] Banna, MH, Shirokoff, J, Molgaard, J, "Effects of two aqueous acidic solutions on polyester and bisphenol A epoxy vinyl ester resins", Mater. Sci. Eng.: A 528 (4-5) 2137–42 (2011)

[79] Crank, J, Park, GS, Diffusion in polymers, Academic Press (1968)

[80] Vanlandingham, MR, Eduljee, RF, Gillespie, JW, "Moisture diffusion in epoxy systems", J Appl. Poly. Sci. 71 787–798 (1998)

[81] George, SC, Thomas, S, "Transport phenomena through polymeric systems", Prog. Poly. Sci. 26 (6) 985–1017 (2001)

[82] Romhild, S, Bergman, G, Hedenqvist, MS, "Transport and adhesion properties of an unlined and a liquid-crystalline polymer-lined vinyl ester thermoset exposed to severe environments", Appl. Poly. Sci. 95 (4) 797–806 (2005)

[83] Wang, Z, Han, E, Liu, F, Ke, W, "Effect of different curing agents on cure reaction and exposure resistance of phenolic-epoxy resins in hot acid solutions", Corrosion 66 (7) 1–9 (2010)

[84] Blankenship, LT, White, MN, Puckett, PM, "Vinyl ester resins: versatile resins for composites", Int. SAMPE Symp. Exhibition (Proc.) 34 (1) 234–245 (1989)

[85] Miller, DR, Macosko, CW, "A New Derivation of Post Gel Properties of Network Polymers", Macromole. 9 (2) 206–211 (1976)

[86] Feng, J, Berger, KR, Douglas, EP, "Water vapor transport in liquid crystalline and non-liquid crystalline epoxies", J. Mater. Sci. 39 (10) 3413–23 (2004)

[87] English, LK, "Liquid-crystal polymers: in a class of their own", Mater. Eng. 103 (3) 36–41 (1985)

[88] Hoyt, AE, Benicewicz, BC, "Rigid rod molecules as liquid crystal thermosets", American Chem. Soc., Poly. Preprints 30 (2) 536–537 (1989)

[89] Grebowicz, JS, "On the formation of liquid crystalline texture in epoxy resins", Macromol. Symp. 104 191–221 (1996)

[90] Kiil, S, "Model-based analysis of photoinitiated coating degradation under artificial exposure conditions", J. Coat. Technol. Res. 9 (4) 375–398 (2012)

[91] Bansal, RK, Sahoo, JC, "Determination of cohesive energy densities of bisphenol-A and epichlorohydrin epoxy resins from swelling measurements", Die Angewandte Makromolekulare Chemie 82 (1265) 149–156 (1979)

[92] Hansen, CM, Hansens solubility parameters. A user's handbook, CRC Press, 2 edn. (2007)

[93] Fried, JR, Polymer science and technology, Prentice Hall Professional Technical Reference, 2 edn. (2003)

[94] Kamaitis, Z, "Structural design of polymer protective coatings for reinforced concrete structures. Part I : Theoretical considerations", Civ. Eng. Management 13 (1) 11–17 (2007)

[95] Sembokuya, HK, Negishi, Y, Kubouchi, M, Tsuda, K, "Corrosion behavior of epoxy resin cured with different amount of hardener in corrosive solutions", Soc. Mater. Sci., Japan 9 (3) 230–234 (2003)

[96] Kalendova, A, "Spinels - reactive pigments affecting the diffusion of corrosive substances through the coatings", Pigm. Resin Technol. 29 (4) 215–221 (2000)

[97] Abacha, N, Kubouchi, M, Sakai, T, Tsuda, K, "Diffusion behavior of water and sulfuric acid in epoxy / organoclay nanocomposites", Appl. Poly. Sci. 112 (2) 1021–29 (2009)

[98] Crank, J, The Mathematics of Diffusion, Clarendon press - Oxford, 2 edn. (1975)

[99] Kalenda, P, "Chemical-resistance values of epoxy resins hardened with polyamines", Pigment Resin Technol. 30 (3) 150–157 (2001)

[100] Hare, CH, "Chemically induced degradation of coatings: Part 3, Pigments", J. Prot. Coat. Linings 17 (2) 58–64 (2000)

[101] Moggridge, GD, Lape, NK, Yang, C, Cussler, EL, "Barrier films using flakes and reactive additives", Prog. Org. Coat. 46 (4) 231–240 (2003)

[102] Pajarito, B, Kubouchi, M, "Flake-filled polymers for corrosion protection", J. Chem. Eng. Japan 46 (1) 18–26 (2013)

[103] Choudalakis, G, Gotsis, aD, "Permeability of polymer/clay nanocomposites: A review", European Poly. J. 45 (4) 967–984 (2009)

[104] Kalenda, P, Kalendova, P, "Improved chemical resistance of epoxy resin-based coating compositions", Dyes Pigments 27 (4) 302–312 (1994)

[105] Ono, S, Tsuda, K, Kubouchi, M, Hojo, H, Nishiyama, T, "Degradation behavior of amine cured epoxy resin and FRP in acid solutions", Proc. ICCM-10 4 215–222 (1995)

[106] Sørensen, PA, Kiil, S, Dam-Johansen, K, Weinell, CE, "Anticorrosive coatings: a review", J. Coat. Technol. Res. 6 (2) 135–176 (2009)

[107] Sørensen, PA, Dam-Johansen, K, Weinell, C, Kiil, S, "Cathodic delamination: Quantification of ionic transport rates along coating-steel interfaces", Prog. Org. Coat. 68 (1-2) 70–78 (2010)

[108] Kotnarowska, D, "Influence of ultraviolet radiation and aggressive media on epoxy coating degradation", Prog. Org. Coat. 37 (3-4) 149–159 (1999)

[109] Schmitz, P, Holubka, J, Xu, Lf, "Mechanism for environmental etch of acrylic melamine-based automotive clearcoats: identification of degradation products", J. Coat. Technol. 72 (904) 39–45 (2000)

[110] Rodgers, W, Garner, D, Cheever, G, "Study of the attack of acidic solutions on melamine-acrylic basecoat/clearcoat paint systems", J. Coat. Technol. 70 (877) 83–95 (1998)

[111] Schmitz, P, Holubka, J, Xu, Lf, "Acid etch of automotive clearcoats II. comparison of degradation chemistry in laboratory and field testing", J. Coat. Technol. 72 (902) 53–61 (2000)

[112] Anderson, E, Capon, B, "Intermolecular general-acid catalysis in acetal hydrolysis", J. Chem. Soc. B-phys. Org. (8) 1033–1037 (1967)

[113] Greene, TW, Peter, GMW, Protective groups in organic synthesis, 5 edn, John Wiley and Sons (2014)

[114] Pritchard, G, Reinforced plastics durability, CRC Press (1999)

[115] Kotnarowska, D, "Epoxy coating destruction as a result of sulphuric acid aqueous solution action", Prog. Org. Coat. 67 (3) 324–328 (2010)

[116] Trahanovsky, W, Oxidation in organic chemistry. Part C: Organic chemistry 5C, Academic Press (1978)

[117] Bauer, DR, "Degradation of organic coatings. I. Hydrolysis of melamine formaldehyde/acrylic copolymer films", Appl. Poly. Sci. 27 (10) 3651–62 (1982)

[118] Hojo, H, Tsuda, K, Ogasawara, K, "Form and rate of corrosion of corrosion-resistant FRP resins", Adv. Composite Mater. 1 (1) 55–67 (1991)

[119] Dang, W, Kubouchi, M, Sembokuya, H, Tsuda, K, "An approach to chemical recycling of epoxy resin cured with amine using nitric acid", Poly. 43 (10) 2953–58 (2002)

[120] Dilafruz, K, Kubouchi, M, Dang, W, Sembohya, H, Tsuda, K, "Chemical recycling bisphenol a type epoxy resin based on degradation in nitric acid", 3rd Int. Symp. Env. Conscious Design Inverse Manufact. pp. 333–338 (2003)

[121] Hojo, H, Tsuda, K, "Effects of chemical environments and stress on corrosion behaviors of glass fiber reinforced plastics and vinyl ester resins", Soc. Plast. Ind., Annual Conf. Proc. (1979)

[122] Huisman, HF, van der Linden, JT, "Degradation of polyurethanes in organic solvents", Org. Coat., Sci. Techn. 6 167–182 (1984)

[123] Stevenson, JS, Kusy, RP, "Structural degradation of polyurethane-based elastomeric modules", J. Mater. Sci.: Mater. Medicine 6 (7) 377–384 (1995)

[124] Tanzi, MC, Mantovani, D, Petrini, P, Guidoin, R, Laroche, G, "Chemical stability of polyether urethanes versus polycarbonate urethanes", J. Biomedical Mater. Res. 36 (4) 550–559 (1997)

[125] ASTM Commitee G02, "G40 - Standard terminology relating to wear and erosion", Tech. rep., ASTM (2013)

[126] Khruschov, M, "Principles of abrasive wear", Wear 28 (1) 69–88 (1974)

[127] Wu, L, Guo, X, Zhang, J, "Abrasive resistant coatings - A review", Lubricants 2 (2) 66–89 (2014)

[128] Hojo, H, Tsuda, K, Yabu, T, "Erosion damage of polymeric material by slurry", Wear 112 17–28 (1986)

[129] Stachowiak, GW, Batchelor, AW, "Abrasive, erosive and cavitation wear", in: Engineering Tribology, eds. GW Stachowiak, AW Batchelor, pp. 501–551, Elsevier B.V., 3 edn. (2006)

[130] Barkoula, NM, Karger-Kocsis, J, "Processes and influencing parameters of the solid particle erosion of polymers and their composites", J. Mater. Sci. 37 (18) 3807–3820 (2002)

[131] Clark, HM, Burmeister, L, "The influence of the squeeze film on particle impact velocities in erosion", Int. J. Impact Eng. 12 (3) 415–426 (1992)

[132] Stachowiak, GW, Batchelor, AW, "Wear of non-metallic materials", in: Engineering Tribology, eds. GW Stachowiak, AW Batchelor, pp. 651–704, Elsevier B.V., 3 edn. (2006)

[133] Arnold, JC, Hutchings, IM, "Flux rate effects in the erosive wear of elastomers", J. Mat. Sci. 24 (3) 833–839 (1989)

[134] Ayranci, I, Machado, MB, Madej, AM, Derksen, JJ, Nobes, DS, Kresta, SM, "Effect of geometry on the mechanisms for off-bottom solids suspension in a stirred tank", Chem. Eng. Sci. 79 163–176 (2012)

[135] Ge, CY, Wang, JJ, Gu, XP, Feng, LF, "CFD simulation and PIV measurement of the flow field generated by modified pitched blade turbine impellers", Chem. Eng. Res. Design 92 (6) 1027–1036 (2014)

[136] Wood, RJK, Jones, TF, Ganeshalingam, J, Miles, NJ, "Comparison of predicted and experimental erosion estimates in slurry ducts", Wear 256 (9-10) 937–947 (2004)

[137] Nazemi, MK, Valix, M, "Evaluation of acid diffusion behaviour of amine-cured epoxy coatings by accelerated permeation testing method and prediction of their service life", Prog. Org. Coat. 97 307–312 (2016)

[138] Carniero, C, Oliveira, F, Nogueira, J, "Permeability of paint film towards chloride ion", J. Coat. Technol. Res. 3 (2) 2–5 (2006)

[139] Kubouchi, M, "Evaluation method of degradation of anti-corrosion epoxy lining for concrete structures", in: Third international conference on sustainable construction materials and technologies

[140] Stuart, B, "Infrared spectroscopy", in: Kirk-Othmer Encyclopedia of Chemical Technology, pp. 1–20, John Wiley and Sons (2005)

[141] Gu, X, Raghavan, D, Nguyen, T, VanLandingham, MR, Yebassa, D, "Characterization of polyester degradation using tapping mode atomic force microscopy: Exposure to alkaline solution at room temperature", Poly. Degrad. Stabil. 74 (1) 139–149 (2001)

[142] Goodhew, PJ, Humphreys, J, Beanland, R, Electron microscopy and analysis, Taylor and Francis Books (2001)

[143] Møller, VB, Dam-Johansen, K, Frankær, SM, Kiil, S, "Simultaneous acid exposure and erosive particle wear of thermoset coatings", Journal of Coatings Technology and Research (2018)

[144] Eyzaguirre, C, Rocks, SS, Klepper, R, Baczek, FA, Chaiko, D, "The FLSmidth rapid oxidative leach (ROL) process: a mechano-chemical approach for rapid metal sulfide dissolution", in: Hydroprocess, vol. 7th, pp. 1–11 (2015)

[145] Lossin, A, "Copper", in: Ullmann's Encyclopedia of Industrial Chemistry, pp. 467–497, Wiley-VCH (2001)

[146] Bai, H, Stephenson, A, Jimenez, J, Jewell, D, Gillis, P, "Modeling flow and residence time distribution in an industrial-scale reactor with a plunging jet inlet and optional agitation", Chem. Eng. Res. and Design 86 (12) 1462–76 (2008)

[147] Voeste, T, Weber, K, Hiskey, B, Brunner, G, "Liquid-solid extraction", in: Ullmann's Encyclopedia of Industrial Chemistry, p. 30 (2012)

[148] Chaiko, D, Baczek, FA, Rocks, SS, Walters, T, Klepper, R, "The FLS rapid oxidative leach (ROL) process. Part I: mechano-chemical process for treating chalcopyrite", in: Com 2015, August (2015)

[149] R.M., G, C.L., C, Solution, minerals, and equilibria, Harper and Row, New York (1965)

[150] Clement, KH, Fangel, P, Jensen, AD, Thomsen, K, Kemiske enhedsoperationer, Polyteknisk Forlag, Copenhagen, Demnark, 5 edn. (2004)

[151] Nienow, AW, "The suspension of solid particles", in: Mixing in the Process Industries, pp. 364–393, Reed Educational and Professional Publishing Ltd (1997)

[152] Oka, YI, Yoshida, T, "Practical estimation of erosion damage caused by solid particle impact: Part 2: Mechanical properties of materials directly associated with erosion damage", Wear 259 102–109 (2005)

[153] King, H, "What is Mohs hardness scale?", URL `http://geology.com/minerals/mohs-hardness-scale.shtml` (2016)

[154] READE, "Mohs' Hardness (Typical) of Abrasives", URL `reade.com/reade-resources/reference-educational/reade-reference-chart-particle-property-briefings/32-mohs-hardness-of-abrasives` (2016)

[155] Møller, VB, Wang, T, Dam-Johansen, K, Frankær, SM, Kiil, S, "Diffusion cell investigations into the acidic degradation of organic coatings", Submitted December to Journal of Coatings Technology and Research (2017)

[156] Yang, C, Smyrl, WH, Cussler, EL, "Flake alignment in composite coatings", J. Membrane Sci. 231 (2004) 1–12 (2004)

[157] Derocher, JP, Gettelfinger, BT, Wang, J, Nuxoll, EE, Cussler, EL, "Barrier membranes with different sizes of aligned flakes", J. Membrane Sci. 254 (1) 21–30 (2005)

[158] Romhild, S, Bergman, G, Hedenqvist, MS, "Short-term and long-term performance of thermosets exposed to water at elevated temperatures", Appl. Poly. Sci. 116 1057–1067 (2010)

[159] Hedenqvist, MS, "Multi-layer modeling of diffusion of water in acrylamide-grafted aliphatic polyesters", Polym. Eng. and Sci. 38 (8) 1313–1323 (1998)

[160] Croll, SG, Shi, X, Fernando, BMD, "The interplay of physical aging and degradation during weathering for two crosslinked coatings", Prog. in Org. Coat. 61 136–144 (2008)

[161] Umino, S, Newman, J, "Diffusion of sulfuric acid in concentrated solutions", J. Electrochem. Soc. 140 (8) 2217–2221 (1993)

[162] Wu, YC, Feng, D, "The second dissociation constant of sulfuric acid at various temperatures by the conductometric method", J. Solut. Chem. 24 (2) 133–144 (1995)

[163] Bitter, JGA, "A study of erosion phenomena - Part I", Wear 6 (1) 5–21 (1963)

[164] Bitter, JGA, "A study of erosion phenomena Part II", Wear 6 (3) 169–190 (1963)

[165] Oka, YI, Okamura, K, Yoshida, T, "Practical estimation of erosion damage caused by solid particle impact: Part 1: Effects of impact parameters on a predictive equation", Wear 259 95–101 (2005)

[166] Lipsett, MG, Bhushan, V, "Modeling erosion wear rates in slurry flotation cells", J. Failure Anal. Prevention 12 51–65 (2012)

Appendix

Contents

A Analytic diffusion model derivations

Cranks derivation of the time-lag equation and the two gravimetric models are as follows:

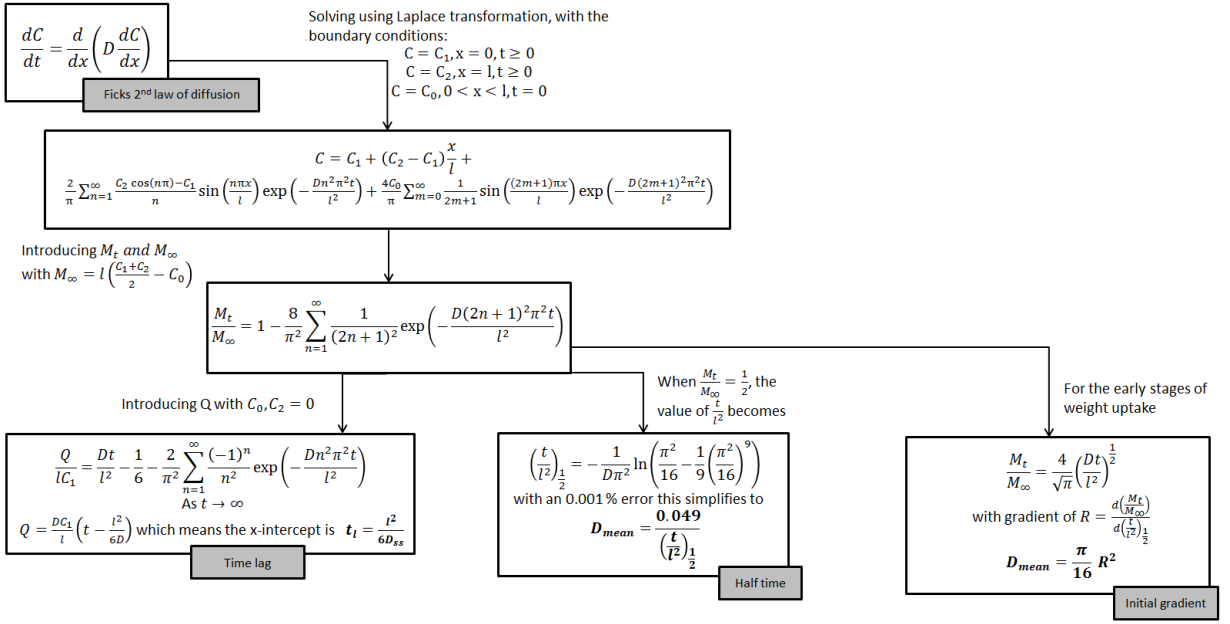

Figure A.1: Derivation of time-lag, gravimetric half time and gravimetric gradient models for determining diffusion coefficients. Assumptions include constant diffusion coefficient and slap geometry. M_t and M_∞ are the amount of substance which enters a slab at time t and time $t = \infty$, respectively. Q denotes the total amount of substance passed through the slab in time t. $\left(\frac{t}{l^2}\right)_{\frac{1}{2}}$ is the value of $\left(\frac{t}{l^2}\right)$ when $\frac{M_t}{M_\infty} = \frac{1}{2}$. D_{ss} represents steady state diffusion coefficient, while D_{mean} is an average diffusion coefficient. Deduced from [98].

B Erosion mathematical models

Table B.1: Parameter values used in the presented models

A	Area
c	Constant determined by the particle type
D	Diameter
$D^{'}$	Reference diameter
E	Total erosion rate
f	Impact frequency
g	Erosion rate
Hv	Particle hardness
K	Normal component of velocity required to initiate erosion
k	Constant determined by the particle type
M	Total mass of impacting particles
m	Mass of a single particle
n	Constant determined by material hardness and particle properties
Q	Volume material removed
t	time
V	Impact speed
$V^{'}$	Reference impact speed
z	Height position
W	Total wear
Greek symbols	
θ	Particle impact angle
ϵ	Specific energy for deformation
ϕ	Specific energy for cutting
Subscripts	
C	Cutting
D	Deformation
p	Particle

The mathematical descriptions of erosion rates give an idea of the relative influence of each individual parameter. Two selected mathematical models have been made to predict the erosion of a single particle colliding with a planar wall. Bitter, J. G. A. presents a model that includes a deformation and cutting wear [163, 164] presented in Eqn. 23, while Oka et *al.* [152, 165], made a wear model that assesses erosion by impingement of a particle on a wall, show in Eqn. 24. Both models stress the impact angle and velocity of the particle, as the most influential parameters, followed by particle hardness and diameter. Some of the parameters mentioned in the beginning of the section are hidden away in empirical constants such as n_1, n_2, K, k_1, k_2 and k_3, see the references for greater detail.

$$
\begin{aligned}
W &= W_D + W_C \\
W_D &= \frac{M(V_p sin(\theta) - K)^2}{2\epsilon} \\
W_C &= \frac{M V_p^2 cos^2(\theta)}{2\phi}
\end{aligned}
\tag{23}
$$

$$
\begin{aligned}
E(\theta) &= g(\theta)E(90) \\
g(\theta) &= sin(\theta)^{n_1}(1 + \mathrm{Hv}(1 - sin(\theta)^{n_2})) \\
E(90) &= c(\mathrm{Hv})^{k_1} \left(\frac{V_p}{V'}\right)^{k_2} \left(\frac{D_p}{D'}\right)^{k_3}
\end{aligned}
\tag{24}
$$

In practice, erosion does not occur with a single particle, but by a combination of many impacts. This too has been modeled, as Lipsett, M. G. [166] combined Oka's equation for abrasive damage. He showed that the particle impact frequency, amount of collisions per area per unit time, is of importance when modeling accumulated erosion. Using the total mass of particles impinging on a cylindrical surface M, with the damage of each particle, he was able to make a model that predicted the total erosive damage over time. With dQ as the volume of material removed, then the erosion rate can be redefined as:

$$
\begin{aligned}
E(\theta) &= \frac{dQ}{M} \\
\frac{dQ}{dt} &= g(\theta)E(90)(m \cdot f \mathrm{d}t \cdot A(z)\mathrm{d}z) = dD'
\end{aligned}
\tag{25}
$$

D' is defined as damage rate, and the cumulative damage can be described by D as shown below.

$$
D = \int_0^t \int_0^h dD' = \int_0^t \int_0^h g(\theta) \cdot E(90) \cdot m \cdot f \cdot A(z)\mathrm{d}z \ \mathrm{d}t \tag{26}
$$

The impact frequency is the parameter worth noting here. The impact frequency is the amount of collisions per unit area and it is determined by the particle concentration, velocity, and impact pattern.

C Coating thickness correlation

The total uncertainty of the Elcometer 355 is the accumulated uncertainty from the equipment itself, the coating roughness, and the experimental deviation. This section will discuss the relative influence of these three parameters as well as the steps taken to reduce measurement inaccuracy and uncertainties. Film thickness measurements are performed after doing a two point calibration. A base calibration on an uncoated substrate, and a thickness calibration on a coating sample of known thickness. Nevertheless, measurements made using the Elcometer 355 were not entirely precise. There was a degree of uncertainty in the equipment. This uncertainty was investigated on coating strips of known thicknesses provided by Elcometer for calibration purposes. The strip thicknesses were, 51.7, 125.9, 245, 525, 952 and 1500 μm. It can be seen from Fig. C.1 that the percentage deviations are highest at lower thicknesses and that the closer one is to the calibration value, the more accurate the measurement.

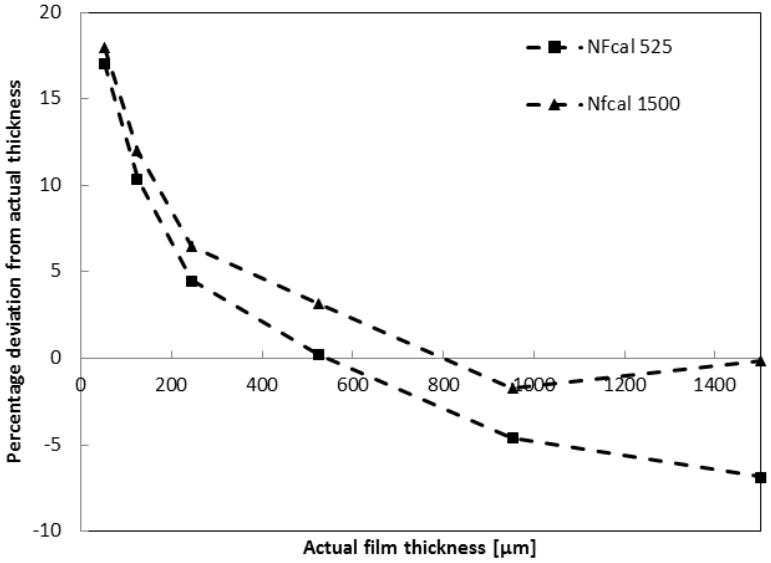

Figure C.1: Percentile deviation from actual thickness values for a non-ferrous (NF) probe. Using either a 525 or 1500 μm thick coating strip for calibration together with the base calibration.

The Elcometer was systematic with its inaccurate measurements, as shown in Fig. C.2 where the average of nine separate readings were performed, using 525 μm strip for calibration. The substrate for the non-ferrous probe was 316 stainless steel. A correction was applied to the collected data, shifting it closer to the actual values. This correction was determined by plotting the relationship between actual and measured thickness values followed by a power regression shown in Fig. C.3. Applying this correction to the original data shifts it closer to actual values as is also shown in Fig. C.2.

Due to the roughness of a coating surface, measurements taken on the same spot would vary slightly. This variation was different from each coating type. Table C.1 shows the four main coating types used in the project and their relative measurement uncertainties.

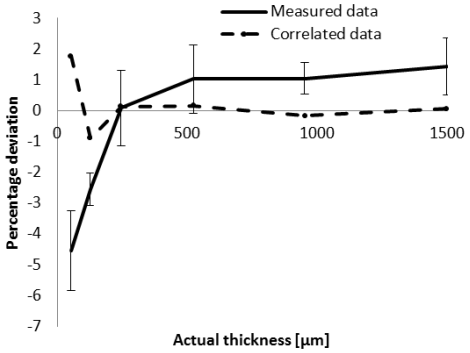

Figure C.2: Non-ferrous film thickness data deviation from actual values, before and after correlation. The calibration was performed using base and 525 μm strip, on 316 SS.

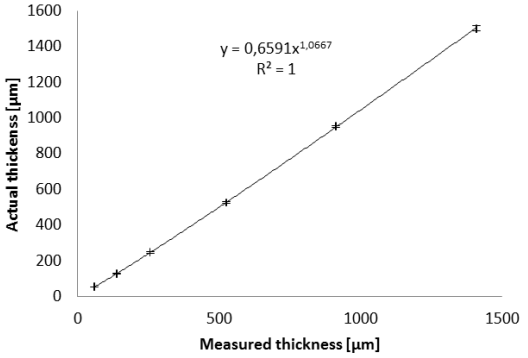

Figure C.3: Plot of actual vs measured thickness of the Elcometer 355, calibration was performed using base and 525 μm strip, on 316 SS. The correction equation is deduced from this relationship and shown together with a fitness parameter.

Table C.1: Elcometer 355 measurement uncertainty for four coating types after post curing before any exposure.

Coating type (code)	Uncertainty [$\pm\mu$ m]
Vinyl ester (VE)	1.9
Polyurethane (PU)	1.1
Novolac epoxy solids (NE1)	1.2
Novolac epoxy (NE2)	0.8

The data in Table C.1 has been gathered by measuring 129 points on unexposed coating samples. Each point was measured three times, and the percentage deviation of these triplicates were gathered and averaged. The average percentile deviation was subtracted by the equipment uncertainty since it is naturally included. It can occur during chemical exposure that the roughness profile changes, leading to increased measurement uncertainty. Though not shown in the table, this uncertainty is included in the collected data, by consequently performing three measurements on every point of measurement.

D UV absorbance

The UV spectrometer had to be calibrated before use. Fig. D.1 shows the calibration line with a linear fit for UV absorption analysis. The readings were performed using wavelengths of 810 nm and samples with known Cu(II) concentration.

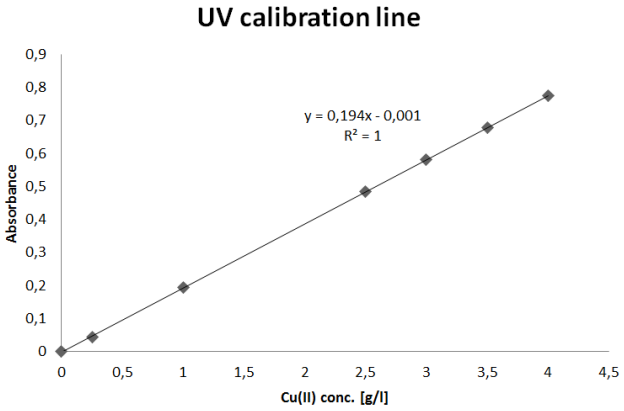

Figure D.1: Calibration line for UV absorption analysis including a linear fit to the data. Commas represent decimal separators.

E Erosive and chemical environment change

In practice, agitated leaching reactors are placed in series, with each reactor at steady state conditions due to continuous feeding of slurry and removal of product. Achieving this in lab scale was not feasible, and experiments are instead run using a single batch instead of a continuous process. This causes a continuous flux in chemical concentrations and particle size distribution. To maintain near constant conditions in the pilot-scale reactor, pH was adjusted using either sulfuric acid or sodium hydroxide. The following sections describe the particles and solution chemistry changes throughout experiments with the pilot-scale reactor.

E.1 Environmental conditions

The copper concentrate particles would react with immersion liquid, altering the pH and Cu(II) concentration, even in Mild conditions. Fig. E.1 shows the evolution of pH and Cu(II) concentration throughout the experimental sessions. It is observed that for Mild conditions, the pH dropped down close to 2.0 after two weeks exposure. This drop is likely the cause of blister formation on NE2, as it occurred at the same time period. The Cu(II) concentration in Harsh conditions saw continuous rise, due to a continued particle leaching until five weeks into the experiment. This indicates that particle mass is continuously being dissolved due to reactions with the sulfuric acid, approximately 13% of the initial particle mass. The effects of Cu(II) concentration on coating erosion resistance are unknown, but the DFT results should be viewed in the light of these changes in chemical conditions.

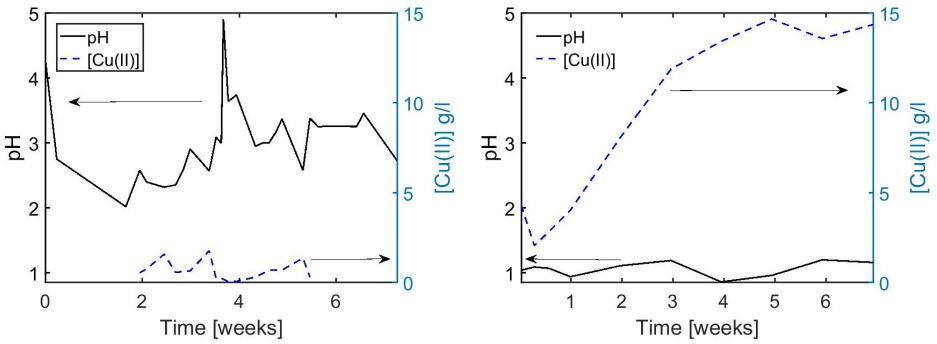

(a) Mild conditions. **(b)** Harsh conditions.

Figure E.1: Cu(II) concentration and pH fluctuation during the reactor experiments, caused by leaching of the copper concentrate.

E.2 Particle analysis

This section provides an overview of how the size distribution (PSD), and particle shape changes throughout the reactor experiments, in Mild and Harsh conditions. PSD was obtained using the Malvern Mastersizer, while shape analysis was performed using microscopical methods. Slurry samples were taken from the reactor while mixing, using a hollow glass tube inserted through the reactor lid.

Shape Fig. E.2 shows the erosive particles in the agitated leaching reactor before and after use. For both Mild and Harsh experiments there are particles with rounded and chipped edges, predominantly with high sphericity, but there are also elongated particles. Transparent particles are silica impurities. At the conclusion of the reactor experiments, the particles did not alter much in shape for either condition, chalcopyrite (black) particles seem more rounded on the edges, while silica particles still maintain chip shapes.

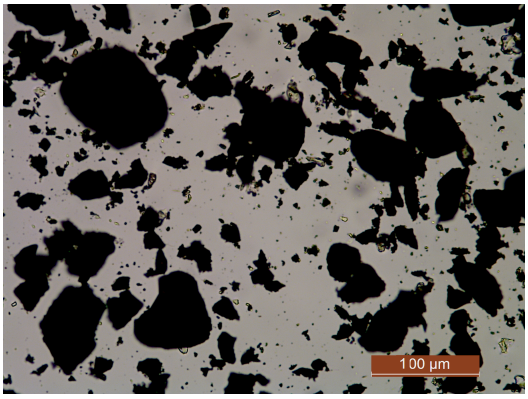

(a) Feed to the reactor, after pre-leaching.

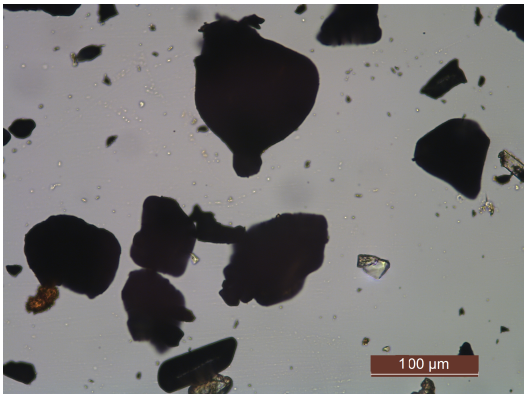

(b) After 7 weeks use in Mild conditions.

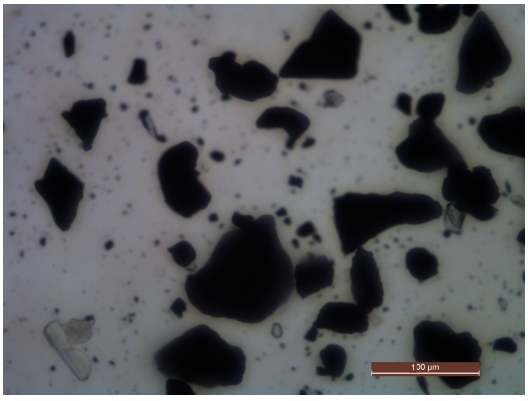

(c) After 7 weeks use in at Harsh conditions.

Figure E.2: Erosive particles before and after use in the reactor.

PSD Fig. E.3a shows a shift from small to large particles throughout the Mild reactor experiment. As the pH dropped, smaller particles (0.1 to 10 μm) would be leached more rapidly, due to their high surface to volume ratio. This pushes the average diameter upwards, but does not signify an increase in large particles, but rather a reduction of small particles.
Fig. E.3b shows that for Harsh conditions, small particles are being consumed initially by the acid, pushing the distribution up. Then as time progresses, larger particles start to break apart, or are reduced in diameter due to leaching, causing a reduction in the PSD. This indicates a reduction in the quantity of the larger particles.

The larger particles have a greater effect on the coating erosion than smaller particles, due to their larger diameter and volume, as shown by the formula for single particle erosion in Appendix B.
Since the quantity of larger particles are not significantly reduced, and only minor changes occur in particle shape, the erosive intensity remains constant throughout the Mild conditions experiment. However, for Harsh conditions it could be expected that erosive intensity is reduced throughout the experiment due to a reduction of larger particles.

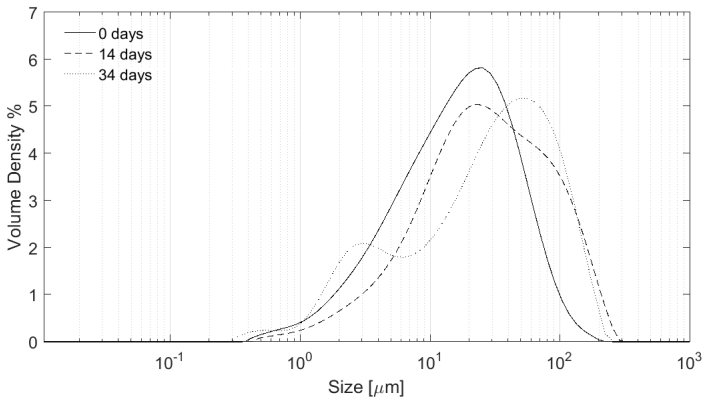

(a) Mild conditions.

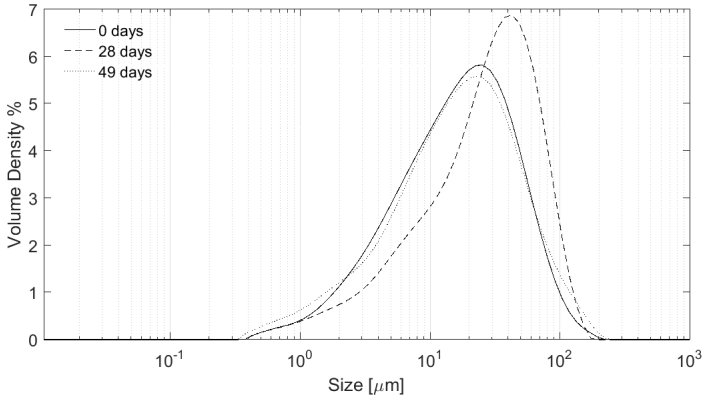

(b) Harsh conditions.

Figure E.3: PSD of particles used in the agitated leaching reactor throughout the experiment. The size class is defined as the mean spherical diameter.

F Details regarding pilot-scale acid leaching reactor

This section includes details of the pilot-scale reactor procedure, materials and safety. It is meant as a quick users guide. This section should be read with the PI diagram in Fig. 15.8.

Inserting coating samples. The reactor lid carrying the mixer, heater and heating sensor can be lifted and lowered using a pneumatic crane via the valve [VP2]. Furthermore, the reactor is placed on wheels and can be easily moved along a short set of rails, into a clearance away from the lid. Once in the open position, coating samples can be inserted into the reactor bottom and fastened.
Sealing the reactor. The reactor is moved beneath the lid, a rubber ring sealing is placed on the reactor, and valve [VP2] is switched to lower the lid. A rubber plug attached to a coated steel rod is used to seal the drainage hole on the bottom of the reactor as shown in Fig. F.1. Valves [V1] and [V5] are closed.

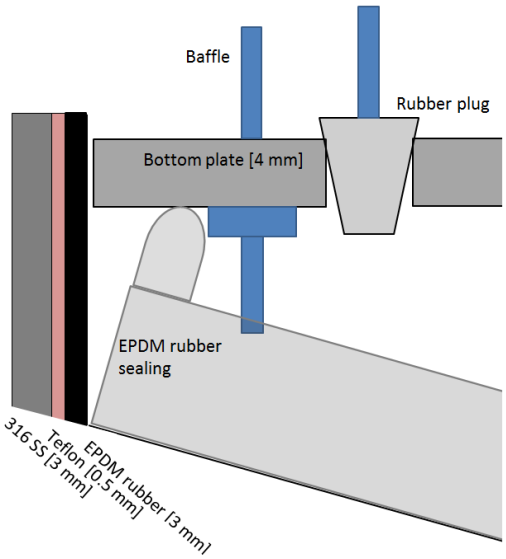

Figure F.1: Cross-section zoom of the reactor bottom. The reactor walls are protected by a teflon and rubber coating. The slurry is prevented from moving beneath the bottom plate using rubber sealings. A drainage hole in the bottom plate is sealed using a rubber plug throughout experimentation.

Slurry from storage to reactor. A mixer [M2] is attached to the storage tank to enable particle suspension while the slurry is pumped back, using [P1], to the reactor. Without the mixer, particles would sediment and remain in the storage tank. The acid pump [P1] has a detachable nozzle which can be inserted in the reactor lid, when the reactor is in its closed position. The acid pump nozzle is removed once all the slurry has been transported, and the hole in the reactor lid can be sealed.
Running an experiment. The desired liquid temperature and stirring speed can be adjusted on the control box, shown in Fig. F.2. Heater [H1] provides the heating, while sensor [T1] determines the liquid temperature. It is important the heater and temperature sensor are immersed during experimentation. Stirring [M1] and heating can commence once coating samples and slurry has been added to the tank

and all the safety condition are met, see Section F.1.

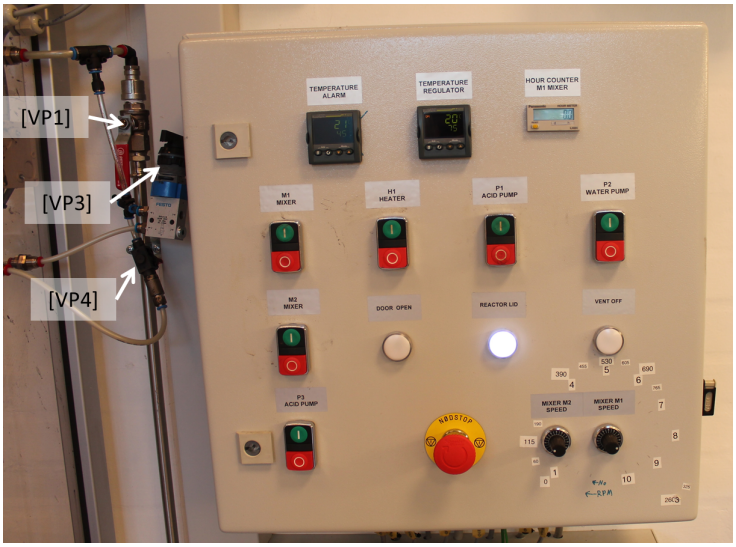

Figure F.2: The electric control box for the pilot-scale leaching reactor and the [VP] 1, 3 and 4 valves, placed outside the set-up fume hood. Displays show temperatures measured by [T1] and [T2], and a counter for experimental time. On/off buttons control mixers, pumps and heater. The warning lights indicate when a safety condition is not met.

Emptying the reactor. To remove the coatings one has to first empty the reactor. By opening the rubber plug and valve [V1], the slurry will fill the pumping tube, make sure [V5] is closed. The acid pump [P3] is inserted in the pumping tube with the exit-nozzle in the storage tank. The [P3] and [M1] are run until the reactor is emptied. Valve [V5] is opened to direct flow into the dump tank, and valve [V2] is directed to the wash water feed, after inserting the spinning cleaning nozzle in the main reactor. The reactor lid can now be lifted using [VP2] and samples removed. **Caution!** A de-clot valve [VP4] is attached to the exit flow pipe from the reactor, its purpose is to prevent blocking of the pipe by blowing air and causing stirring. Use only when the exit flow pipe is blocked, and use with caution, too high pressures can spray slurry out of the reactor.
Preventing evaporation. The reactor is kept at ambient pressure using a hole in the lid. A reflux condenser is attached to this hole, recirculating any evaporating liquids and aerosols to the reactor to maintain a constant liquid volume. Cooling water is pumped into the condenser from Tank 3 using [P2], but can also be directed into a spinning spray nozzle, using valve [V2] for cleaning the reactor after use. During experimentation the [V2] should be directed into the reflux-condenser.

F.1 Safety and materials

To ensure safe operation and proper containment of the corrosive environment all construction materials were chosen carefully, and safety switches and sensors were included to prevent any erroneous use of the set-up.

Safety conditions were included to shut down and prevent operation of the acid pump, mixers and heaters should the following occur. Fume-hood doors open, ventilation shut off, or reactor lid be raised. An extra safety switch is attached to the temperature sensor in the reflux condenser, should the exit gas become too warm, indicative of failed/poor condensation, operations will shut down.
Regarding materials, the main scaffolding, reactor and impellers are made of 316-L stainless steel, an acid resistant metal. The internal baffles where made of Hastalloy C-22. The temperature sensor and bath heater inserted in the main reactor are made of acid-resistant ceramic material, and so is the reflux condenser. The main reactor valve [V1] is made of polypropylene (PP), so are all fittings in the main reactor lid, and the acid-pump nozzle. The storage tank is made of high density polyethylene (HDPE). The secondary containment tank is made of polyethylene (PE). As extra safety, the main reactor has been coated with a commercial PTFE coating, for chemical resistance. This coating is also protected from erosion and marring by a mechanically fastened EPDM rubber sheet. Should a spill occur, then the secondary containment tank is able to contain a greater volume of liquid than the main reactor.

G Water erosion

The effects of water erosion were tested by exposing coating samples to warm stirred water in the pilot-scale reactor. Fig. G.1 shows DFT change by section of reactor samples immersed in mild conditions without erosive particles. There is no evident pattern such as one can find when erosion is present. This provides evidence that water erosion can be neglected.

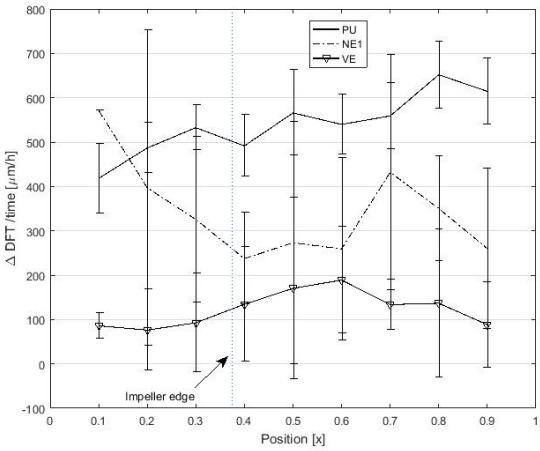

Figure G.1: Following 326 h immersion in mild conditions without erosive particles.

H Matlab code

The following is an example of the code used to simulate the concentration change in the Receiver chamber of the diffusion cell and compare it with experimental values.

```
% Explicit modeling of acid diffusion through a slap, with concentration
% dependent diffusion coefficient and concentration accumulation.
% Using a three-step time dependency of the D-coeff
clear all; clc; clf;
%% loading experimental data
load('C:\\Users\\vibum\\Dropbox\\DTU\\PhD\\Diffusion cell set-up\\Data and ...
    results\\Data treatment\\Ting_diffusion_data.mat');

p=1;                            %sample nr
time=time_NE4D_data(:,p);       % Experimental time [h]
cH2SO4=Hconc_NE4D_data(:,p);    % Concentration of H+ ion [mol/m3]
l=thickness_NE4D_data(p)*10^-6; % Thickness of the coating [m]

%%%%%%%%%%%%%%%%%%%%%% Data and Values %%%%%%%%%%%%%%%%%%%%%%%%%%%%%%%%%%

%c0=10^(-(0.9))*1000;% [mol/m3] for VE,PU,NE1 and NE2
c0=10^(-(-0.03))*1000; % for NE4 [mol/m3]; Concentration in the feed chamber
pHstart=6.5;    % start conditions inside the coating and in the R chamber water
area=SA;        % Surface area available for diffusion insert value in [m]
volume=Vr;      % Receiver chamber volume insert value in [m]

% D-coeff values before acid breakthrough
D_C0=0.1e-15;   % [m^2/s]
alpha=0.000;    % [mol/m^3]^-1
t_frac_bt=0.5;  %timefraction for changing Dcoeff at acid breakthough

% D-coeff values during the transient stage
D_C1=2.8e-15;
alpha1=alpha;
t_frac_trans=0.72; %timefraction for changing Dcoeff at steady state

% D-coeff values for the steady state flux
D_C2=5e-15;
alpha2=alpha;

%% Distance and time grid for simulation
% If the solution does not converge, consider increasing the j value

a=0; b=l; % Range of dimensionless distance: a≤X≤b
i=30; %Distance is divided into i intervals
lvector=linspace(a,l,i);
ΔX=(b-a)/i;

t0=0; tf=time(end,1);  % Dimensionless time span: t0≤T≤tf
j=5000000; %Time is divided into j intervals
```

```
t=linspace(t0,tf,j); % tspan
ΔT=(tf-t0)*3600/j;


%% Initial and boundary conditions
c=zeros(j,i);       %creating a zero matrix to print values on

c_R=zeros(1,j)+10^(-pHstart)*1000;  % Receiver chamber initial concentration
c(1,:)=10^(-pHstart)*1000;          % Initial conditions
c(:,1)=c0; c(:,i)=10^(-pHstart)*1000; %Boundary conditions

%% Main solver loop
for m=1:j-1
        %discritized pde, with concentration dependent D-coeff
    for n=2:i-1
        c(m+1,n)=c(m,n)+(ΔT*D_C0/ΔX^2)*...
            (exp(alpha*(c(m,n+1)+c(m,n))/2)...
            *(c(m,n+1)-c(m,n))-exp(alpha*(c(m,n)+c(m,n-1))/2)...
            *(c(m,n)-c(m,n-1)));
    end

    %Flux of bisulfate ion at l=l_0;
    F(m)=area*D_C0*exp(alpha*c(m,i))*(c(m,i-1)-c(m,i))/ΔX;

    %Concentration of bisulfate ion at l=l_0
    c_R(m+1)=c_R(m)+F(m)*ΔT/volume;

    %Upgrading boundary conditions
    c(m+1,i)=c_R(m+1);

    %Changing D-ceoff values
      if m== round(j*t_frac_bt) % at acid breakthrough
        D_C0=D_C1;
        alpha=alpha1;
      end
      if m== round(j*t_frac_trans) % at steady state flux
        D_C0=D_C2;
        alpha=alpha2;
      end
end
%converting results to pH values
pHsim=-log10(c_R/1000);
pHexp=-log10(cH2SO4/1000);

%% Plotting results
%lin1 = {'-k','--k',':k','-.k','-vk'};
lin1 = {'-k','-dk','-^k','-ok','-vk'};
lin2 = {'-','--',':','-.','-v'};

f1=1/(24);%unit converter, hours to days

%plotting experimental values against simulated values: Receiver chamber
figure (1)
```

```
hold on
    yyaxis left
plot(time*f1,pHexp,'x')     %Plot of experimental results
plot(t*f1,pHsim,'-','LineWidth',1.3) %Plot of result of explicit method
 xlabel('Time [days]')
 ylabel('pH')
 ylim([0 8])
 yyaxis right
plot(time*f1,cH2SO4,'o') %Plot of experimental results
plot(t*f1, c_R,'--','LineWidth',1.3) %Plot of result of explicit method
  ylabel('Concentration [mol/m^3]')
  legend('Experimental pH', 'Model pH','Experimental concentration'...
      , 'Model concentration', 'Location', 'best')
  legend('boxoff')
  set(gca,'FontSize',17)
  set(gca,'LineWidth',1.5)
  set(gcf, 'Position',[400 200 800 650])
  axis('tight')
  ylim([0 20])
annotation('arrow',[0.2525 0.15875],...
    [0.449769230769231 0.450769230769231],'Color',[0 0.5 0.9],'LineWidth',1.5);
annotation('arrow',[0.76375 0.87875],...
    [0.203076923076923 0.203076923076923],'Color',[1 0.4 0],'LineWidth',1.5);
 set(gcf, 'Position',[400 200 800 650])
 yL = get(gca,'YLim');
  line([t(round(j*t_frac_bt))*f1 t(round(j*t_frac_bt))*f1]...
      ,yL,'LineStyle',lin2{3},'color','black','LineWidth',1.5);
  line([t(round(j*t_frac_trans))*f1 t(round(j*t_frac_trans))*f1]...
      ,yL,'LineStyle',lin2{3},'color','black','LineWidth',1.5);
hold off


f2=1/(3600*24);%unit converter, seconds to days
%plotting the concentration curves inside the coating film at set points in
%time
 figure (2)
      plot(lvector*10^(6),c(round(j*t_frac_bt*0.01),:),lin1{5}, ...
          lvector*10^(6),c(round(j*t_frac_bt*0.05),:)...
          ,lin1{2},lvector*10^(6),c(round(j*t_frac_bt),:),lin1{3}...
          ,lvector*10^(6),c(round(0.8*j*((t_frac_trans-t_frac_bt)*0.5+t_frac_bt)),:)...
          ,lin1{4},lvector*10^(6),c(round(j),:),lin1{1},'LineWidth',1.5)
      title('Concentration curve at different times')
      xlabel('Position in the film [\mum]')
      ylabel('Concentration [mol/m^3]')
      set(gca,'FontSize',17)
  set(gca,'LineWidth',1.5)
  set(gcf, 'Position',[400 200 800 650])
      legend(['time=' num2str(round(j*t_frac_bt*0.01)*ΔT*f2) ' [days]']...
          ,['time=' num2str(round(j*t_frac_bt*0.05)*ΔT*f2) ' [days]']...
          ,['time=' num2str(round(j*t_frac_bt)*ΔT*f2) ' [days]']...
          ,['time=' ...
              num2str(round(j*0.8*((t_frac_trans-t_frac_bt)*0.5+t_frac_bt))*ΔT*f2) ...
              ' [days]']...
```

```
148             ,['time=' num2str(round(j)*ΔT*f2) ' [days]'],'Location', 'best')
149         legend('boxoff')
150     set(gcf, 'Position',[400 200 800 650])
```

I Dimensionless diffusion model

The following is a description of a dimensionless version of the diffusion cell mathematical model, with a plot to show the feedback effect of concentration increase in the Receiver chamber. To observe the feedback from the increasing concentration in the Receiver chamber one can make the model presented in Section 26.1 dimensionless by introducing the dimensionless variables

$$y = \frac{C}{C_D} \tag{27}$$

$$z = \frac{x}{l_0} \tag{28}$$

$$\tau = \frac{t}{t_{\text{ref}}} \tag{29}$$

$$t_{\text{ref}} = \frac{l_0^2}{D_0} \tag{30}$$

yielding a dimensionless diffusion model

$$\frac{\partial y}{\partial \tau} = \frac{\partial}{\partial z}\left(D_x(y)\frac{\partial y}{\partial z}\right) \tag{31}$$

with the flux to the Receiver chamber becoming

$$\frac{\partial y}{\partial \tau} = -\gamma D_x(y=1)\frac{\partial y}{\partial z}\Big|_{z=1} \tag{32}$$

with the dimensionless diffusion coefficient

$$D_x(y) = D_1 \cdot \exp(\kappa \cdot y) \tag{33}$$

and with the dimensionless constants being

$$\kappa = \alpha \cdot c_0 \tag{34}$$

$$\gamma = \frac{l_0 \cdot A}{V_R} \tag{35}$$

$$D_1 = \frac{D_0}{D_{\text{ref}}} \tag{36}$$

Fig. I.1 shows the simulated dimensionless concentration as time passes for a given set of dimensionless values. The figure shows how an up-concentration in the Receiver chamber causes the concentration gradient across the coating film to gradually decrease. This then causes the ion flux level off after the steady state has been reached.

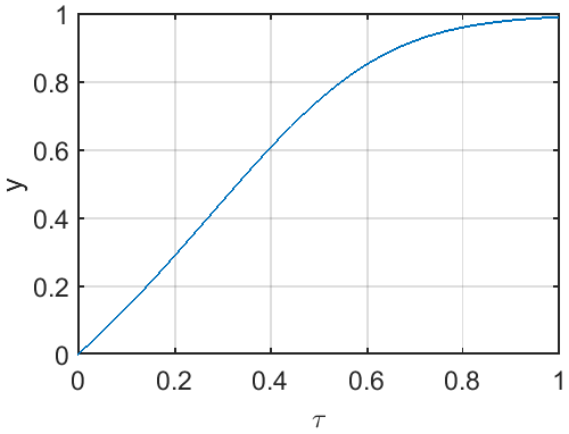

Figure I.1: Dimensionless simulated ion concentration-time profile in a diffusion cell Receiver chamber. Simulated using $\kappa = 3.77$, $\gamma = 0.0049$ and $D_1 = 35$

J Diffusion model results

The following is a graphical overview of the simulated Receiver chamber concentration and pH profiles, fitted to experimental values for the diffusion cell experiments. The D_{0B}, D_{0T}, D_{0ss} and α values used can be found in Table 29.1.

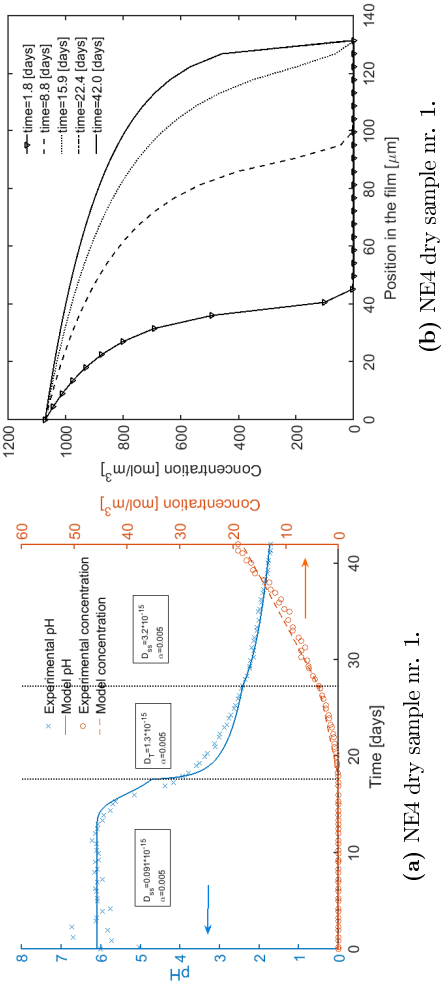

(a) NE4 dry sample nr. 1.

(b) NE4 dry sample nr. 1.

(c) NE4 dry sample nr. 2.

(d) NE4 dry sample nr. 2.

Figure J.1: NE4 Dry experimental and simulated results. Left figures show the pH and corresponding H^+ ion concentration change in the Receiver chamber. Figures to the right shows the simulated concentration profiles inside the coatings at different points in time.

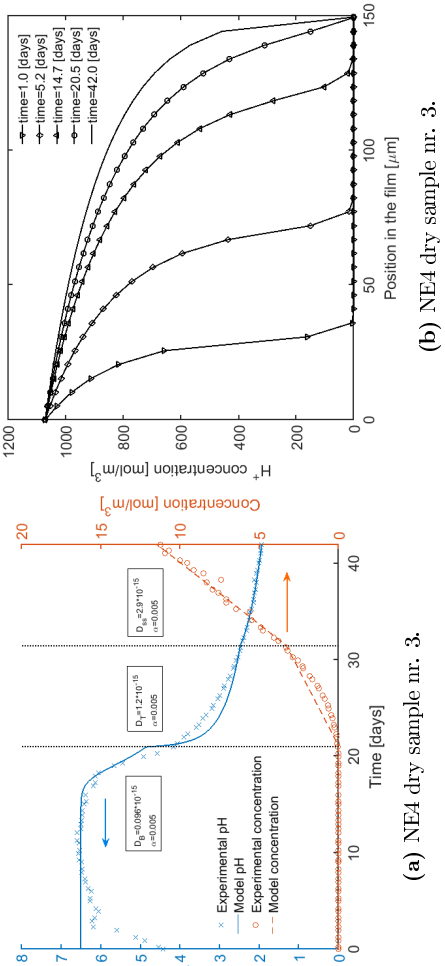

(a) NE4 dry sample nr. 3.

(b) NE4 dry sample nr. 3.

(c) NE4 dry sample nr. 4.

(d) NE4 dry sample nr. 4.

Figure J.2: NE4 Dry experimental and simulated results. Left figures show the pH and corresponding H^+ ion concentration change in the Receiver chamber. Figures to the right shows the simulated concentration profiles inside the coatings at different points in time.

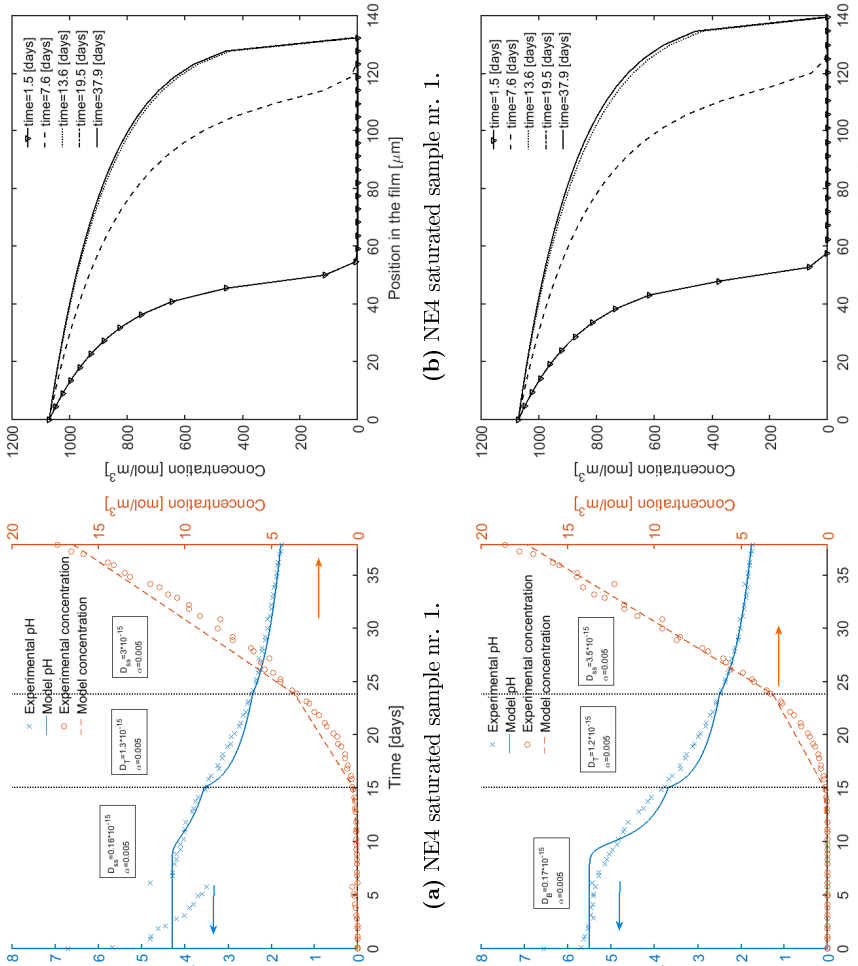

(a) NE4 saturated sample nr. 1.

(b) NE4 saturated sample nr. 1.

(c) NE4 saturated sample nr. 2.

(d) NE4 saturated sample nr. 2.

Figure J.3: NE4 Saturated experimental and simulated results. Left figures show the pH and corresponding H^+ ion concentration change in the Receiver chamber. Figures to the right shows the simulated concentration profiles inside the coatings at different points in time.

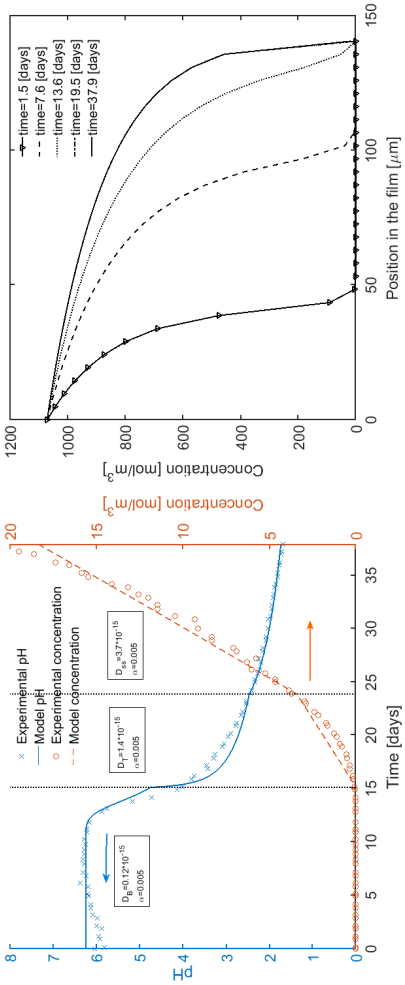

(a) NE4 saturated sample nr. 3.

(b) NE4 saturated sample nr. 3.

Figure J.4: NE4 Saturated experimental and simulated results. Left figures show the pH and corresponding H^+ ion concentration change in the Receiver chamber. Figures to the right shows the simulated concentration profiles inside the coatings at different points in time.

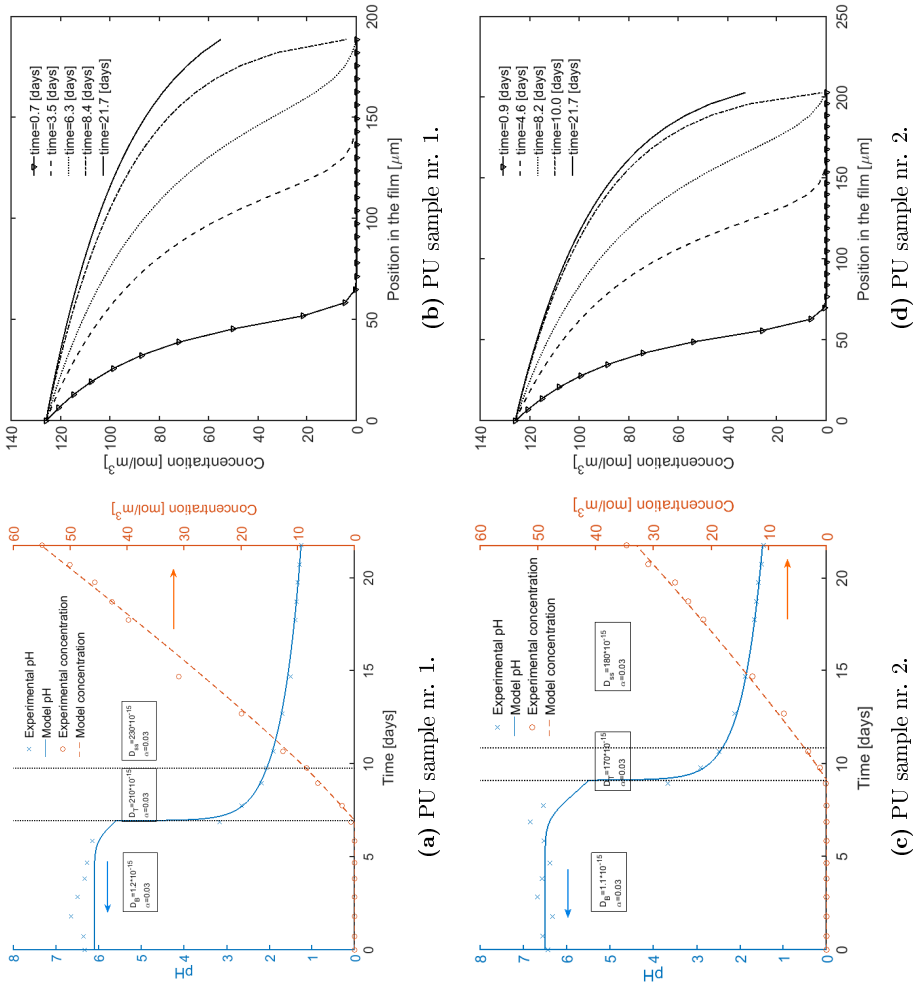

(a) PU sample nr. 1. **(b)** PU sample nr. 1. **(c)** PU sample nr. 2. **(d)** PU sample nr. 2.

Figure J.5: PU experimental and simulated results. Left figures show the pH and corresponding H^+ ion concentration change in the Receiver chamber. Figures to the right shows the simulated concentration profiles inside the coatings at different points in time.

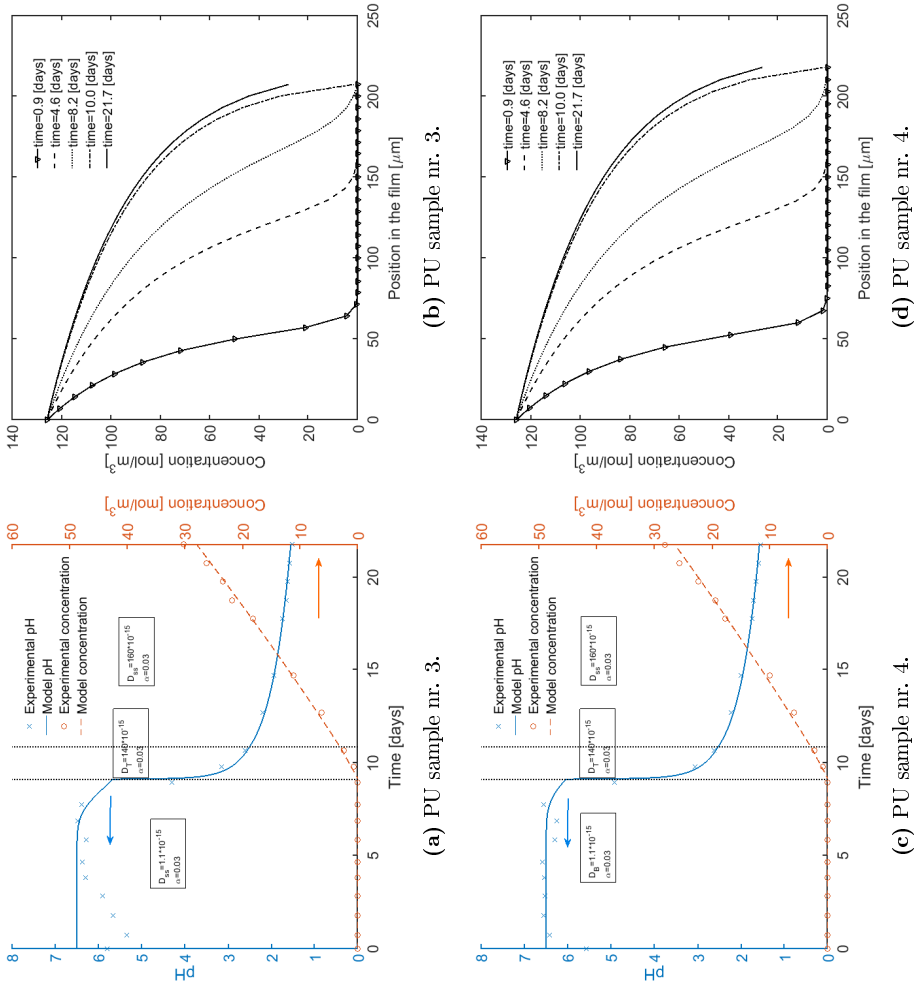

(a) PU sample nr. 3. **(b)** PU sample nr. 3.

(c) PU sample nr. 4. **(d)** PU sample nr. 4.

Figure J.6: PU experimental and simulated results. Left figures show the pH and corresponding H^+ ion concentration change in the Receiver chamber. Figures to the right shows the simulated concentration profiles inside the coatings at different points in time.

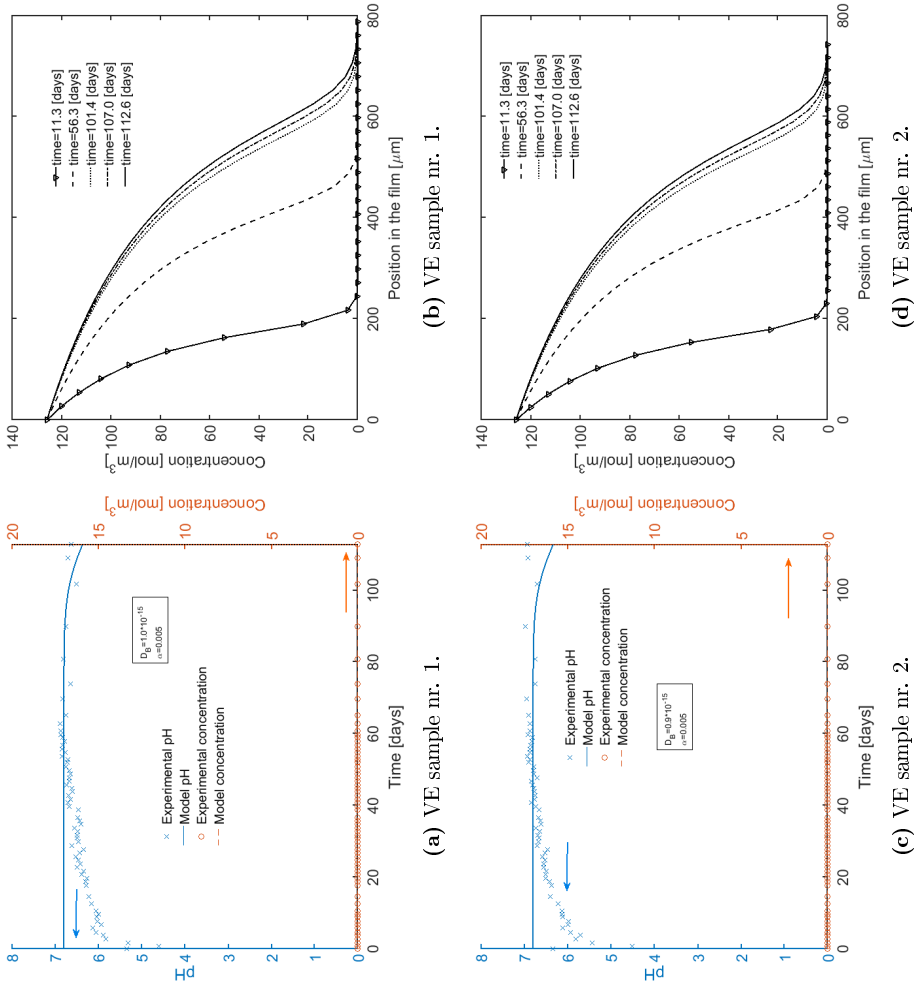

(a) VE sample nr. 1. **(b)** VE sample nr. 1.

(c) VE sample nr. 2. **(d)** VE sample nr. 2.

Figure J.7: VE experimental and simulated results. Left figures show the pH and corresponding H^+ ion concentration change in the Receiver chamber. Figures to the right shows the simulated concentration profiles inside the coatings at different points in time.

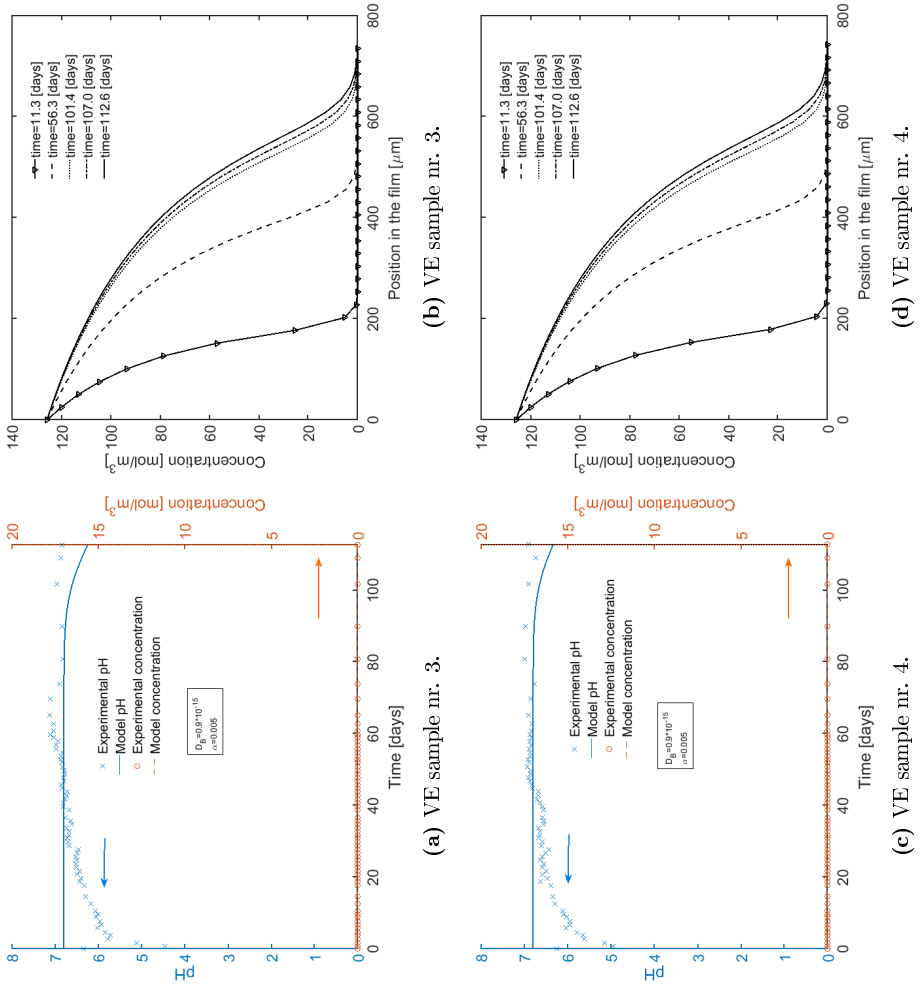

(a) VE sample nr. 3. **(b)** VE sample nr. 3.

(c) VE sample nr. 4. **(d)** VE sample nr. 4.

Figure J.8: VE experimental and simulated results. Left figures show the pH and corresponding H^+ ion concentration change in the Receiver chamber. Figures to the right shows the simulated concentration profiles inside the coatings at different points in time.

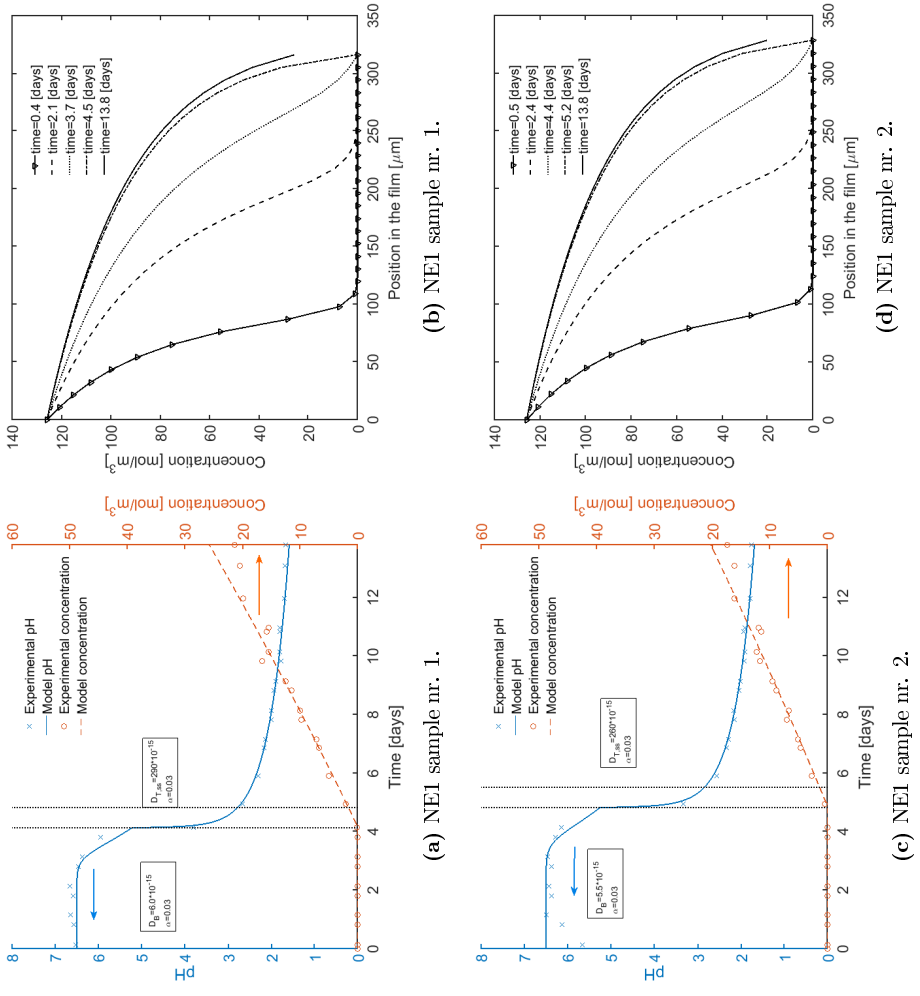

(a) NE1 sample nr. 1. **(b)** NE1 sample nr. 1. **(c)** NE1 sample nr. 2. **(d)** NE1 sample nr. 2.

Figure J.9: NE1 experimental and simulated results. Left figures show the pH and corresponding H^+ ion concentration change in the Receiver chamber. Figures to the right shows the simulated concentration profiles inside the coatings at different points in time.

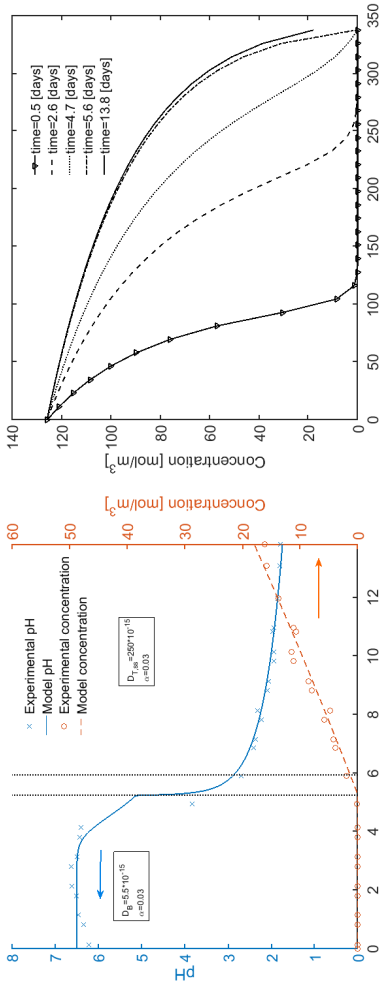

(a) NE1 sample nr. 3.

(b) NE1 sample nr. 3.

(c) NE1 sample nr. 4.

(d) NE1 sample nr. 4.

Figure J.10: NE1 experimental and simulated results. Left figures show the pH and corresponding H^+ ion concentration change in the Receiver chamber. Figures to the right shows the simulated concentration profiles inside the coatings at different points in time.

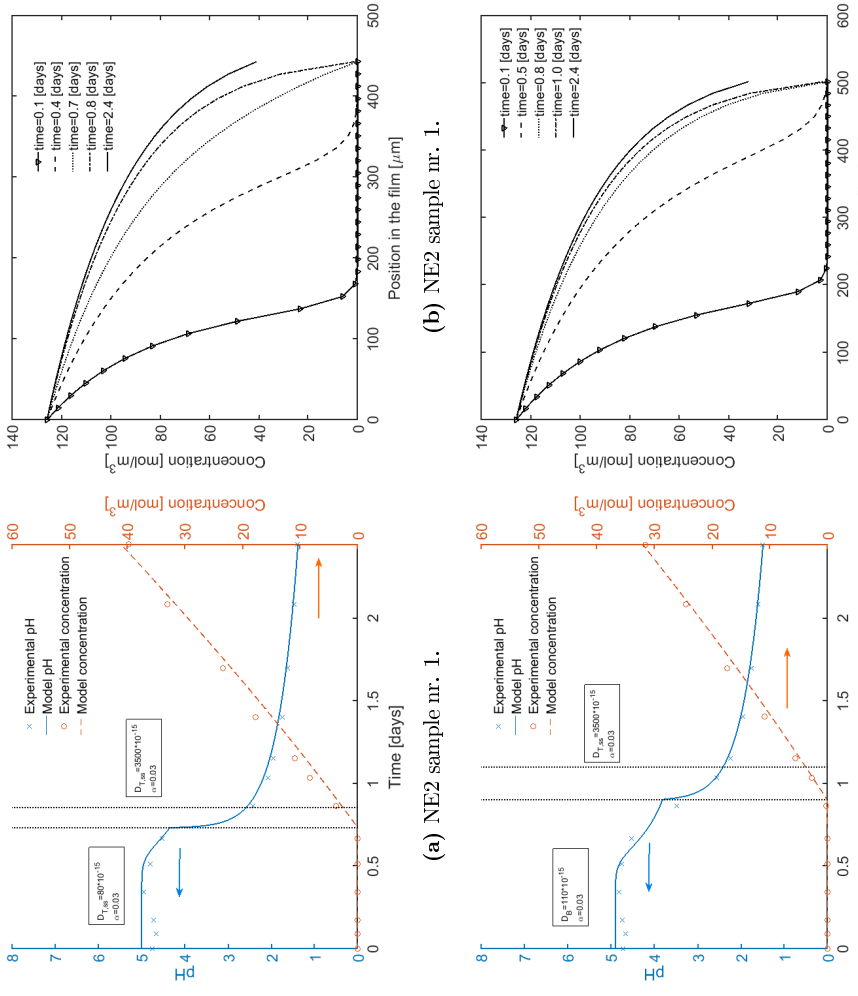

(a) NE2 sample nr. 1. **(b)** NE2 sample nr. 1. **(c)** NE2 sample nr. 2. **(d)** NE2 sample nr. 2.

Figure J.11: NE2 experimental and simulated results. Left figures show the pH and corresponding H^+ ion concentration change in the Receiver chamber. Figures to the right shows the simulated concentration profiles inside the coatings at different points in time.

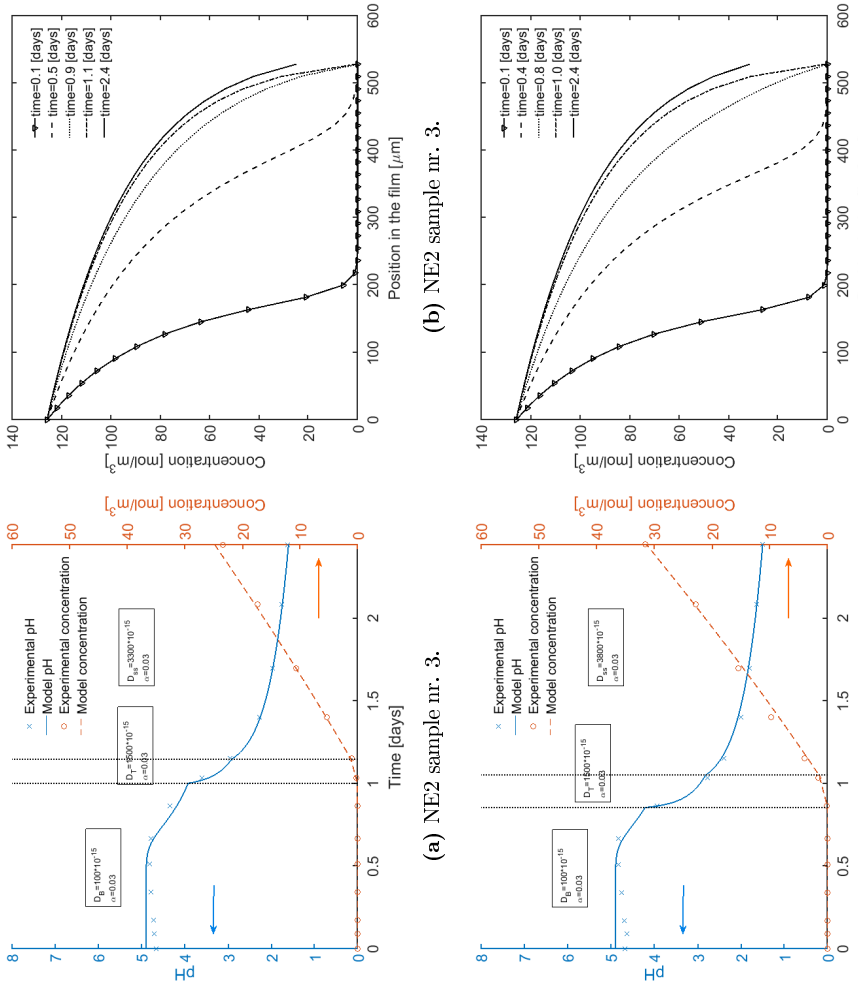

(a) NE2 sample nr. 3.

(b) NE2 sample nr. 3.

(c) NE2 sample nr. 4.

(d) NE2 sample nr. 4.

Figure J.12: NE2 experimental and simulated results. Left figures show the pH and corresponding H^+ ion concentration change in the Receiver chamber. Figures to the right shows the simulated concentration profiles inside the coatings at different points in time.

K Simple breakthrough time diffusion coefficients

Table K.1 provides and overview of the D_B values for each coating sample used in the diffusion cell. The D_B value is evaluated by using Eqn. 7, with t equating the breakthrough time, and l being the sample thickness.

Table K.1: Breakthrough time diffusion coefficients overview for all experiments using diffusion cells. D_B is derived from Eqn. 7.

Condition	Coating code	Sample nr.	Thickness [μm]	$D_B \cdot 10^{-14} [m^2/s]$
Preliminary	NE4	1	131.3±4.5	1.11±0.08
Dry (21±1°C)	NE4	2	139.9±7.0	1.31±0.13
	NE4	3	149.3±7.8	1.21±0.13
	NE4	4	113.8±9.2	1.36±0.21
Saturated (21 ± 1°C)	NE4	1	132.3±8.9	1.81±0.24
	NE4	2	139.4±6.7	1.58±0.15
	NE4	3	140.5±6.5	1.50±0.14
Harsh	PU	1	188.7±5.2	6.46±0.36
(68.5 ± 2.5°C)	PU	2	203.0±4.6	5.32±0.24
	PU	3	207.5±4.6	5.56±0.25
	PU	4	218.0±8.7	5.87±0.47
	VE	1	788.0±20.7	6.38±0.34[a]
	VE	2	743.0±17.4	5.67±0.27[a]
	VE	3	735.0±36.5	5.55±0.55[a]
	VE	4	743.0±21.6	5.67±0.33[a]
	NE1	1	316.0±8.5	27.87±1.49
	NE1	2	328.5±12.2	25.24±1.87
	NE1	3	337.5±10.9	26.64±1.72
	NE1	4	343.5±6.8	27.51±1.09
	NE2	1	443.0±13.8	338.6±21.1
	NE2	2	502.0±8.7	379.5±13.1
	NE2	3	528.0±8.3	339.0±10.7
	NE2	4	528.0±10.4	372.4±14.7

[a] These are the largest possible values, calculated assuming acid penetration occurred at the termination of the experiment. No actual acid breakthrough was observed and the D_B is expected to be much lower.

Department of Chemical and Biochemical Engineering - CoaST
Technical University of Denmark
Søltofts Plads, Building 229
2800 Kgs. Lyngby
Denmark
Phone: +45 45 25 28 00
Web: www.kt.dtu.dk

Printed by STEP